Widespread Polymodal Chemosensory Receptor Expression in *Drosophila* Olfactory Neurons

Darya Task[1], Chun-Chieh Lin[1,4,5], Ali Afify[1], Hongjie Li[2], Alina Vulpe[3], Karen Menuz[3], Christopher J. Potter[1]*

ABSTRACT

Drosophila olfactory neurons have long been thought to express only one chemosensory receptor modality. Using a new genetic knock-in strategy, we targeted the four co-receptors representing the chemosensory modes in *Drosophila* (*Orco*, *Ir25a*, *Ir8a*, *Ir76b*). Co-receptor knock-in expression patterns were verified as accurate representations of endogenous expression. We find extensive overlap in expression among the different co-receptors. As defined by innervation into antennal lobe glomeruli, *Ir25a* is broadly expressed in 88% of olfactory neuron classes and is co-expressed in 64% of Orco+ neuron classes, including all neuron classes in the maxillary palp. *Orco*, *Ir8a*, and *Ir76b* expression patterns are also expanded. Single sensillum recordings from Orco-expressing *Ir25a* mutant antennal and palpal neurons identify significant changes in olfactory responses. These results suggest polymodal expression and function of chemosensory receptors is common in olfactory neurons. We present a new map of the olfactory system reflecting this polymodal expression.

Keywords: insect, olfaction, odorant receptor, ionotropic receptor, sensory neuron, CRISPR, *QF2*, antennal lobe, HACK, knock-in.

INTRODUCTION

The sense of smell is crucial for many animal behaviors, from conspecific recognition and mate choice (Dweck et al., 2015; Stengl, 2010) to location of a food source (Auer et al., 2020; Hansson and Stensmyr, 2011) to avoidance of predators (Kondoh et al., 2016; Papes et al., 2010) and environmental dangers (Mansourian et al., 2016; Stensmyr et al., 2012). Peripheral sensory organs detect odors in the environment using a variety of chemosensory receptors (Carey and Carlson, 2011; Su et al., 2009). The molecular repertoire of chemosensory receptors expressed by the animal, and the particular receptor expressed by any individual olfactory neuron, define the rules by which an animal interfaces with its odor environment. Investigating this initial step in odor detection is critical to understanding how odor signals first enter the brain to guide behaviors.

The olfactory system of the vinegar fly, *Drosophila melanogaster*, is one of the most extensively studied and well understood (Depetris-Chauvin et al., 2015). *Drosophila* is an attractive model for studying olfaction due to its genetic tractability, numerically simpler nervous system (compared to mammals), complex olfactory-driven behaviors, and similar organizational principles to vertebrate olfactory systems (Ache and Young, 2005; Wilson, 2013). Over sixty years of research have elucidated many of the anatomical, molecular, and genetic principles underpinning fly olfactory behaviors (Gomez-Diaz et al., 2018; Harris, 1972; Pask and Ray, 2016; Siddiqi, 1987; Stocker, 2001; Venkatesh and Singh, 1984; Vosshall and Stocker, 2007; Yan et al., 2020). Recent advances in electron microscopy and connectomics are revealing higher brain circuits involved in processing of olfactory information (Bates et al., 2020; Berck et al., 2016; Frechter et al., 2019; Horne et al., 2018; Marin et al., 2020; Zheng et al., 2018); such endeavors will aid the full mapping of neuronal circuits from sensory inputs to behavioral outputs.

The fly uses two olfactory appendages to detect odorants: the antennae and the maxillary palps (Fig 1A) (Stocker, 1994). Each of these is covered by sensory hairs called sensilla, and each sensillum houses between one and four olfactory sensory neurons or OSNs (Fig 1B) (de Bruyne et al., 2001; Venkatesh and Singh, 1984). The dendrites of these neurons are found within the sensillar lymph, and they express chemosensory receptors from three gene families: *odorant receptors* (*ORs*), *ionotropic receptors* (*IRs*) and *gustatory receptors* (*GRs*) (Fig 1C, left) (Benton et al., 2009; Clyne et al., 1999; Gao and Chess, 1999; Jones et al., 2007; Kwon et al., 2007; Vosshall et al., 1999; Vosshall et al., 2000). These receptors bind odorant molecules that enter the sensilla from the environment, leading to the activation of the OSNs, which then send this olfactory information to the fly brain (Fig 1D), to the first olfactory processing center – the antennal lobes (ALs) (Fig 1E) (reviewed in: (Depetris-Chauvin et al., 2015; Gomez-Diaz et al., 2018; Pask and Ray, 2016). The standard view regarding the organization of the olfactory system in *Drosophila* is that each class of olfactory neuron expresses receptors from only one of the chemosensory modalities (either *ORs*, *IRs*, or *GRs*), and all neurons of that class project their axons to one specific region in the AL called a glomerulus (Fig 1C, right) (Couto et al., 2005; Fishilevich and Vosshall, 2005; Gao et al., 2000; Laissue et al., 1999; Pinto et al., 1988; Vosshall et al., 2000). This pattern of projections creates a map in which the OR+ domains (Fig 1E, teal) are segregated from the IR+ domains (Fig 1E, purple) as well as the GR+ domain (Fig 1E, dark blue). The OR+ domains (38 glomeruli) are found primarily in more anterior glomeruli, while the IR+ (19 glomeruli) and GR+ (1 glomerulus) domains occupy more posterior portions of the antennal lobes. One exception is the Or35a+ OSN class, which expresses an *IR* (*Ir76b*) in addition to the *OR* and *Orco*, and innervates the VC3 glomerulus (Fig 1E, striped glomerulus) (Benton et al., 2009; Couto et al., 2005; Fishilevich and Vosshall, 2005). Different OSN classes send their information to different glomeruli, and the specific combination of OSN classes and glomeruli that are activated by a given smell (usually a blend of different odorants) constitutes an olfactory 'code' which the fly

[1]The Solomon H. Snyder Department of Neuroscience, Center for Sensory Biology, Johns Hopkins University School of Medicine, Baltimore, MD 21205, USA, [2]Department of Biology, Stanford University, Stanford, CA 94305, USA, [3]Physiology & Neurobiology Department, Institute for Systems Genomics, and Connecticut Institute for the Brain and Cognitive Sciences, University of Connecticut, Mansfield, CT 06269, USA. [4]Mortimer B. Zuckermann Mind Brain Behavior Institute, Columbia University, New York, NY 10027, USA. [5]Present Address: The Department of Pathology and Laboratory Medicine, Giesel School of Medicine, Dartmouth-Hitchcock Medical Center, Lebanon, NH 03756, USA. ***Correspondence**: cpotter@jhmi.edu (CJP)

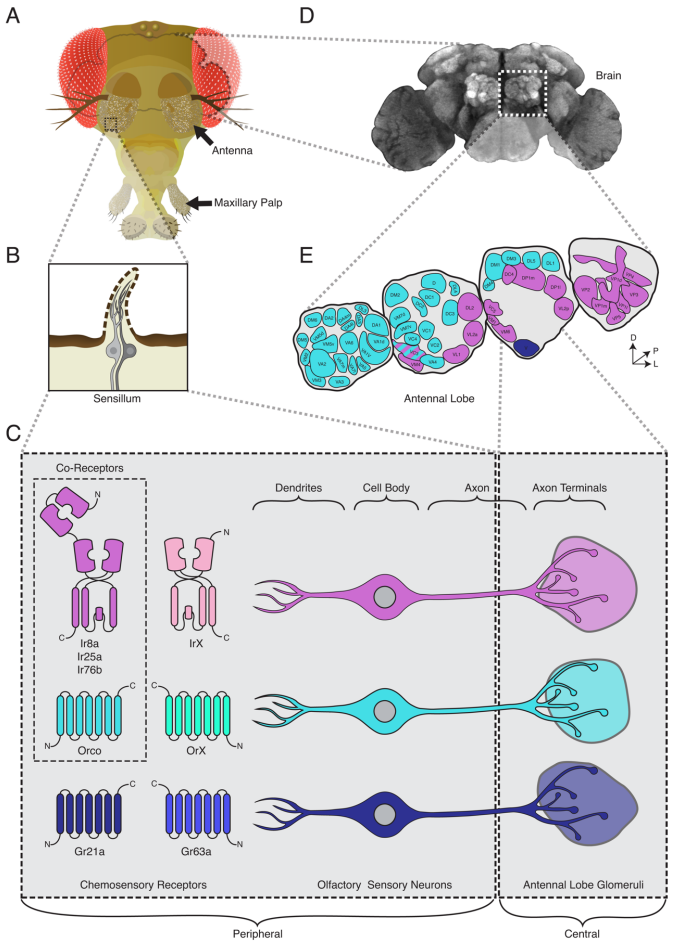

Figure 1. The standard view of odor coding in *Drosophila melanogaster.*
A. The adult fly head (left) has two olfactory organs: the antennae and the maxillary palps (arrows). Olfactory neurons from these organs project to the fly brain (D), to the first center involved in processing of olfactory information, the antennal lobes (E). **B.** The olfactory organs are covered by sensory hairs called sensilla (left). Each sensillum contains between one and four olfactory sensory neurons (two example neurons are shown in grey). The dendrites of these neurons extend into the sensilla, and the axons target discrete regions of the antennal lobes called glomeruli (E). Neuronal compartments (dendrites, cell body, axon, axon terminals) are labeled in (C). **C.** Left: in the periphery, each olfactory sensory neuron is traditionally thought to express chemosensory receptors from only one of three modalities on its dendrites: ionotropic receptors (IRs, pink and purple), odorant receptors (ORs, teal and green), or gustatory receptors (GRs, light and dark blue). IRs and ORs require obligate co-receptors (dotted box outline) to form functional ion channels. All ORs utilize a single co-receptor, Orco (teal), while IRs can utilize one (or a combination) of three possible co-receptors (purple): Ir8a, Ir25a, or Ir76b. The two GRs form a functional carbon dioxide detecting channel expressed in only one class of neurons. All other olfactory neurons express one of the four co-receptors. Right: olfactory sensory neurons expressing ORs, IRs, and GRs are thought to project to mutually exclusive glomeruli in the AL of the central brain, forming the olfactory map shown in (E). **D.** Fly brain stained with anti-nc82 synaptic marker, with left antennal lobe (AL) outlined by dotted white box. **E.** AL map with glomeruli color-coded by the chemosensory receptor modality (ORs, IRS, or GRs) expressed in the olfactory sensory neurons projecting to them. Only one glomerulus (VC3, striped) receives inputs from multimodal neurons. Compass: D = dorsal, L = lateral, P = posterior.

brain translates into an appropriate behavior (Grabe and Sachse, 2018; Haverkamp et al., 2018; Seki et al., 2017).

The receptors within each chemosensory modality form heteromeric ion channels (Abuin et al., 2011; Butterwick et al., 2018; Sato et al., 2008). The *ORs* require a single co-receptor, *Orco*, to function (Fig 1C, middle row) (Benton et al., 2006; Larsson et al., 2004; Vosshall and Hansson, 2011). The ligand binding *OrX* confers odorant specificity upon the neuron, while the co-receptor *Orco* is necessary for trafficking of the *OR* to the dendritic membrane and formation of a functional ion channel (Benton et al., 2006; Larsson et al., 2004). Likewise, the *IrXs* require one or more *IR* co-receptors: *Ir8a*, *Ir25a*, and/or *Ir76b* (Fig 1C, top row). The *IR* co-receptors are similarly required for trafficking and ion channel function (Abuin et al., 2011; Abuin et al., 2019; Ai et al., 2013). The *GR* gene family generally encodes receptors involved in taste typically expressed outside the olfactory system (such as in the labella or the legs) (Dunipace et al., 2001; Park and Kwon, 2011; Scott, 2018; Scott et al., 2001); however, *Gr21a* and *Gr63a* are expressed in one antennal OSN class, and form a complex sensitive to carbon dioxide (Fig 1C, bottom row) (Jones et al., 2007; Kwon et al., 2007).

The majority of OSNs have been mapped to their corresponding receptors, sensilla, and glomeruli in the fly brain (Bhalerao et al., 2003; Couto et al., 2005; Fishilevich and Vosshall, 2005; Frank et al., 2017; Grabe et al., 2016; Hallem and Carlson, 2006; Hallem et al., 2004; Knecht et al., 2017; Marin et al., 2020; Ray et al., 2008; Silbering et al., 2011). This detailed map has allowed for exquisite investigations into the developmental, molecular, electrophysiological, and circuit/computational bases of olfactory neurobiology. This work has relied on transgenic lines to identify and manipulate OSN classes (Ai et al., 2013; Brand and Perrimon, 1993; Couto et al., 2005; Fishilevich and Vosshall, 2005; Kwon et al., 2007; Lai and Lee, 2006; Larsson et al., 2004; Menuz et al., 2014; Potter et al., 2010; Silbering et al., 2011). These transgenic lines use segments of DNA upstream of the chemosensory genes that are assumed to reflect the enhancers and promoters driving expression of these genes. While a powerful tool, transgenic lines may not contain all of the necessary regulatory elements to faithfully recapitulate the expression patterns of the endogenous genes. Some transgenic lines label a subset of the cells of a given class, while others label additional cells: for example, the transgenic *Ir25a-Gal4* line is known to label only a portion of cells expressing Ir25a protein (as revealed by antibody staining) (Abuin et al., 2011); conversely, *Or67d-Gal4* transgenes incorrectly label two glomeruli, whereas a *Gal4* knock-in at the *Or67d* genetic locus labels a single glomerulus (Couto et al., 2005; Fishilevich and Vosshall, 2005; Kurtovic et al., 2007). While knock-ins provide a faithful method to capture a gene's expression pattern, generating these lines has traditionally been cumbersome.

In this paper, we present the implementation of a more efficient knock-in strategy. We use this strategy to target the four main chemosensory co-receptor genes in *Drosophila (Orco, Ir25a, Ir8a, Ir76b)*. Besides producing valuable reagents, these knock-ins reveal accurate co-receptor expression and enable genetic access to essentially all olfactory neurons in the fly. The new knock-in strategy is easy and highly effective. We further reveal that chemosensory co-receptors exhibit polymodal expression in overlapping subsets of olfactory neurons, challenging the current view of odor coding in *Drosophila melanogaster*. In particular, *Ir25a* is expressed in the majority of olfactory neurons, including most Orco+ olfactory neurons. Recordings in *Ir25a* mutant sensilla in Orco+ neurons reveal subtle, yet significant, changes in odor responses. These data suggest that olfactory neurons have the potential to be multimodal sensors and invite a re-examination of odor coding in *Drosophila*. A comprehensive model of co-receptor expression is presented, which will inform future investigations of polymodal chemosensory processing.

RESULTS

An Optimized Genetic Knock-In Strategy

We previously developed the HACK technique for CRISPR/Cas9 mediated homology directed repair (HDR) for *in vivo* gene conversion of various binary expression system components, such as the conversion of transgenic *Gal4* to *QF2* (Brand and Perrimon, 1993; Jinek et al., 2012; Lin and Potter, 2016a, b; Potter et al., 2010; Riabinina et al., 2015; Xie et al., 2018). The HACK strategy combines a targeting cassette (a genetic element for insertion and a selection marker flanked by homology arms) and guide RNA expression in a single plasmid (Lin and Potter, 2016a). Here, we adapt this strategy for the generation of gene targeted knock-ins. Specifically, we use HACK to insert a *T2A-QF2* cassette and RFP selection marker before the stop codon of multiple genes of interest (Fig 2A and Fig S1A-C). By introducing the T2A ribosomal skipping peptide, the knock-in will produce the full-length protein of the gene being targeted as well as a functional QF2 transcription factor (Fig 2A, Protein Products). This approach should capture the endogenous expression pattern of the gene under the control of the gene's native regulatory elements, while retaining the gene's normal function (Baena-Lopez et al., 2013; Bosch et al., 2020; Chen et al., 2020; Diao et al., 2015; Diao and White, 2012; Du et al., 2018; Gnerer et al., 2015; Gratz et al., 2014; Kanca et al., 2019; Lee et al., 2018; Li-Kroeger et al., 2018; Lin and Potter, 2016a; Vilain et al., 2014; Xue et al., 2014). We chose to target the four chemosensory co-receptor genes to examine the logic of odor coding in *Drosophila melanogaster*.

The HACK knock-in approach requires two components: a donor construct and Cas9 (Lin and Potter, 2016a). The donor includes *gRNAs* specific to the target gene, as well as the template for HDR-mediated insertion of *T2A-QF2* into the genome (Fig 2A, middle row). This template includes ~1kb homology arms directly up and downstream of the gene's stop codon flanking a cassette containing *T2A-QF2* and a *3XP3-RFP* fluorescent eye marker (Fig S2A-C). Outside of these homology arms, the construct has two *RNA polymerase III U6* promoters driving independent expression of two *gRNAs* specific to the region around the target gene's stop codon (Port et al., 2014). Two *gRNAs* were used to increase the probability of successfully inducing double stranded breaks (DSBs) in the target (Port et al., 2014). The knock-in construct replaces the target gene's stop codon (Fig 2A, bottom row), and introduces a transcriptional stop at the end of *QF2*. Additional details describing knock-in generation can be found in Methods.

To investigate the effect of *T2A-QF2* knock-in on gene function, we performed single sensillum recordings (SSR) on *Orco-T2A-QF2^{HACK}* and *Ir8a-T2A-QF2^{HACK}* knock-in flies, comparing their responses to *wildtype* flies to panels of Orco- and Ir8a-dependent odorants (Fig S3) (Abuin et al., 2011; de Bruyne et al., 2001; Lin and Potter, 2015). In ab2 basiconic sensilla, *Orco-T2A-QF2^{HACK}* knock-in flies had slightly lower baseline activity as compared to *wildtype* (Fig S3A); however, there were no significant differences in odor-evoked activity between these two genotypes across all stimuli tested (Fig S3B). In ac2 coeloconic sensilla, responses of *Ir8a-T2A-QF2^{HACK}* knock-in flies to Ir8a-dependent odorants (Abuin et al., 2011) were similar to *wildtype* controls (example trace in Fig S3C, quantification in Fig S3D). See Supplemental Data 2 and Methods for additional details.

Polymodal Expression of Orco

We examined the expression of *Orco-T2A-QF2^{HACK}* by crossing it to a *QUAS-GFP* reporter. GFP expression was detected in the adult antennae and maxillary palps (Fig 2B), as previously described (Larsson et al., 2004). No GFP expression was detected in the adult ventral nerve cord (Fig S4A, top row). In the larva, GFP expression was detected in the

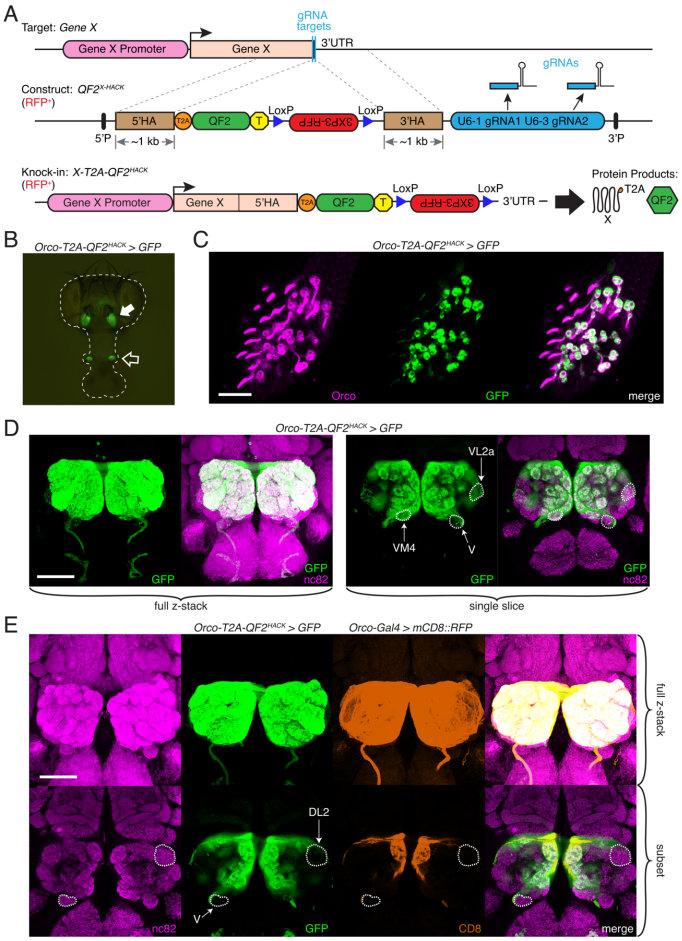

Figure 2. Knock-in of *T2A-QF2* at the *Orco* genetic locus reveals expanded polymodal chemosensory expression.

A. Schematic of HACK knock-in technique. Top: two double-stranded breaks are induced on either side of the target gene stop codon with gRNAs (blue) expressed from the *QF2$^{X\text{-}HACK}$* construct (middle) in the presence of Cas9 (see Fig S1). The construct includes *T2A-QF2* and a floxed *3XP3-RFP* marker. The knock-in introduces a transcriptional stop (yellow T) after QF2. Bottom: the knock-in produces two protein products (right) from the targeted mRNA: target X protein and the *QF2* transcription factor[32]. The *X-T2A-QF2^{HACK}* knock-in line can be crossed to a reporter line (e.g. *QUAS-GFP*) to examine the endogenous expression pattern of the target gene. **B.** The HACK technique was used to generate an *Orco-T2A-QF2^{HACK}* knock-in line. In the fly head, the knock-in drives GFP expression in the antennae (filled arrow) and maxillary palps (hollow arrow), as previously reported[81]. **C.** Anti-Orco antibody staining in palp labeled by *Orco-T2A-QF2^{HACK}* knock-in (see Table S2). The cytoplasmic *GFP* reporter primarily labels cell bodies, while the Orco antibody labels cell bodies and dendrites. Scale bar = 25 µm. N = 3. **D.** *Orco-T2A-QF2^{HACK}* driven GFP expression in the antennal lobes. The knock-in weakly labels additional glomeruli associated with other chemosensory modalities, including VM4 (Ir76b+ neurons), V (Gr21a+/Gr63a+ neurons), and VL2a (Ir8a+ neurons). In the single slice, gain has been increased in the GFP channel to visualize weakly labeled glomeruli. The nc82 antibody labels synapses (magenta) and is used as a brain counterstain in this and subsequent brain images. N = 5. **E.** Co-labeling experiments of transgenic *Orco-Gal4* driving *UAS-mCD8::RFP* (anti-CD8, orange) and the *Orco-T2A-QF2^{HACK}* knock-in driving GFP. The *Orco-Gal4* line labels most, but not all, glomeruli labeled by the knock-in. Top: maximum intensity projection of full z-stack. Bottom: subset of the z-stack (projection of three consecutive slices) showing two glomeruli sparsely labeled by the knock-in but not labeled by the transgenic *Gal4* line: the V (Gr21a/Gr63+) and DL2 (Ir8a+) glomeruli. N = 3. Scale bars in (D) and (E) are 50 µm. See also Fig S1-S5, Tables S1 and S2, and Suppl Data 1.

larval olfactory dorsal organs (Fig S4B, top row) (Larsson et al., 2004). No obvious GFP expression was detected outside of these olfactory organs in the larva or adult; however, we did not examine sperm expression (*Orco* expression has previously been reported in insect sperm) (Dubey et al., 2016; Pitts et al., 2014). All subsequent analyses focused on the adult olfactory system.

To validate the *Orco-T2A-QF2^{HACK}* knock-in line, we performed whole-mount antibody staining of *Drosophila* maxillary palps (Fig 2C). We found a high degree of correspondence between anti-Orco antibody staining and knock-in driven GFP in palpal olfactory neurons, with 96% of all cells being double labeled, suggesting the knock-in faithfully recapitulates the endogenous expression pattern (Table S2). The few cells not co-labeled may be due to either issues of antibody penetration or weak GFP signal in some cells. The GFP reporter is cytoplasmic and thus strongly labels cell bodies (Shearin et al., 2014), while the antibody labels both cell bodies and dendrites, reflecting the distribution of Orco protein.

In the brain, an initial examination of *Orco-T2A-QF2^{HACK}* driven GFP expression suggested the knock-in recapitulated the known expression pattern (Fig 2D, left two panels). However, closer examination revealed several additional glomeruli previously not thought to belong to the *Orco* expression domain. These include VM4, which is strongly labeled (Fig 2D, medial dotted outline), and receives inputs from Ir76b+ olfactory neurons; the V glomerulus (Fig 2D and E, ventral dotted outlines), which receives inputs from the Gr21a+/Gr63a+ olfactory neurons, and is very sparsely labeled by the knock-in; and VL2a (Fig 2D, lateral dotted outline), which is labeled more weakly than VM4 but more strongly than V, and receives inputs from Ir8a+ olfactory neurons. We further observed weak *Orco-T2A-QF2^{HACK}* innervation in DP1l (Ir8a+), DL2 (Ir8a+) (Fig 2E, dorsal dotted outline), and VL1 (Ir25a+) (See Supplemental Data 6). Occasionally, the DC4 glomerulus (Ir8a+) was also innervated (see Fig 1B, right, for the previously reported Orco+ expression pattern in teal). This suggests that *Orco* overlaps with all other known chemosensory receptor modalities (at least within a population of these olfactory neurons). This result was unexpected, and we examined if this expanded expression pattern may have been overlooked in a previously established transgenic *Orco-Gal4* line (Larsson et al., 2004). We performed co-labeling experiments in the brain, with *Orco-T2A-QF2^{HACK}* driving GFP expression, and transgenic *Orco-Gal4* driving mCD8::RFP expression (Fig 2E; see also Supplemental Data 4). While the expression patterns look similar, they are not identical. The inset shows an example glomerulus, VM4, which appears to be labeled by the knock-in but not the transgenic *Gal4* line. The reporter alone controls are shown in Fig S2F (these reporters were used for all knock-in and co-labeling experiments shown in Fig 3 – 5). Further examination of the *Orco-Gal4* line with a strong GFP reporter (Shearin et al., 2014) (Fig S5, top row) revealed that, surprisingly, even the transgenic line drives weak expression in VL2a (lateral dotted outline) and VM4 (medial dotted outline) glomeruli, which was not previously reported. However, the *Orco-Gal4* line appears to be missing expression in DL2, V, and VL1 glomeruli. In total, the *Orco-T2A-QF2^{HACK}* knock-in consistently labels 6 additional glomeruli (and one sporadically), expanding the known olfactory neurons expressing this co-receptor.

Expanded Expression of Ir8a and Identification of a New Glomerulus

We next examined expression of the *Ir8a-T2A-QF2^{HACK}* knock-in line. Unlike *Orco*, *Ir8a* expression had previously been localized only to the antenna, in olfactory neurons found in coeloconic sensilla and in the sacculus. The knock-in line drove GFP expression only in the antenna (Fig 3A). There was no obvious expression in the larval stage (Fig S4B, second row); thus we focused on *Ir8a-T2A-QF2^{HACK}* characterization in the adult.

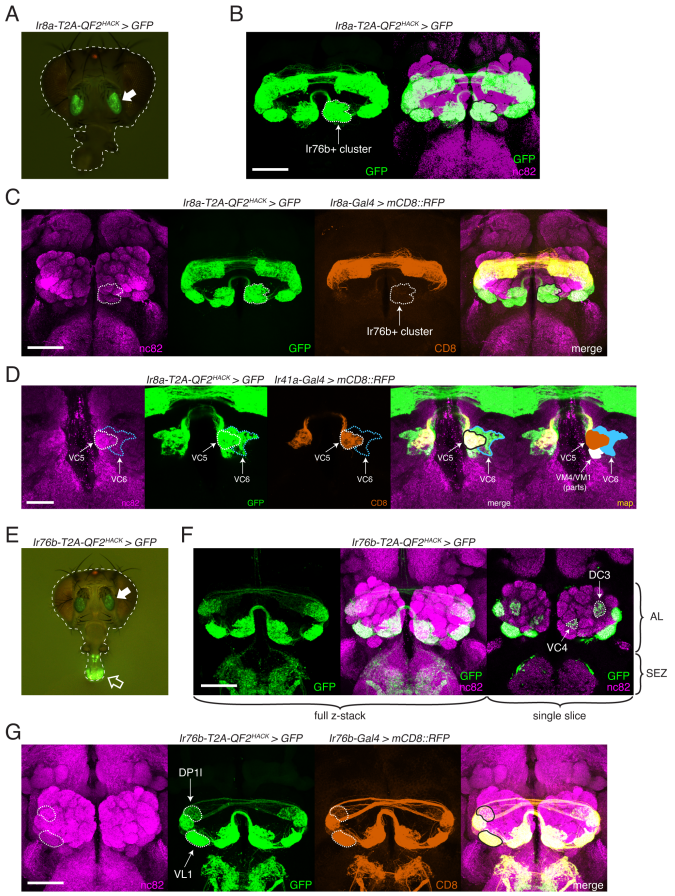

Figure 3. The *Ir8a-T2A-QF2^{HACK}* and *Ir76b-T2A-QF2^{HACK}* knock-ins reveal broader expression in antennal olfactory neurons.
A. In the fly head, the *Ir8a-T2A-QF2^{HACK}* knock-in drives GFP expression only in the antennae (arrow), as previously reported[1]. **B.** The *Ir8a-T2A-QF2^{HACK}* knock-in drives GFP expression in additional glomeruli from those previously reported, including a cluster of Ir76b+ glomeruli (dotted outline). N = 7 (3 male, 4 female). **C.** Co-labeling experiments of the *Ir8a-T2A-QF2^{HACK}* knock-in driving GFP and a transgenic *Ir8a-Gal4* line driving *UAS-mCD8::RFP* (anti-CD8, orange) reveal that the *Gal4* line similarly labels the Ir76b+ cluster, albeit weakly. Additional differences between expression in the knock-in and transgenic lines are detailed in Fig S5 and Suppl Data 1. N = 3. **D.** Co-labeling experiments with *Ir41a-Gal4* driving mCD8::RFP (orange) show the *Ir8a-T2A-QF2^{HACK}* knock-in labels the VC5 glomerulus (white dotted outline), and also a previously unidentified glomerulus lateral and posterior to VC5 (blue dotted outline). The new glomerulus has been named VC6. The right panel shows a superimposed antennal lobe map of this region, with the VC5 glomerulus filled in orange, the VC6 glomerulus filled in blue, and portions of two additional neighboring glomeruli (VM1 and VM4) colored white. **E.** Image of a fly head. *Ir76b-T2A-QF2^{HACK}* knock-in drives GFP expression in the antennae (filled arrow) and labella (hollow arrow), reflecting the known roles of this co-receptor in olfaction and gustation, respectively[10, 146]. **F.** In the brain, *Ir76b-T2A-QF2^{HACK} > GFP* olfactory neurons innervate the antennal lobes (AL), while gustatory neurons from the labella innervate the subesophageal zone (SEZ). The *Ir76b-T2A-QF2^{HACK}* knock-in labels several Orco+ glomeruli not previously reported, such as DC3 and VC4. In the single slice, gain has been increased in the GFP channel to visualize weakly labeled glomeruli. N = 7 (2 male, 5 female). **G.** Co-labeling experiments comparing expression in the *Ir76b-T2A-QF2^{HACK}* knock-in driving GFP to a transgenic *Ir76b-Gal4* line driving mCD8::RFP (orange) reveal both lines label more glomeruli than previously reported, including VL1 (Ir25a+) and DP1l (Ir8a+). The *Ir76b-Gal4* line labels additional glomeruli compared to the knock-in and lacks expression in several glomeruli labeled by the knock-in (see Fig S5 and Suppl Data 1). N = 4.

(legend continued on next page)

As with the *Orco-T2A-QF2^{HACK}* knock-in, examination of *Ir8a-T2A-QF2^{HACK} > GFP* expression in the adult antennal lobes revealed robust labeling of glomeruli not previously reported as Ir8a+ (Fig 3B; see also Supplemental Data 4). Interestingly, most of these additional glomeruli belong to a cluster innervated by Ir76b+ neurons (Fig 3B, dotted outline) (Silbering et al., 2011), suggesting that all three IR co-receptors are expressed in these olfactory neurons. This cluster includes four glomeruli: VM1, VM4, VC3, and VC5. Comparing the expression of the knock-in to the Benton lab's transgenic *Ir8a-Gal4* line (Fig 3C, orange) (Abuin et al., 2011), we found that this same cluster was also labeled by the *Gal4* line (dotted outline), but was previously missed because the expression was weak. However, when this transgenic line is examined with a stronger reporter (Shearin et al., 2014) (Fig S5, second row), the Ir76b+ cluster is clearly labeled (large, medial dotted outline). In addition, we found the VL1 glomerulus (Ir25a+) to be labeled by both the knock-in and the *Ir8a-Gal4* line. The knock-in also consistently but weakly labels one Orco+ glomerulus (VA3), and sporadically labels another Ir25a+ glomerulus (VM6), neither of which were observed in the transgenic *Ir8a-Gal4* line (See Supplemental Data 6). The expression pattern of the knock-in appears to more closely resemble a different transgenic *Ir8a-Gal4* line generated by the Suh group (Ai et al., 2013).

The *Ir8a-T2A-QF2^{HACK}* knock-in strongly labels a previously undescribed postero-central glomerulus. By performing a co-labeling experiment with *Ir41a-Gal4*, which labels the VC5 glomerulus (part of the Ir76b+ cluster identified above), we narrowed down the anatomical location of the new glomerulus and ruled out VC5 as the target of these axons (Fig 3D). While the *Ir8a-T2A-QF2^{HACK}* knock-in clearly labels VC5 (white dotted outline), it also labels a new glomerulus that is lateral and slightly posterior to VC5 (blue dotted outline). This glomerulus is dorsal and posterior to VM1 and VM4 (portions of which can be seen in the map in Fig 3D, right panel), and appears to fill in the antennal lobe space between the VC5, VM6, VP2, and VP1m glomeruli. Based on its anatomical location, we named this new glomerulus VC6, or ventro-central glomerulus 6. Taking this new glomerulus into account, *Ir8a-T2A-QF2^{HACK}* labels 13 glomeruli consistently (and one sporadically). While it was previously reported that an *Ir8a-Gal4* transgenic line may label up to 10 glomeruli, only 6 of these were formally identified (Silbering et al., 2011).

Polymodal Expression of Ir76b in the Antenna

In contrast to *Orco* and *Ir8a*, *Ir76b* has previously been implicated in both olfaction and gustation and has been shown to be expressed in adult fly antennae, labella (mouthparts), legs, and wings (Abuin et al., 2011; Chen and Amrein, 2017; Croset et al., 2010; Ganguly et al., 2017; Hussain et al., 2016; Sanchez-Alcaniz et al., 2018; Zhang et al., 2013). We examined the *Ir76b-T2A-QF2^{HACK}* knock-in line and found a similar pattern of expression in the periphery, with GFP expression in the antennae and labella (Fig 3E, filled and hollow arrows, respectively), and neuronal innervations in the ventral nerve cord or VNC (the fly spinal cord equivalent) corresponding to axons originating from the legs and wings (Fig S4A, third row). We also detected broad expression in the larva, both in the head and throughout the body wall (Fig S4B, third row).

In the adult brain, the GFP+ neurons from the antennae project to the antennal lobes (AL), and GFP+ neurons from the labella project to the subesophageal zone (SEZ) (Fig 3F) (Hussain et al., 2016; Zhang et al., 2013). However, as with the *Orco* and *Ir8a* knock-in lines, the *Ir76b-T2A-QF2^{HACK}* knock-in labels more glomeruli than previously described. In addition to the four previously reported Ir76b+ glomeruli (VM1, VM4, VC3, VC5), the *Ir76b-T2A-QF2^{HACK}* knock-in labels several Orco+ glomeruli, such as DC3 (Fig 3F, right panel, lateral dotted outline) and VC4 (Fig 3F, medial dotted outline). We also detected weak expression in three anterior Orco+ glomeruli (VA3, VA5, and VA6), one posterior Orco+ glomerulus (DL1), as well as variable expression (defined as found in less than 50% of brains examined) in two anterior Orco+ glomeruli (VA7m and DA1). The *Ir76b-T2A-QF2^{HACK}* knock-in labels four Ir8a+ glomeruli (DP1m, DP1l, VL2a, and VL2p), and an additional Ir25a+ glomerulus (VL1). In total, the *Ir76b-T2A-QF2^{HACK}* knock-in labels 15 glomeruli consistently (and two sporadically), which is approximately four times more glomeruli than previously reported (Silbering et al., 2011) (See Supplemental Data 6 for examples of all new glomerular innervation). Interestingly, we found the *Ir76b-T2A-QF2^{HACK}* knock-in does not label the newly identified VC6 glomerulus, even though it labels the neighboring VC5 glomerulus.

We performed co-labeling experiments to compare the antennal lobe expression of the *Ir76b-T2A-QF2^{HACK}* knock-in (Fig 3G, green) to a transgenic *Ir76b-Gal4* line (orange). Surprisingly, most of the additional glomeruli identified above can be found in the *Ir76b-Gal4* line, including VL1 (Ir25a+, ventral dotted outline) and DP1l (Ir8a+, dorsal dotted outline), as well as VL2a (Fig S5, third row). However, the *Gal4* transgene appears to be missing the VA5 and DC3 Orco+ glomeruli (see Supplemental Data 4). Furthermore, the *Ir76b-Gal4* line labels additional glomeruli not seen in the knock-in (Fig S5, third row, Orco+ cluster). Thus, of the transgenic *Gal4* lines examined, *Ir76b-Gal4* appears the least accurate.

Broad Ir25a Expression Across Olfactory Organs

Ir25a has been implicated in a broad array of cellular and sensory functions, from olfaction (Abuin et al., 2011; Benton et al., 2009; Silbering et al., 2011) and gustation (Chen and Amrein, 2017; Chen and Dahanukar, 2017; Jaeger et al., 2018), to thermo- and hygro-sensation (Budelli et al., 2019; Enjin et al., 2016; Knecht et al., 2017; Knecht et al., 2016), to circadian rhythm modulation (Chen et al., 2015). In the adult olfactory system, *Ir25a* expression has previously been reported in three types of structures in the antenna: coeloconic sensilla, the arista, and the sacculus (Abuin et al., 2011; Benton et al., 2009). We examined the *Ir25a-T2A-QF2^{HACK}* knock-in line, and found GFP expression in the adult VNC (Fig S4A, fourth row), broad expression in the larva (Fig S4B, fourth row), and expression in the adult antennae and labella (Fig 4A, filled and hollow arrows, respectively). GFP expression was also detected in the maxillary palps (Fig 4A, arrowhead), which have not previously been reported to express *Ir25a*. The maxillary palps are considered a simple olfactory organ, possessing only one type of olfactory sensillum (basiconic), and six classes of olfactory neurons, all of which express *Orco* and *ORs* (Couto et al., 2005; de Bruyne et al., 1999; Fishilevich and Vosshall, 2005). Until now, no *IR* receptor expression has previously been reported in the palps.

In the adult brain, the *Ir25a-T2A-QF2^{HACK}* knock-in drives GFP expression in the SEZ, and broadly in the ALs. Many Orco+ glomeruli are labeled, as shown in Fig 4B. These glomeruli appear to correspond to Orco+ neurons not just from the maxillary palps, but also from the antennae, suggesting broad co-expression of these two chemosensory receptor modalities. To confirm this, we performed anti-Orco antibody staining on antennal cryosections in *Ir25a-T2A-QF2^{HACK} > GFP* animals and found examples of Orco+ GFP+ double-labeled cells (Fig 4C, insets). We next verified Ir25a protein expression in the maxillary palps. We performed whole-mount anti-Ir25a antibody staining

For clarity, all single channel outlines in (B-D) and (G) are white or blue dotted lines, while the composite image outlines are black or blue solid lines, respectively. Brain images are max intensity projections of full z-stacks, except the right panel in (F). All brain scale bars are 50 µm, apart from (D), which is 25 µm. In (A) and (E), the *3XP3-RFP* knock-in marker can be weakly detected in the eyes and ocelli of both the *Ir8a-T2A-QF2^{HACK}* and *Ir76b-T2A-QF2^{HACK}* knock-in lines. See also Fig S4 and S5.

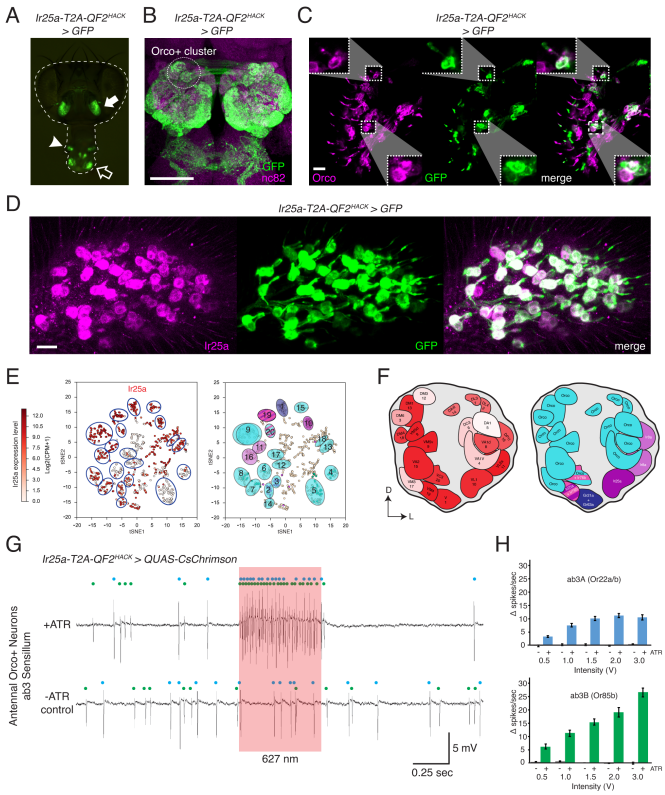

Figure 4. *Ir25a-T2A-QF2^{HACK}* reveals broad co-receptor expression in the fly olfactory system.

A. In the fly head, the *Ir25a-T2A-QF2^{HACK}* knock-in drives GFP expression in the antennae (filled arrow) and labella (hollow arrow), which has been reported previously[10, 26]. Expression in the maxillary palps (arrowhead) has not been previously reported. **B.** In the brain, the *Ir25a-T2A-QF2^{HACK}* knock-in drives GFP expression broadly in the ALs and SEZ. Ir25a+ neurons innervate many Orco+ glomeruli, such as those in the dotted circle. See Suppl Data 1. N = 15 (9 male, 6 female). Scale bar = 50 µm. **C.** Anti-Orco antibody staining in cryosections of *Ir25a-T2A-QF2^{HACK} > GFP* antennae. Double labeled cells (Orco+ and GFP+) are highlighted in magnified insets. Scale bar = 10 µm. **D.** Whole-mount maxillary palp staining with anti-Ir25a antibody in *Ir25a-T2A-QF2^{HACK} > GFP* flies. The knock-in and Ir25a antibody co-label the majority of olfactory neurons in the palps (see Table S3). Scale bar = 10 µm. N = 5. **E.** scRNAseq dataset from pupal antennae[84] reveals *Ir25a* expression in many olfactory neuron clusters that map to Orco+, GR+, or Ir8a+ glomeruli. tSNE plots show *Ir25a* expression in 20 decoded antennal OSN clusters mapped to 21 glomeruli. Transcriptomic clusters are numbered 1 – 20 in the right plot, and color-coded according to chemosensory receptor modality, as in (F). Cluster 9 maps on to two adjacent glomeruli: VM5d and VM5v. **F.** Antennal lobe maps summarizing *Ir25a* expression by OSN class and glomerular target. Glomerular names and cluster numbers are indicated in the left map, while standard chemosensory modalities are indicated in the right map (teal = *Orco*, pink = *Ir76b*, light purple = *Ir8a*, dark purple = *Ir25a*, dark blue = *Gr21a* + *Gr63a*). *Ir76b* does not have unique glomeruli but overlaps with either *Orco* or *Ir25a* (indicated by striped fill). In the left map, opacity of the red fill indicates the proportion of cells in that cluster expressing *Ir25a*, as seen in (E). See also Suppl Data 3. Compass: D = dorsal, L = lateral**. G.** Verification of *Ir25a* expression in antennal ab3 sensilla using optogenetics. Single sensillum recordings (SSR) from ab3 Orco+ neurons in *Ir25a-T2A-QF2^{HACK} > QUAS-CsChrimson* flies. Representative traces from ab3 using 1.5V of 627 nm LED light (red box) to activate *CsChrimson*. Bottom trace is control animal not fed the required all-trans retinal cofactor (-ATR). Spikes from ab3A and ab3B neurons are indicated by blue and green dots, respectively. **H.** Quantification of neuronal activity in response to light at various LED intensities (N = 7 – 12). These experiments support *Ir25a* expression in both ab3A (*Or22a/b*, top) and ab3B neurons (*Or85b*, bottom). See also Fig S4-S6, Table S3, and Suppl Data 2 and 3.

in *Ir25a-T2A-QF2^{HACK} > GFP* palps and found broad *Ir25a* expression in palpal olfactory neurons (Fig 4D). Quantification of co-expression of Ir25a and GFP revealed a high degree of overlap (98%; Table S3).

In comparison to the palp, the antenna is a more complex olfactory organ: it has more than ten times the number of olfactory neurons, four times the number of sensillar types (and multiple subtypes), and expresses over 50 different ORs, IRs, or GRs (Couto et al., 2005; de Bruyne et al., 2001; Dobritsa et al., 2003; Fishilevich and Vosshall, 2005; Silbering et al., 2011). It is therefore more challenging to examine *Ir25a* co-expression in the antennae in a comprehensive, quantifiable, and unbiased way using antibody staining. Instead, we analyzed a previously published single cell RNAseq (scRNAseq) dataset from pupal antennae (Li et al., 2020) to investigate *Ir25a* expression in various olfactory sensory neuron (OSN) classes in greater detail. This dataset mapped 20 transcriptomic clusters (Fig 4E, right tSNE plot) to 21 glomerular targets in the brain (Fig 4F, right AL map). These OSN classes include Ir25a+ neurons (VL1 glomerulus); Ir76b+ neurons (VC3 and VM4); Ir8a+ neurons (VL2a and DP1l); Gr21a/Gr63a+ neurons (V); and multiple classes of Orco+ neurons (such as DM1, DC3, DL3, VA1d, among others). These clusters also include example OSN classes from all types of sensilla (basiconic, intermediate, trichoid, and coeloconic). Fig 4E shows the expression level in red of *Ir25a* in these clusters, which is mapped onto the respective glomeruli in Fig 4F (left). The proportion of cells in each cluster expressing *Ir25a* is indicated by the opacity of the red fill in the corresponding glomeruli in the left AL map in Fig 4F. The scRNAseq analysis reveals *Ir25a* expression in 62% of OSNs, or about 630 of 1,016 neurons, at this developmental timepoint (42 – 48 h after puparium formation or APF) (CPM threshold ≥ 7; see Methods and Supplemental Data 3). These results are also consistent with a recent single-nucleus RNAseq study performed on adult *Drosophila* antennae (McLaughlin et al., 2020). Cluster analysis of the pupal scRNAseq data reveals broad Ir25a+ expression in previously unreported chemosensory receptor clusters, such as cluster 1 (V glomerulus, GR+, 97.3% of cells) and cluster 15 (VA2 glomerulus, Orco+, 96.2% of cells), and sparse to no expression in others, such as cluster 12 (DM3, Orco+, 11.1% of cells) (see Supplemental Data 3 for cell counts for all clusters). The scRNAseq dataset also confirms *Ir25a* expression in some basiconic, intermediate, and trichoid sensilla (all sensillar types previously considered *IR* negative).

To examine *Ir25a* expression in OSN classes not included in the scRNAseq dataset (such as Or22a/b+ neurons in ab3 sensilla, innervating the DM2 glomerulus), we employed an optogenetic approach. We used the *Ir25a-T2A-QF2^{HACK}* knock-in to drive expression of *QUAS-CsChrimson*, a red-shifted channelrhodopsin (Klapoetke et al., 2014), and performed SSR from sensilla previously known to house only Orco+ neurons. If these neurons do express *Ir25a*, then stimulation with red light should induce neuronal firing. We recorded from ab3 sensilla, which have two olfactory neurons (A and B; indicated with blue and green dots, respectively, in Fig 4G). Both neurons responded to pulses of 627 nm light at various intensities in a dose-dependent manner (example trace in Fig 4G, quantification in Fig 4H), confirming *Ir25a* expression in these neurons. No light-induced responses were found in control flies not fed all-trans retinal (-ATR), a necessary co-factor for channelrhodopsin function (see Methods). We used similar optogenetic experiments to examine *Ir25a* expression in OSN classes in which glomerular innervation by the knock-in was ambiguous, including the DM5 (ab2B, Or85a/Or33b+) and D glomeruli (ab9A, Or69aA/aB+) (Fig S6). These experiments confirmed that *Ir25a* is expressed in ab2A neurons (Or59b+, DM4; also seen with scRNAseq), but indicated that *Ir25a* is not expressed in ab2B neurons (Or85a/Or33b+, DM5; not in scRNAseq dataset) (Fig S6A and B). Furthermore, we found that *Ir25a* is expressed in ab9B (Or67b+, VA3; not in scRNAseq dataset), but not

in ab9A (Or69aA/aB+, D glomerulus; not in scRNAseq dataset) (Fig S6C and D; see also Supplemental Data 2).

Given the broad expression pattern revealed by the *Ir25a-T2A-QF2^{HACK}* knock-in, we wondered whether some of these additional glomeruli had been missed in the original *Ir25a-Gal4* transgenic line, perhaps due to weak expression and reporter limitations. When crossed to a strong reporter (Shearin et al., 2014), the *Ir25a-Gal4* line does label a few Orco+ glomeruli (Fig S5, fourth row); however, its expression is much narrower than the knock-in, as revealed by co-labeling experiments (Fig 5A, top row). This transgenic line was originally reported to label only a subset of Ir25a+ neurons, as evidenced by a comparison of the *Ir25a-Gal4* line to anti-Ir25a antibody staining; however, it was assumed that neurons not captured by the transgenic line would reside in coeloconic sensilla (or perhaps the arista or sacculus), the original locations for all IR+ OSNs. This was found in some cases, such as Ir64a+ neurons (DP1m, Fig S5A, second row), which reside in the sacculus and express the *Ir8a* co-receptor. In total, six Ir8a+ glomeruli/OSN classes were labeled by the *Ir25a-T2A-QF2^{HACK}* knock-in: five strongly (DP1m, DP1l, DL2, VL2a, VL2p) and one weakly (DC4). These data indicate that all olfactory neuron classes expressing *IRs* also express *Ir25a* to some degree (see Supplemental Data 4). Furthermore, as is the case with *Orco*, the *Ir25a* knock-in overlaps to some extent with all other chemosensory receptor modalities, including the GR+ olfactory neurons (as mentioned previously), all Ir76b+ neurons, and up to 33 classes of the Orco+ OSNs previously thought to express only Orco (31 glomeruli labeled consistently, 2 glomeruli labeled sporadically; for full list of glomeruli, see Supplemental Data 4; for example images of all new glomeruli innervated by this knock-in line, see Supplemental Data 6). These Orco+ OSNs include as many as 27 antennal populations, and all six OSN classes in the maxillary palps (one example is shown in Fig 5A, bottom row). The palpal glomeruli are all labeled either strongly or intermediately. Finally, the *Ir25a-T2A-QF2^{HACK}* knock-in also labels the new VC6 glomerulus (Fig 5B, blue outline) identified in the *Ir8a* knock-in line. The right panel in Fig 5B shows a superimposed antennal lobe map of this region, to illustrate the glomeruli that border the VC6 glomerulus: VC6 (blue fill) is bounded by VC5 medially (orange fill), VM6 ventrally (white fill), and VP1m laterally (white fill). The VP2 glomerulus, which can be found posterior to VC6, is not visible at this z position.

Table S4 summarizes the chemosensory receptor expression patterns for all four knock-in lines across all OSNs, sensillar types, and glomeruli. The *Orco-T2A-QF2^{HACK}* knock-in consistently labels 44 glomeruli (6 more than previously reported); the *Ir8a-T2A-QF2^{HACK}* knock-in consistently labels 13 glomeruli (7 more than previously identified); the *Ir76b-T2A-QF2^{HACK}* knock-in consistently labels 15 glomeruli (11 more than previously identified); and the *Ir25a-T2A-QF2^{HACK}* knock-in consistently labels 51 glomeruli (39 more than previously identified).

Multimodal Contributions to Olfactory Neuron Physiology

How might the broad, combinatorial co-expression of various chemosensory modalities affect olfactory neuron function? One way to begin to address this question is to examine olfactory responses in neuronal populations co-expressing just two of the four chemosensory receptor modalities (*Orco* and *Ir25a*). We chose to test eight OSN classes that have strong or intermediate *Ir25a* expression previously assigned only to the Orco+ sensory modality– two in the antennae, and six in the maxillary palps. The two antennal OSN classes are found in the same ab3 sensillum (ab3A, Or22a/b+, DM2 glomerulus; and ab3B, Or85b+, VM5d glomerulus). The six palpal OSN classes represent the entire olfactory neuron population of the maxillary palps (pb1A, Or42a+, VM7d; pb1B, Or71a+, VC2; pb2A, Or33c/Or85e+, VC1; pb2B, Or46a+, VA7l; pb3A,

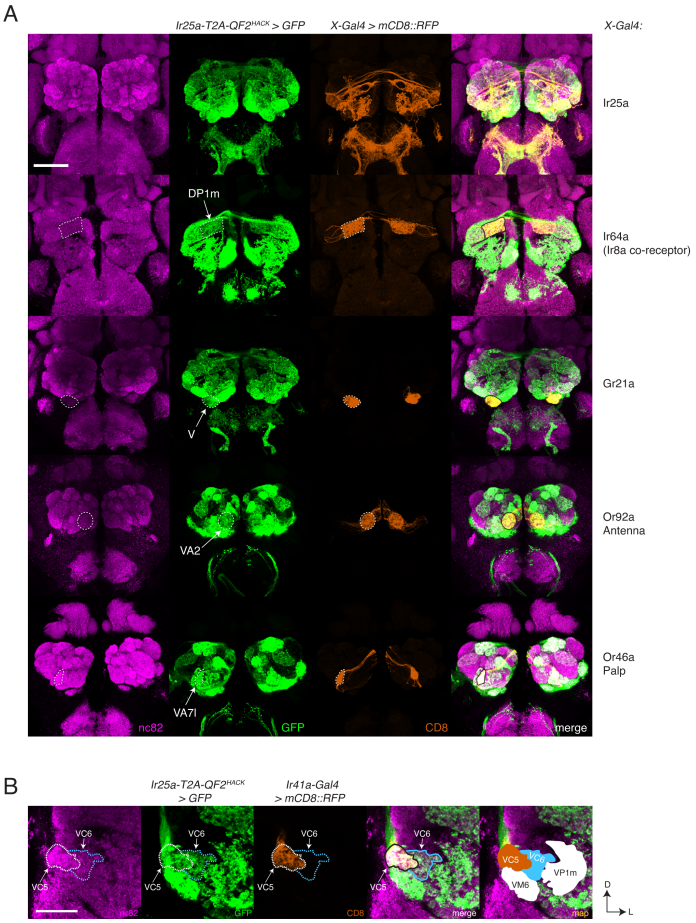

Figure 5. Polymodal expression of *Ir25a-T2A-QF2^{HACK}*.
A. Co-labeling experiments with various transgenic *Gal4* lines driving mCD8::RFP (orange) in the *Ir25a-T2A-QF2^{HACK}* knock-in driving GFP (green). The *Ir25a-Gal4* transgenic line (top row) labels a subset of the *Ir25a-T2A-QF2^{HACK}* knock-in expression pattern. The *Ir25a-T2A-QF2^{HACK}* knock-in labels neurons from all other chemosensory receptor modalities, including other *IRs* (such as *Ir64a*, DP1m glomerulus, previously reported as only expressing the *Ir8a* co-receptor; second row), *Gr21a/Gr63a* (V glomerulus; third row), and *ORs* from both the antennae (*Or92a*, VA2 glomerulus; fourth row) and maxillary palps (*Or46a*, VA7l glomerulus; bottom row). Top row shows maximum intensity projection of z-stack; all other images are from single slices. N = 3 – 10 flies per co-label experiment. Scale bar = 50 µm. **B.** High magnification image of portion of left antennal lobe. The new VC6 glomerulus labeled by the *Ir8a-T2A-QF2^{HACK}* knock-in (Fig 3D) is also labeled by the *Ir25a-T2A-QF2^{HACK}* knock-in. Co-labeling experiment with *Ir41a-Gal4 > mCD8::RFP* (orange) and *Ir25a-T2A-QF2^{HACK}* knock-in driving GFP (green) confirms that the knock-in innervates both VC5 (white dotted outline) and VC6 (blue outline). The right panel shows a superimposed antennal lobe map of this region, with the VC5 glomerulus (orange), VC6 glomerulus (blue), and two additional neighboring Ir25a+ glomeruli (VM6 and VP1m; white). Scale bar = 25 µm. Compass: D = dorsal, L = lateral. In (A) and (B), single channel outlines are white or blue dotted lines, while composite image outlines are black or blue solid lines, respectively.

Or59c+, VM7v; pb3B, Or85d+, VA4). In both the antennae and the palps, we compared the olfactory responses of OSNs to a panel of 13 odorants in three genotypes: *wildtype*, *Ir25a^{2}* mutant, and *Orco^{2}* mutant flies. This panel included odorants typically detected by *ORs*, such as esters and aromatics, and odorants typically detected by *IRs*, such as acids and amines (Silbering et al., 2011). In the previously accepted view of olfaction in *Drosophila*, Orco+ neurons express only Orco/OrX complexes, and all olfactory responses in the neurons can be attributed to these complexes. Thus, in an *Ir25a^{2}* mutant background, there should be

no difference in olfactory responses from *wildtype* if either a) *Ir25a* is not expressed in these neurons, or b) *Ir25a* is expressed, but is not playing a functional role in these neurons. In an *Orco*^{2} mutant background, there would be no trafficking of Orco-OrX complexes to the dendritic membrane, and no formation of functional ion channels (Benton et al., 2006; Larsson et al., 2004). Thus, in the traditional view of insect olfaction, *Orco*^{2} mutant neurons should have no odor-evoked activity. However, in the new polymodal model of olfaction, if *Ir25a* is contributing to olfactory responses in Orco+ neurons, then mutating this receptor might affect the response profiles of these neurons. Similarly, *Orco*^{2} mutant neurons that co-express *Ir25a* might retain some odor-evoked activity.

We first examined olfactory responses in palp basiconic sensilla. In the palps, three types of basiconic sensilla (pb1, pb2, and pb3) contain two neurons each (A and B) (Fig 6A), for a total of six OSN classes (Couto et al., 2005; de Bruyne et al., 1999; Fishilevich and Vosshall, 2005; Goldman et al., 2005; Ray et al., 2008; Ray et al., 2007). We found robust responses to several odorants in our panel in both the *wildtype* and *Ir25a*^{2} mutant flies, including odorants like 1-octen-3-ol typically considered as an OR ligand (Fig 6B), and IR ligands like pyrrolidine. Neither odor-evoked nor spontaneous activity was detected in the *Orco*^{2} mutant (Fig 6B, bottom row; see also Fig S6E). This was true of all sensilla tested in the palps. There was also no spontaneous or odor-evoked activity in an *Ir25a*^{2}; *Orco*^{2} double mutant (Fig S6F). Given the lack of neuronal activity in the *Orco*^{2} mutant, we focused subsequent analyses in the palps on the two other genotypes: *wildtype* and *Ir25a*^{2}.

The response in the pb1A neuron to 1-octen-3-ol was significantly higher in the *Ir25a*^{2} mutant compared to the *wildtype* (Mann-Whitney *U* test, $p = 0.0016$), as was the response to methyl salicylate ($p = 0.0177$), while the response to ethyl acetate was higher in *wildtype* ($p = 0.008$) (Fig 6C; see figure legend for *U* statistics and Supplemental Data 2 for results of all statistical analyses). The differences in responses across all six OSN classes in the palps between *wildtype* and *Ir25a*^{2} mutant flies are summarized in Fig 6D. In each neuron class, we found one to three odorants whose response profiles differed between the two genotypes. However, the specific stimuli eliciting different responses, and the directionality of those responses, varied. For example, 2,3-butanedione elicited higher responses in the *Ir25a*^{2} mutant in both pb2B and pb3A neurons, but lower responses in the mutant (higher in the *wildtype*) in pb3B. These results suggest that *Ir25a* may be involved in gain control in palpal OSNs, but the mechanism may be context dependent.

These results support the model that *Ir25a* plays a functional role in Orco+ palpal neurons. It was surprising then that there were no olfactory responses in the absence of *Orco*. This might suggest that *Ir25a* function in these neurons is *Orco*-dependent. Another possibility is that the olfactory neurons had degenerated in the *Orco*$^-$ mutant (Chiang et al., 2009; Hueston et al., 2016), as has been found in ant *Orco*$^-$ mutants (Trible et al., 2017; Yan et al., 2017). The axons of *Orco*$^-$ mutant neurons have been reported to degenerate in the antennal lobes over time due to a lack of activity, with signs of blebbing and retraction becoming evident around 4 – 6 days post eclosion (DPE) (Chiang et al., 2009). OSN classes in the antennae do occasionally lose their cell bodies in the absence of either *Orco* or the native *OrX*, but this happens at a much later timepoint than the axonal degeneration (14 DPE) (Hueston et al., 2016). To our knowledge, neurodegeneration in *Orco*$^-$ mutants has not been examined in palpal olfactory neurons. To examine the effects of the loss of *Orco* on palpal OSNs, we performed whole-mount antibody staining on maxillary palps using the pan-neuronal marker, *elav* (O'Neill et al., 1994; Robinow and White, 1991). This marker should label all ~120 olfactory neurons in the palps, as well as a small population (~20) of presumed mechanosensory neurons (Singh and Nayak, 1985).

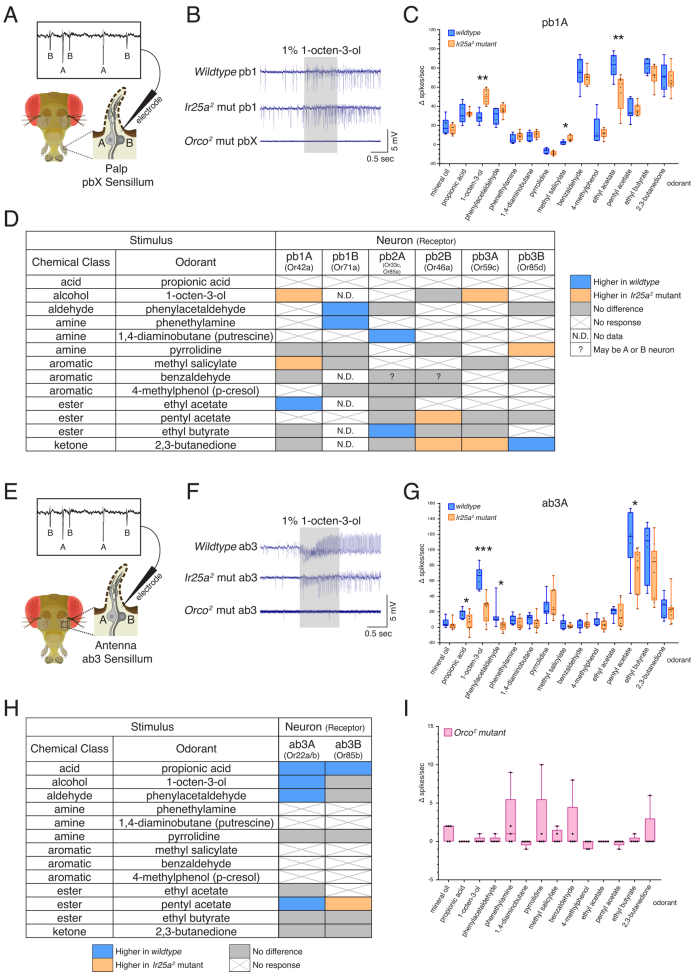

Figure 6. *Ir25a* contributes to olfactory responses in Orco+ neurons in the antennae and maxillary palps.

A.-I. SSR experiments performed from palps and antennae in three genetic backgrounds: *wildtype*, *Ir25a*^{2} mutant, and *Orco*^{2} mutant flies. A panel of 13 odorants were tested. In all box plots, * $p < 0.05$, ** $p < 0.01$, and *** $p < 0.001$. **A.** Cartoon of a fly head, zooming in on a single sensillum in the palp. Each palpal sensillum (pbX) contains two neurons, A and B. An electrode is inserted into the sensillum, and neuronal activity is recorded in response to odorants. Activity of the A and B neurons can be distinguished based on their spike amplitudes (top). **B.** Representative traces from recordings in pb1 sensilla in the three genotypes in response to 1% 1-octen-3-ol. Sensilla were identified based on responses to reference odorants[27]. The *Orco*^{2} mutant did not exhibit odor-evoked activity nor spontaneous activity making it difficult to determine the identity of the recorded sensillum (denoted as pbX). See Fig S6 for additional SSR recordings. **C.** Quantification of responses to the panel of odorants in *wildtype* (blue; N = 5 – 9 flies) and *Ir25a*^{2} mutant (orange; N = 6 – 10 flies) pb1A neurons. Responses were higher in the *Ir25a*^{2} mutant than in the *wildtype* for 1-octen-3-ol and methyl salicylate, and lower in the *Ir25a*^{2} mutant for ethyl acetate. Mann-Whitney U tests indicated these differences were statistically significant: 1-octen-3-ol: $Mdn_{Ir25amut} = 50$, $Mdn_{wildtype} = 28$, $U(N_{Ir25amut} = 8, N_{wildtype} = 5) = 0$, $p = 0.0016$; methyl salicylate: $Mdn_{Ir25amut} = 5$, $Mdn_{wildtype} = 2$, $U(N_{Ir25amut} = 7, N_{wildtype} = 5) = 3$, $p = 0.0177$; ethyl acetate: $Mdn_{Ir25amut} = 63.5$, $Mdn_{wildtype} = 83.5$, $U(N_{Ir25amut} = 8, N_{wildtype} = 6) = 4$, $p = 0.008$. See also Suppl Data 2. **D.** Summary of differences in responses across all six neuron classes in the palps between *wildtype* and *Ir25a*^{2} mutant flies. Comparisons were made using Mann-Whitney *U* tests (see also Suppl Data 2). Orange indicates higher response in *Ir25a*^{2} mutant, blue indicates higher response in *wildtype*. Grey is no difference in responses between genotypes, X indicates no response to the given stimulus, and N.D. is no data (strong A neuron response obscured B neuron spikes preventing quantification).

(legend continued on next page)

We compared anti-elav antibody staining in *wildtype* and *Orco*^{2} mutant flies at three timepoints: 3, 7, and 15 DPE (Fig S7A). In the *wildtype*, we found consistent neuronal cell counts across timepoints. The *Orco*^{2} mutant palps of 3-day-old flies were indistinguishable from *wildtype* (Fig S7A, left column). However, by 15 DPE extensive loss of cell bodies was detectable (Fig S7A, right column). This neurodegeneration was evident at 7 DPE (middle column), suggesting that cell body loss in the palps occurs more quickly and potentially more broadly than in the antennae. Overall, *Orco*^{2} mutants lose 60 – 70% of their palpal neurons. These results are quantified in Fig S7B. Both 7 and 15 DPE *Orco*^{2} mutants had significantly fewer elav+ cells compared to all *wildtype* timepoints as well as 3 DPE *Orco*^{2} mutants ($p \leq 0.0002$), but were not statistically significantly different from each other ($p = 0.4055$) (one-way ANOVA with Tukey's HSD; see figure legend for F statistic and Supplemental Data 5 for exact p values for all pairwise comparisons). There was no difference between any of the *wildtype* conditions ($p > 0.99$), nor between the 3 DPE *Orco*^{2} mutant and any of the *wildtype* timepoints ($p > 0.79$).

The SSR experiments in Fig 6A-D were performed at 4 – 8 DPE. Therefore, it is likely that at least some *Orco*^{2} mutant palpal neurons had degenerated, which would potentially confound our interpretation. We repeated the experiments in young (1 – 3 DPE) flies but similarly detected neither odor-evoked activity nor spontaneous activity in mutant palpal neurons (Fig S6H). This suggests one of three possibilities: first, *Orco*^{2} mutant neurons in the palps could already be dysfunctional at this early stage, despite not yet showing cell loss, and *Ir25a*-dependent activity is not sufficient to maintain either baseline or stimulus-induced activity; second, *Ir25a* function may be *Orco*-dependent in these cells, or act downstream of *Orco*, such that loss of *Orco* function affects *Ir25a* function; third, we did not stimulate neurons with an *Ir25a*-dependent odorant. The latter possibility would not, however, explain why there is no spontaneous activity in these cells. Future experiments will be needed to address these possibilities.

We next examined olfactory responses in antennal basiconic ab3 sensilla in *wildtype*, *Ir25a*^{2} mutant, and *Orco*^{2} mutant flies (Fig 6E – I). As in the palps, antennal ab3 sensilla contain two neurons, A and B (Fig 6E). In contrast to the palps, *Orco*^{2} mutant ab3 sensilla did occasionally show spontaneous activity (Fig 6F, bottom row; see Fig S6G for additional example traces). Although there are two Orco+ neurons in this sensillum, we consistently observed only a single spike amplitude in the *Orco*^{2} mutant. Thus, we cannot determine at this time whether this activity arises from the A or B neuron. We occasionally observed small responses (≤ 10 Δ spikes/sec) in the *Orco*^{2} mutant; however, across all flies tested, these responses were not significantly different from the mineral oil control (Fig 6I; statistical analyses can be found in Supplemental Data 2). For these reasons, *Orco*^{2} mutant flies were excluded from the analyses in Fig 6G and Fig 6H.

As in the palps, we found significant differences in the responses of both ab3A and ab3B neurons to odorants between the two genotypes. Comparison of all ab3A responses between *wildtype* and *Ir25a*^{2} mutant are shown in Fig 6G, and results from both the A and B neurons are summarized in Fig 6H (Mann-Whitney U, as in A-C; see Supplemental Data 2 for U values and all analyses). In the ab3A neuron, *wildtype* showed higher responses to propionic acid ($p = 0.0441$), 1-octen-3-ol ($p = 0.0004$), phenylacetaldehyde ($p = 0.015$), and pentyl acetate ($p = 0.0164$). Interestingly, two of these four odorants are typically associated with *IRs* (propionic acid and phenylacetaldehyde). In the ab3B neuron, only two odorants elicited significantly different responses between the *wildtype* and *Ir25a*^{2} mutant: propionic acid (response higher in *wildtype*, as with ab3A; $p = 0.0388$), and pentyl acetate (response higher in mutant, in contrast to ab3A; $p = 0.0385$). While responses to propionic acid are small in both ab3 neurons, they are abolished in the *Ir25a*^{2} mutant background (Kruskal-Wallis with uncorrected Dunn's comparing odorant responses to mineral oil control; ab3A $p = 0.3957$; ab3B $p = 0.5184$), suggesting that propionic acid detection in ab3 may be *Ir25a*-dependent.

The Polymodal Map of Olfaction in Drosophila

Polymodal expression of insect chemosensory receptors suggests multiple receptors may influence the response properties of an olfactory neuron, as we have shown in ab3 and palpal sensilla. To aid future investigations of polymodal signaling, we synthesized our results into a comprehensive new map of the antennal lobe. Fig 7 summarizes the expression patterns of all the co-receptor knock-in lines and presents a new model for odor coding in *Drosophila melanogaster*. In Fig 7A, the expression pattern of each knock-in line is presented separately (see also Supplemental Data 4). The new antennal lobe map is updated with the recent re-classification of VP1 into three glomeruli (Marin et al., 2020) and includes the newly identified VC6 glomerulus (this paper), bringing the total number of antennal lobe glomeruli to 58. In Fig 7A, the original glomerular innervation pattern for each co-receptor is shown in green, with new innervation revealed by the *T2A-QF2*^{HACK} knock-in lines color coded by intensity: strongly labeled glomeruli are in orange, intermediate glomeruli in yellow, and weakly labeled glomeruli are in pink. Glomeruli labeled in less than 50% of brains examined are designated variable (grey), and glomeruli not labeled by the given knock-in are in white. The new VC6 glomerulus is labeled with grey stripes.

In the previous view of odor coding in *Drosophila*, the Orco/OR domain primarily occupied the anterior AL, while the IR domains innervated more posterior glomeruli. While the former is still, for the most part, accurate (Fig 7A, *Orco*), the latter is not: both *Ir8a-T2A-QF2*^{HACK} and *Ir76b-T2A-QF2*^{HACK} label several more anterior glomeruli (such as VA3 or VA6), and *Ir25a-T2A-QF2*^{HACK} labels the majority of glomeruli throughout the anterior to posterior axis (Fig 7A,

D. In the *wildtype*, for one sensillum-odorant combination (pb2 and benzaldehyde), it could not be distinguished if responses were arising from the A or B neuron or both (indicated by a question mark). **E.** Fly head cartoon, zooming in on a single sensillum in the antenna. We recorded from ab3 sensilla, which contain two neurons, A and B. As in the palps, responses from these neurons can be distinguished by spike amplitude (top). **F.** Representative traces from recordings in ab3 sensilla in the three genotypes in response to 1% 1-octen-3-ol. In *Orco*^{2} mutant ab3 sensilla spontaneous activity was observed, but there was no significant odor-evoked activity (see Fig S6 for additional examples). *Wildtype* N = 7 sensilla from 5 flies; *Ir25a*^{2} mutant N = 10 sensilla from 5 flies. **G.** Quantification of responses in *wildtype* (blue; N = 7) and *Ir25a*^{2} mutant (orange; N = 9) ab3A neurons. Responses were significantly higher in *wildtype* compared to *Ir25a*^{2} mutant ab3A neurons for four odorants (Mann-Whitney U results in parentheses; all $N_{wildtype} = 7$ and $N_{Ir25amut} = 9$): propionic acid ($Mdn_{wildtype} = 21$, $Mdn_{Ir25amut} = 7$, $U = 12.5$, $p = 0.0441$); 1-octen-3-ol ($Mdn_{wildtype} = 67$, $Mdn_{Ir25amut} = 29$, $U = 1.5$, $p = 0.0004$); phenylacetaldehyde ($Mdn_{wildtype} = 10$, $Mdn_{Ir25amut} = 3$, $U = 9$, $p = 0.015$); and pentyl acetate ($Mdn_{wildtype} = 118$, $Mdn_{Ir25amut} = 77$, $U = 9$, $p = 0.0164$). Difference between *wildtype* and *Ir25a*^{2} mutant to phenylacetaldehyde is significantly different even with the large *wildtype* outlier removed ($p = 0.0336$).
H. Summary of differences in responses in the two neuron classes in ab3 between *wildtype* and *Ir25a*^{2} mutant flies. Comparisons for ab3B were made using Mann-Whitney U tests (see Suppl Data 2). Orange is higher response in *Ir25a*^{2} mutant, blue is higher response in *wildtype*, grey is no difference between genotypes, and X is no response. One *Ir25a*^{2} mutant fly was excluded from analyses as it had high responses to the mineral oil control (40 – 53 Δ spikes/sec), not seen in any other animal of any genotype. **I.** Weak responses in *Orco*^{2} mutant flies to certain stimuli (≤ 10 Δ spikes/sec) were occasionally detected. While there were some statistically significant differences from mineral oil control (pentyl acetate $p = 0.0109$, propionic acid $p = 0.0434$, ethyl acetate $p = 0.0434$, 1,4-diaminobutane $p = 0.0109$, p-cresol $p = 0.0021$), these were not deemed biologically significant due to very small Δ spike values relative to zero. N = 5 flies. See also Fig S6 and S7, and Suppl Data 2.

top right). The expansion of the Ir25a+ domain is the most dramatic of the four co-receptors: previously, Ir25a+ glomeruli accounted for 21% of the AL (12/57 glomeruli) (Enjin et al., 2016; Frank et al., 2017; Marin et al., 2020; Silbering et al., 2011); the *Ir25a-T2A-QF2^{HACK}* knock-in consistently labels 88% of the AL (51/58 glomeruli, excluding variable). This represents a greater than fourfold expansion. Similarly, the number of Ir76b+ glomeruli increased approximately fourfold, from 7% of the AL (4/57 glomeruli) (Silbering et al., 2011), to 26% (15/58, excluding variable). The Ir8a+ domain has doubled, from 11% of the AL originally (6/57 glomeruli) (Silbering et al., 2011) to 22% (13/58 glomeruli, excluding variable). Interestingly, in contrast to Ir25a+ and Ir76b+ glomeruli, the Ir8a+ domain is almost exclusively restricted to glomeruli receiving inputs from coeloconic sensilla or the sacculus. The most modest increase in reported expression is in the Orco+ domain: from 67% of the AL (38/57 glomeruli) (Couto et al., 2005; Fishilevich and Vosshall, 2005), to 76% (44/58, excluding variable).

The expression overlap in the antennal lobe of the four co-receptor modalities is summarized in the Venn diagram shown in Fig 7B (excluding the variably labeled glomeruli from Fig 7A). The table at the right lists the names of the glomeruli which correspond to the sections of the Venn diagram. This analysis reveals 6 glomeruli labeled by all four knock-in lines; furthermore, it shows that the Ir8a+ and Ir76b+ domains do not have glomeruli unique to them. Most of the antennal lobe is innervated by Orco+ and Ir25a+ neurons (26 glomeruli that are only Orco+ Ir25a+, plus an additional 11 that have Orco, Ir25a, and one or both other co-receptors). The Orco+ and Ir25a+ domains reveal glomeruli unique to them (6 glomeruli that are only Orco+, 8 glomeruli that are only Ir25a+). Expression analyses also reveal that Ir8a does not co-express with Orco alone or Ir76b alone.

A unified AL map organized by chemosensory modality (ORs, IRs, and GRs) is shown in Fig 7C (right panel), and the left two panels extend this information into the periphery. Here we include the GR+ innervation of the V glomerulus. However, a knock-in line for either *Gr21a* or *Gr63a* does not currently exist; thus, it is possible these receptors might also be more broadly expressed than previous transgenic lines indicate. All four OR and IR co-receptors are expressed in the antenna, while olfactory neurons in the palps express *Orco* and *Ir25a*. In the antennae, there are many different classes of olfactory sensory neurons expressing various combinations of chemosensory receptors and co-receptors: there are Orco+ only neurons (Fig 7C, middle panel, #2), such as those innervating the VM2 and VM3 glomeruli (teal); IrCo+ only neurons (purple), which include neurons expressing one, two, or all three *IR* co-receptors (such as VM6, VC6, or DP1m respectively) (Fig 7C, middle panel, #1); and neurons expressing both *Orco* and *IrCo(s)* (teal and purple stripe) (Fig 7C, middle panel, #3 and 4).

The expression data suggests that different populations of olfactory neurons might be targeting a shared glomerulus. Our data indicate that both Orco+ and Ir25a+ neurons innervate the GR+ V glomerulus (dark blue; see also Fig 7A). Based on the sparse innervation of the V glomerulus by the *Orco-T2A-QF2^{HACK}* knock-in (Fig 2D), we hypothesize that *Orco* may be expressed in only a subset of Gr21a/Gr63a+ neurons. This contrasts the *Ir25a-T2A-QF2^{HACK}* knock-in, which, based on both co-labeling experiments and the scRNAseq data, appears to label most (if not all) Gr21a/Gr63a+ neurons. Thus, two sub-populations of neurons maybe co-converging upon the same V glomerulus: neurons that express *Gr21a/Gr63a* and *Ir25a* (dark blue and purple stripes), and neurons that express *Gr21a/Gr63a, Ir25a* and *Orco* (dark blue, purple, and teal stripes) (Fig 7C, middle panel, #5). Such co-convergence has recently been shown in the olfactory system of *Aedes aegypti* mosquitoes (Younger, Herre et al., 2020). Similarly, the sparse *Orco-T2A-QF2^{HACK}* knock-in innervation of the DP1l glomerulus suggests that there are OSN populations expressing mostly *IRs*, but with

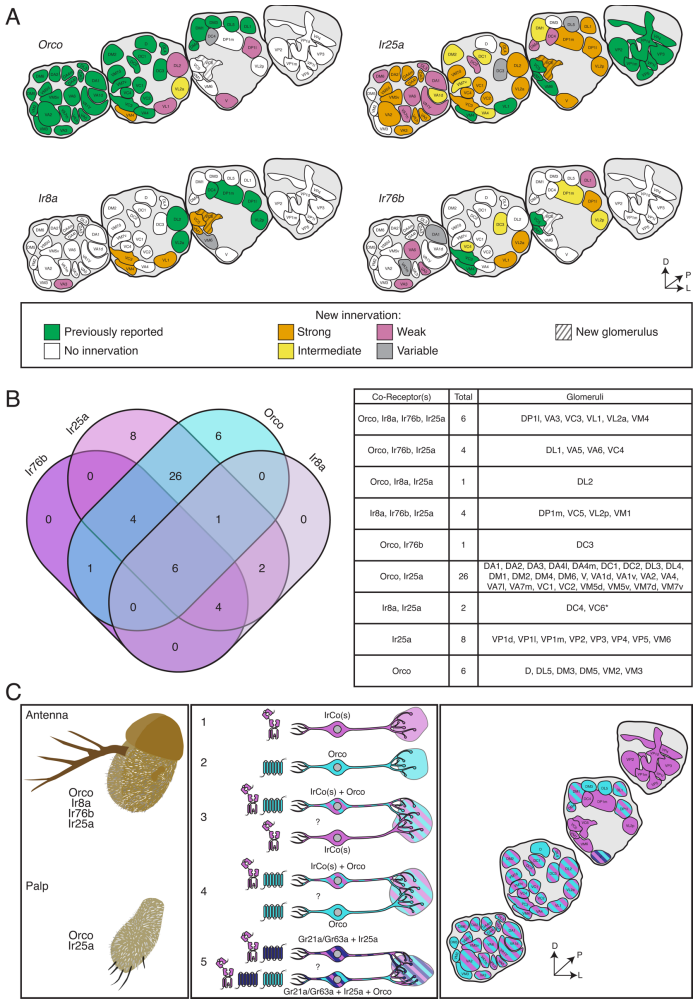

Co-Receptor(s)	Total	Glomeruli
Orco, Ir8a, Ir76b, Ir25a	6	DP1l, VA3, VC3, VL1, VL2a, VM4
Orco, Ir76b, Ir25a	4	DL1, VA5, VA6, VC4
Orco, Ir8a, Ir25a	1	DL2
Ir8a, Ir76b, Ir25a	4	DP1m, VC5, VL2p, VM1
Orco, Ir76b	1	DC3
Orco, Ir25a	26	DA1, DA2, DA3, DA4l, DA4m, DC1, DC2, DL3, DL4, DM1, DM2, DM4, DM6, V, VA1d, VA1v, VA2, VA4, VA7l, VA7m, VC1, VC2, VM5d, VM5v, VM7d, VM7v
Ir8a, Ir25a	2	DC4, VC6*
Ir25a	8	VP1d, VP1l, VP1m, VP2, VP3, VP4, VP5, VM6
Orco	6	D, DL5, DM3, DM5, VM2, VM3

Figure 7. The polymodal olfactory map in *Drosophila*.
A. Summary of AL expression for all knock-in lines (from all brains examined in Fig 2 – 4; *Orco* N = 8, *Ir8a* N = 10, *Ir76b* N = 11, *Ir25a* N = 15). The previously reported innervation pattern for each co-receptor is shown in green; new innervation reported here is color-coded according to strength of glomerular labeling: strong (orange), intermediate (yellow), weak (pink). Glomeruli labeled in <50% of brains examined are designated variable (grey); glomeruli not labeled are white. The novel VC6 glomerulus reported here is indicated by grey stripes. See also Suppl Data 4. **B.** Overlap of chemosensory modalities in the AL. In the Venn diagram (left), *IR* co-receptors are color-coded in shades of purple, while *Orco* is in teal, as in Fig 1. Numbers indicate how many glomeruli are found in the given intersection of co-receptors out of 58 total. Variably labeled glomeruli were excluded from these analyses. The table lists the names of the glomeruli in each section of the Venn diagram. The new VC6 glomerulus is indicated with an asterisk. **C.** A polymodal view of olfaction in *Drosophila*. Left: in the periphery, all four co-receptors are expressed in the antenna (top), while palpal neurons express *Orco* and *Ir25a* (bottom). Middle: Many different classes of OSNs express various combinations of chemosensory receptors and co-receptors. While some neurons express only *IrCos* (purple, #1) or *Orco* (teal, #2), many neurons co-express these chemosensory modalities (indicated with striped fill, #3 and 4). Within the latter group, there may be OSN populations in which *IRs* are the dominant modality, and *OR* expression is sparse (#3), and other populations where *ORs* are the primary receptors and *IR* expression is infrequent (#4). GR+ neurons (dark blue) also express *Ir25a* (#5, dark blue and purple striped fill), and some of these neurons additionally express *Orco* (#5, dark blue, purple, and teal striped fill). Question marks indicate potential instances of co-convergence of different sub-types of OSNs onto the same glomeruli. Right: a comprehensive map of the antennal lobe shows that most glomeruli are polymodal. Compass in (A) and (C): D = dorsal, L = lateral, P = posterior. See also Suppl Data 4.

a subset of neurons that additionally express *Orco* (Fig 7C, middle panel, #3). The converse may also be possible (Fig 7C, middle panel, #4): OSN populations which have some neurons expressing only *Orco*, and a subset expressing both *Orco* and *IrCo(s)* co-converging onto the same glomerulus. There is some evidence for this in the palps: the anti-Orco antibody and the *Orco-T2A-QF2^{HACK}* knock-in label approximately 119 cells on average (Table S2), while the anti-Ir25a antibody and the *Ir25a-T2A-QF2^{HACK}* knock-in label about 94 cells (Table S3). There are approximately 120 OSNs in the maxillary palps (Singh and Nayak, 1985); this suggests that *Orco* is expressed in all olfactory neurons in the palps, while *Ir25a* is expressed in a large subset (nearly 80%) of palpal neurons. The scRNAseq data suggests this may also be the case in the antennae: in a number of Ir25a+ clusters, a subset of the OSN population expresses *Ir25a* transcripts (such as cluster 2, DL4 glomerulus, Or49a+/Or85f+, which is ~67% Ir25a+).

DISCUSSION

Here we present evidence in *Drosophila melanogaster* of widespread polymodal chemosensory receptor expression, contrasting a previously accepted view of segregated, mutually exclusive chemosensory domains. By generating targeted knock-ins of the four main chemosensory co-receptors (*Orco*, *Ir8a*, *Ir76b*, and *Ir25a*), we demonstrate that all four co-receptors have broader olfactory neuron expression than previously appreciated. Co-expression of these chemosensory modalities was found in the periphery and in the central projections to the brain. The *Ir25a* co-receptor was previously thought to be expressed only in a small subset of olfactory neurons (coeloconic, sacculus, and arista neurons), but we present evidence that it is expressed in subsets of nearly all olfactory sensory neuron (OSN) classes that innervate the majority of the fly antennal lobes (ALs). We further demonstrate that co-expression of chemosensory modalities has functional relevance for olfactory neurons, and that the *Ir25a* co-receptor may be involved in gain control in Orco+ OSNs, both in the antennae and maxillary palps. We present a new AL map which will aid future inquiries into the roles that specific chemosensory modalities are playing in distinct OSN populations.

A model for OR/IR segregation was initially supported by developmental evidence. Two pro-neural genes specify the development of sensory structures on the antennae: *amos* and *atonal*. *Amos* mutants lack basiconic and trichoid sensilla, while *atonal* mutants do not develop coeloconic sensilla, the arista, or the sacculus (Goulding et al., 2000; Gupta and Rodrigues, 1997; Jhaveri et al., 2000a; Jhaveri et al., 2000b). It was observed that *amos* mutants lose *Orco* expression while retaining *Ir25a* expression (Benton et al., 2009). Our results do not conflict with this view. However, the converse conclusion – that *atonal* mutants have *Orco* but not *Ir25a* expression – is not consistent with co-receptor knock-in expression (the same is true for *Ir76b*, but not *Ir8a*). Based upon the strength of the corresponding glomerular innervations, it does appear that the previously reported Ir25a+ neurons have stronger (or more consistent) *Ir25a* expression, while the new Ir25a+ olfactory neurons in the antennae reported here (e.g. *OR*-expressing OSNs) are generally weakly or stochastically labeled. This might also explain why *Ir25a* expression was initially overlooked in these Orco+ neural populations. Furthermore, our results are consistent with RNAseq analyses performed on *atonal* mutant antennae, which showed that both *Ir25a* and *Ir76b* expression, but not *Ir8a* expression, remained (Menuz et al., 2014). The developmental pattern is different in the maxillary palps, where it is *atonal* and not *amos* which is required for development of the basiconic sensilla (Gupta and Rodrigues, 1997). Interestingly, the *Ir25a* knock-in expression corresponds well with the *atonal* developmental program across the olfactory appendages: the strongest expression of *Ir25a* is in coeloconic sensilla, but outside of these sensilla the strongest and most consistent *Ir25a* expression is in palp basiconic sensilla.

Polymodal chemosensory receptor expression may help clarify previously confounding observations regarding *Drosophila* odor coding. For example, a population of olfactory neurons in the sacculus expresses the *Ir64a* tuning receptor along with the *Ir8a* co-receptor (Ai et al., 2013; Ai et al., 2010). Unlike most other OSN populations, Ir64a+ neurons project to two different glomeruli: DC4 and DP1m. These two glomeruli exhibit different olfactory response profiles, with DC4 being narrowly tuned to acids or protons, while DP1m is more broadly tuned. The molecular mechanism for these differences was previously unclear as it was thought these neurons expressed the same receptors. However, the co-receptor knock-in data presented here reveals that the Ir64a+ OSN sub-populations do, in fact, express different combinations of chemosensory receptors: in addition to the *Ir8a* co-receptor, neurons innervating DC4 express *Ir25a* (and occasionally *Orco*) (see Fig 7). In contrast, neurons innervating DP1m express *Ir8a*, *Ir25a*, and *Ir76b*. Thus, perhaps it is *Ir76b* expression in DP1m-targeting Ir64a+ neurons which makes them olfactory generalists. This idea is supported by experiments in which *Ir64a* was expressed in neurons targeting the VM4 glomerulus, conferring a DP1m-like, rather than a DC4-like, response profile to VM4 (Ai et al., 2010). We show here that VM4-targeting neurons express *Ir8a*, in addition to *Ir25a* and *Ir76b* (as well as *Orco*): thus, molecularly, the VM4 neuron profile is more similar to DP1m (co-expressing all *IrCos*) than DC4 (co-expressing two *IrCos*), and the key distinguishing component appears to be *Ir76b*. It would be interesting to repeat such misexpression experiments in an *Ir76b^{-}* mutant background to test this hypothesis.

While we demonstrate here that multiple chemosensory modalities can be co-expressed in the same olfactory neurons, it remains to be determined if this also applies to tuning (odor-binding) receptors. Previous studies suggest that OrX tuning receptors are generally limited to a single class of olfactory neurons, with the sole exception being *Or33b* (Couto et al., 2005; Fishilevich and Vosshall, 2005). However, many IrX tuning receptors remain to be characterized and could be co-expressed in multiple olfactory neurons. For example, recordings from ab1, ab3, and ab6 sensilla indicate responses to the typical IR odors 1,4-diaminobutane, ammonia, and butyric acid, respectively (de Bruyne et al., 2001), suggesting tuning IrXs may be involved. We show that *Ir25a* plays a functional role in Orco+ neurons in the antennae and palps; this suggests that these Orco+ neurons could also express as yet unidentified ligand binding *IrXs*. In the palps, we did not find odorants that were entirely dependent upon *Ir25a* expression in these neurons; however, in antennal ab3 sensilla, we did find one odorant (propionic acid) which elicited a small response in *wildtype* neurons, and no response in *Ir25a^{2}* mutant neurons. It remains possible that potential IrXs expressed in the palps might be narrowly tuned towards an odorant not tested in our limited odorant panel. These results suggest that testing a broader array of ligands could reveal *IR*-dependent responses in Orco+ OSNs. Identification of potential tuning *IrXs* in Orco+ OSNs would likely aid our understanding of *IR* function in these neurons.

The widespread expression of Ir25a in the fly olfactory system raises the possibility that it might have roles in addition to its function as an IrX co-receptor. For example, Ir25a has been found to play a developmental role in forming the unique structure of Cold Cells in the arista (Budelli et al., 2019). Evolutionary studies also suggest that Ir25a is the most ancient of all the insect chemosensory receptors (Croset et al., 2010), and the currently broad expression might reflect its previous ubiquitous role in chemosensory signaling. Ir25a may also be involved in downstream olfactory signal transduction or amplification, as suggested by the work presented here, and as has recently been shown for a pickpocket ion channel (Ng et al., 2019). Experiments addressing

potentially expanded roles for Ir25a will be aided by the new multimodal chemosensory map presented here.

We have also identified a new glomerulus, VC6. Given that this glomerulus is labeled by both the *Ir25a-T2A-QF2^{HACK}* and *Ir8a-T2A-QF2^{HACK}* knock-in lines, the cell bodies of these neurons must be in the antenna. Based on its location and receptor expression, this glomerulus could receive either olfactory information, or thermosensory/hygrosensory information (Marin et al., 2020). We did not find *Ir8a-T2A-QF2^{HACK}* labeling of the arista; thus, these neurons are likely to be either in coeloconic sensilla, or in the sacculus. Future experiments will be necessary to determine these neurons' location, molecular profile (e.g. tuning receptor expression), and response profile. There are several tuning *IRs* whose transcripts have previously been detected in the antennae, but which were not mapped to specific neurons and could be promising candidates for this new OSN class (Benton et al., 2009; Menuz et al., 2014).

We also present evidence that *Orco^{-}* mutant olfactory neurons rapidly degenerate in the palps. While a similar phenomenon was previously described for antennal axons innervating the AL, and in some populations of antennal OSN cell bodies (Chiang et al., 2009; Hueston et al., 2016), the degeneration phenotype in the palps is far more pronounced. This presents a potentially new model system for studying neurodegeneration and activity-dependent neuronal maintenance. In contrast to the antenna, neuronal loss in *Orco* mutant palps is rapid (within 6 or 7 days post eclosion vs 14 days post eclosion in antennae); the palp is a simpler olfactory organ, and neuronal changes are easier to study and quantify by whole-mount staining in the palps. The rapid neurodegeneration of *Orco* mutant palpal neurons makes it experimentally challenging to address the independent role of *Ir25a* in palpal OSNs; whether IR-dependent activity enables a subpopulation of these neurons to be spared in the *Orco* mutant background remains to be determined.

The work presented here was aided by the use of a highly effective new knock-in strategy. The HACK KI strategy could be easily adapted for targeting knock-ins to other *Drosophila* genes, potentially making *Drosophila* knock-in generation routine. The HACK genetic strategy could also be applicable to other animal systems, especially non-model organisms, such as *Anopheles* mosquitoes, for which it has traditionally been difficult to generate genetic reagents. This approach has several advantages over the transgenic approaches previously employed. First, knock-ins recapitulate endogenous gene expression patterns. Second, in organisms with large genomes such as *Anopheles gambiae* and *Aedes aegypti* it is often difficult to identify the enhancer/promoter region for a gene of interest (Holt et al., 2002; Nene et al., 2007; Riabinina et al., 2016). To do so often requires cloning large fragments of DNA, which can still result in failed transgenic lines driving no or incomplete expression (Riabinina et al., 2016). Third, knock-ins (particularly of binary expression system components) can be more versatile than transgenic lines: depending on the design, a single knock-in line can both capture gene expression while also generating a mutant for that gene (Gratz et al., 2015). Fourth, the HACK *T2A-QF2* knock-in cassette is smaller than comparable *Gal4* knock-in cassettes, which should increase efficiency of HDR (Li et al., 2014), and *QF2* often drives stronger expression than *Gal4* (Riabinina et al., 2015). Finally, in organisms such as *Anopheles* and *Aedes* mosquitoes, the *Gal4/UAS* system has encountered limitations due to poor activity (Lynd and Lycett, 2012). Tools employing the *Q* System, such as HACK, may prove generalizable to more organisms (Matthews et al., 2019; Persad et al., 2020; Riabinina et al., 2016; Subedi et al., 2014; Wei et al., 2012).

Co-expression of chemosensory modalities might function to increase the signaling capabilities of an olfactory neuron. For example, the signaling of an Orco+ olfactory neuron may be guided primarily by the tuning OrX, and the sensitivity range extended to include odors detectable by an IrX. Co-expression might also allow synergism, such that weak activation of a co-expressed receptor could increase neuronal activity to levels sufficient to drive behavior. This might be useful in tuning behavioral response to complex odors, such that certain combinations of odors lead to stronger olfactory neuron responses. Alternatively, a co-expressed receptor inhibited by odorants might be able to attenuate a neuron's response to odor mixtures. Co-expressed chemosensory receptors might also modulate the perceived valence of an olfactory stimulus through the same olfactory circuit or channels. For example, a recent study showed that CO_2, which is normally aversive to flies, can be attractive in certain contexts (van Breugel et al., 2018). While the aversive response requires the known CO_2 receptors, *Gr21a* and *Gr63a*, the attractive response was shown to be *Ir25a*-dependent. However, previous calcium imaging experiments in the antennal lobes have shown that CO_2 primarily activates a single glomerulus, the V glomerulus, which receives inputs from the Gr21a+/Gr63a+ neurons (Suh et al., 2004). Our *Ir25a-T2A-QF2^{HACK}* knock-in line reveals that *Ir25a* is expressed in this OSN class. This raises the possibility that the same neurons, through a different chemosensory receptor modality, could drive both attractive and aversive behavior in different contexts (MacWilliam et al., 2018). Co-expression of chemosensory receptors could be a mechanism to increase the functional flexibility of a numerically limited olfactory system.

Drosophila often serve as a model for many other insect olfactory systems, and information gleaned from *Drosophila* is frequently extrapolated to other insects (for example, DeGennaro et al., 2013; Fandino et al., 2019; Riabinina et al., 2016; Trible et al., 2017; Yan et al., 2017). The work presented here raises the possibility that other insects may also exhibit polymodal expression of chemosensory receptors. Exciting new work in *Aedes aegypti* mosquitoes suggests that this may indeed be the case: mosquito olfactory neurons can co-express Orco/IrCo/Gr receptors; in the CO_2-sensing olfactory neuron, this polymodal co-expression functionally expands the range of activating odors (Younger, Herre et al., 2020). This suggests that polymodal expression of chemosensory receptors may be an important feature of insect olfactory neurons.

Author Contributions

Conceptualization: D.T. (knock-in analysis, SSR, neurodegeneration), C-C.L. (HACK development, knock-in analysis, SSR, optogenetics), A.V. (SSR), K.M. (SSR, IRs, palp analysis), C.J.P. (all aspects); **Methodology**: D.T. (cloning and generation of knock-ins (*Ir25a*, *Ir8a*, *Ir76b*), immunohistochemistry, SSR, statistics, AL maps, neurodegeneration), C-C.L. (HACK, genetics, cloning and generation of knock-ins (*Orco*, *Ir8a*, *Ir76b*), cloning and generation of *QUAS-CsChrimson*, SSR, optogenetics), A.A. (SSR), H.L. (scRNAseq), A.V. (SSR), K.M. (SSR, IR expression), C.J.P. (all aspects); **Formal Analysis**: D.T. (knock-ins, SSR, neurodegeneration), C-C.L. (knock-ins, SSR), A.A. (SSR), H.L. (scRNAseq); **Investigation**: D.T. (knock-in generation and validation (*Ir25a*, *Ir8a*, *Ir76b*), immunohistochemistry, AL analysis, neurodegeneration), C-C.L. (HACK development, knock-in generation and validation (*Orco*, *Ir8a*, *Ir76b*), *QUAS-CsChrimson* generation and validation, optogenetics, SSR – palp, ab2), A.A. (SSR – ab3), H.L. (scRNAseq), A.V. (SSR – coeloconic); **Writing, Original Draft**: D.T. and C.J.P.; **Writing, Review & Editing**: D.T., C-C.L., A.A., H.L., A.V., K.M., C.J.P.; **Visualization**: D.T. (olfactory system/fly cartoons, AL maps, microscopy images, SSR, Venn diagram, tables), C-C.L. (genetics cartoons, crossing schemes, SSR, optogenetics), H.L. (scRNAseq), C.J.P.; **Supervision**: K.M. and C.J.P.; **Funding Acquisition**: C.J.P.

Declaration of Interests

The authors declare no competing interests.

Acknowledgments

We thank E. Marr and K. Robinson for splinkerette genetic mapping, Y.-T. Chang for cloning of *pHACK*^{Ir8a} components, O. Riabinina for initial *QUAS-CsChrimson* characterization, S. Maguire for preliminary SSR experiments, P. Mohapatra for RNAseq insights, D. Baktash for help with figures, J. Konopka for advice on statistical analyses, S. Shankar for discussion of AL mapping, and R. Mann for providing lab resources. Many thanks to the following labs for sharing antibody and fly stock reagents: Leslie B. Vosshall (Rockefeller), Richard Benton (UNIL), Paul Garrity (Brandeis), Marco Gallio (Northwestern), Greg Suh (NYU), and Thomas R. Clandinin (Stanford). We thank the Center for Sensory Biology Imaging Facility (NIH P30DC005211) for use of the LSM700 confocal microscope, and the Johns Hopkins School of Public Health Malaria Research Institute for use of the Olympus SZX7 microscope equipped with QImaging QIClick Cooled digital CCD camera. We thank J. Raji, S. Maguire, and J. Konopka for comments on the manuscript and members of the Potter and Menuz labs for discussion. We thank the Vosshall lab for sharing their *Aedes* data before publication. This work was supported by a Shelanski award to C.-C. L; grants from the National Institutes of Health to H.L. (K99 AG062746); grants from the National Institutes of Health to K.M. (NIGMS R35GM133209; NIDCD 1R21DC017868); grants from the Department of Defense to C.J.P. (W81XWH-17-PRMRP) and from the National Institutes of Health to C.J.P. (NIAID R01AI137078; NIDCD R01DC013070).
Portions of this work appear in Chapter 3 of D.T.'s doctoral dissertation.

MATERIALS AND METHODS

Key Resources Table

REAGENT or RESOURCE	SOURCE	IDENTIFIER
Antibodies		
Mouse anti-nc82	DSHB	Cat# nc82; RRID: AB_2314866
Rat anti-cd8	Thermo Fisher Scientific	Cat# 14-0081-82; RRID: AB_467087
Rat anti-elav	DSHB	Cat# Rat-Elav-7E8A10; RRID: AB_528218
Rabbit anti-Orco	Gift from Leslie Vosshall; (Larsson et al., 2004)	N/A
Rabbit anti-Ir25a	Gift from Richard Benton; (Benton et al., 2009)	RRID: AB_2567027
Goat anti-mouse Cy3	Jackson ImmunoResearch	Cat# 115-165-166; RRID: AB_2338692
Goat anti-mouse Alexa 647	Jackson ImmunoResearch	Cat# 115-605-166; RRID: AB_2338914
Goat anti-rat Cy3	Jackson ImmunoResearch	Cat# 112-165-167; RRID: AB_2338251
Goat anti-rat Alexa 647	Jackson ImmunoResearch	Cat# 112-605-167; RRID: AB_2338404
Goat anti-rabbit Cy3	Jackson ImmunoResearch	Cat# 111-165-144; RRID: AB_2338006
Goat anti-rabbit Alexa 647	Jackson ImmunoResearch	Cat# 111-605-144; RRID: AB_2338078
Chemicals, Peptides, and Recombinant Proteins		
Mineral oil	Sigma-Aldrich	CAS# 8042-47-5
Ethyl acetate	Sigma-Aldrich	CAS# 141-78-6
Pentyl acetate	Sigma-Aldrich	CAS# 628-63-7
Benzaldehyde	Sigma-Aldrich	CAS# 100-52-7
Ethyl butyrate	Sigma-Aldrich	CAS# 105-54-4
Hexanol	Sigma-Aldrich	CAS# 111-27-3
E2-hexenal	Sigma-Aldrich	CAS# 6728-26-3
Geranyl acetate	Sigma-Aldrich	CAS# 105-87-3
2-heptanone	Sigma-Aldrich	CAS# 110-43-0
1-octen-3-ol	Sigma-Aldrich	CAS# 3391-86-4
2,3-butanedione	Sigma-Aldrich	CAS# 431-03-8
Phenylacetaldehyde	Sigma-Aldrich	CAS# 122-78-1
Phenethylamine	Sigma-Aldrich	CAS# 64-04-0
Propionic acid	Sigma-Aldrich	CAS# 79-09-4

1,4-diaminobutane	Sigma-Aldrich	CAS# 110-60-1
Pyrrolidine	Sigma-Aldrich	CAS# 123-75-1
P-cresol	Sigma-Aldrich	CAS# 106-44-5
Methyl salicylate	Sigma-Aldrich	CAS# 119-36-8
Paraffin Oil	ACROS Organics	CAS# 8012-95-1
Water	SIGMA Life Science	CAS# 7732-18-5
Acetic acid	Fisher Scientific	CAS# 64-19-7
Ammonium hydroxide	Fisher Scientific	CAS# 7664-41-7
Cadaverine	Sigma-Aldrich	CAS# 462-94-2
Hexanol	ACROS Organics	CAS# 111-27-3
2,3-butanedione	ACROS Organics	CAS# 431-03-8
Phenethylamine	ACROS Organics	CAS# 64-04-0
Propanal	ACROS Organics	CAS# 123-38-6
1,4-diaminobutane	ACROS Organics	CAS# 110-60-1
All trans-retinal	Sigma-Aldrich	CAS# 116-31-4
Critical Commercial Assays		
In-Fusion Cloning	Clontech Labs	Cat# 639645
DNeasy Blood and Tissue Kit	Qiagen	Cat# 69506
Deposited Data		
Raw and analyzed data	This paper	Available upon request
scRNAseq data	(Li et al., 2020)	https://github.com/Hongjie-Li/FlyORN
Experimental Models: Organisms/Strains		
D. melanogaster: *Orco-T2A-QF2^{HACK}* knock-in	This paper	BDSC: TBD
D. melanogaster: *Ir8a-T2A-QF2^{HACK}* knock-in	This paper	BDSC: TBD
D. melanogaster: *Ir76b-T2A-QF2^{HACK}* knock-in	This paper	BDSC: TBD
D. melanogaster: *Ir25a-T2A-QF2^{HACK}* knock-in	This paper	BDSC: TBD
D. melanogaster: Pin/CyO; QUAS-CsChrimson #11c/TM6b	This paper	BDSC: TBD
D. melanogaster: *Ir21a-T2A-Gal4* knock-in	Gift from Paul Garrity; (Marin et al., 2020)	N/A
D. melanogaster: *Ir68a-T2A-Gal4* knock-in	Gift from Paul Garrity; (Marin et al., 2020)	N/A
D. melanogaster: w[*]; P(w[+mC]=Gr21a-GAL4.9.323)2/CyO; Dr[1]/TM3, Sb[+]	Bloomington *Drosophila* Stock Center	BDSC: 57600; FlyBase: FBti0162643
D. melanogaster: w[*]; P(w[+mC]=Ir25a-GAL4.A)236.1; TM2/TM6B, Tb[1]	Bloomington *Drosophila* Stock Center	BDSC: 41728; FlyBase: FBti0148895
D. melanogaster: Ir64a-Gal4	Gift from Greg Suh lab; (Ai et al., 2010)	N/A
D. melanogaster: w[*]; P(w[+mC]=Ir76b-GAL4.916)226.8; TM2/TM6B, Tb[+]	Bloomington *Drosophila* Stock Center	BDSC: 41730; FlyBase: FBti0153291
D. melanogaster: w[*]; P(w[+mC]=Ir8a-GAL4.A)204.8; TM2/TM6B, Tb[1]	Bloomington *Drosophila* Stock Center	BDSC: 41731; FlyBase: FBti0148897
D. melanogaster: w[*]; P(w[+mC]=Or22a-GAL4.7.717)14.2	Bloomington *Drosophila* Stock Center	BDSC: 9951; FlyBase: FBti0101805
D. melanogaster: w[*]; P(w[+mC]=Or22a-GAL4.7.717)14.21	Bloomington *Drosophila* Stock Center	BDSC: 9952; FlyBase: FBti0101805
D. melanogaster: w[1118]; P(w[+mC]=Or46a-GAL4.G)32.1.y	Bloomington *Drosophila* Stock Center	BDSC: 23291; FlyBase: FBti0076800

D. melanogaster: w[*]; P(w[+mC]=Or67b-GAL4.F)68.3/TM6B, Tb[1]	Bloomington *Drosophila* Stock Center	BDSC: 9995; FlyBase: FBti0101858
D. melanogaster: w[*]; P(w[+mC]=Or92a-GAL4.F)62.1	Bloomington *Drosophila* Stock Center	BDSC: 23139; FlyBase: FBti0101867
D. melanogaster: w[*]; P(w[+mC]=Orco-GAL4.W)11.17; TM2/TM6B, Tb[1]	Bloomington *Drosophila* Stock Center	BDSC: 26818; FlyBase: FBti0101150
D. melanogaster: germline *Cas9*: *y[1] M(RFP[3xP3.PB] GFP[E.3xP3]=vas-Cas9)ZH-2A w[1118]/FM7c*	Bloomington *Drosophila* Stock Center	BDSC: 51323; FlyBase: FBti0154823
D. melanogaster: germline *Cas9: w[1118]; PBac(y[+mDint2]=vas-Cas9)VK00027*	Bloomington *Drosophila* Stock Center	BDSC: 51324; FlyBase: FBti0154822
D. melanogaster: germline *Cas9: y[1] M(w[+mC]=Act5C-Cas9.P)ZH-2A w[*]*	Bloomington *Drosophila* Stock Center	BDSC: 54590; FlyBase: FBti0159182
D. melanogaster: QUAS reporter*: y[1] w[1118]; P(w[+mC]=QUAS-mCD8::GFP.P)5B/TM6B, Tb[1]*	Bloomington *Drosophila* Stock Center	BDSC: 30003; FlyBase: FBti0129937
D. melanogaster: QUAS reporter*: y[1] w[*]; PBac(y[+mDint2] w[+mC]=10XQUAS-6XGFP)VK00018/CyO, P(Wee-P.ph0)Bacc[Wee-P20]*	Bloomington *Drosophila* Stock Center	BDSC: 52264; FlyBase: FBti0162759
D. melanogaster: UAS reporter*: w[*]; P(y[+t7.7] w[+mC]=15XUAS-IVS-mCD8::GFP)attP2*	Bloomington *Drosophila* Stock Center	BDSC: 32193; FlyBase: FBti0131935
D. melanogaster: UAS reporter*: w[*]; P(y[+t7.7] w[+mC]=10XUAS-IVS-mCD8::GFP)attP40*	Bloomington *Drosophila* Stock Center	BDSC: 32186; FlyBase: FBti0131963
D. melanogaster: UAS reporter*: w[*]; P(y[+t7.7] w[+mC]=10XUAS-IVS-mCD8::RFP)attP2*	Bloomington *Drosophila* Stock Center	BDSC: 32218; FlyBase: FBti0131950
D. melanogaster: UAS reporter*: w[*]; P(y[+t7.7] w[+mC]=10XUAS-IVS-mCD8::RFP)attP40*	Bloomington *Drosophila* Stock Center	BDSC: 32219; FlyBase: FBti0131967
D. melanogaster: UAS reporter*: y[1] w[*]; PBac(y[+mDint2] w[+mC]=20XUAS-6XGFP)VK00018/CyO, P(Wee-P.ph0)Bacc[Wee-P20]*	Bloomington *Drosophila* Stock Center	BDSC: 52261; FlyBase: FBti0162758
D. melanogaster: y[1] w[67c23] P(y[+mDint2]=Crey)1b; sna[Sco]/CyO	Bloomington *Drosophila* Stock Center	BDSC: 766; FlyBase: FBti0012692
D. melanogaster: Orco^{2} mutant*: w[*]; TI(w[+m*]=TI)Orco[2]*	Bloomington *Drosophila* Stock Center	BDSC: 23130; FlyBase: FBti0168777
D. melanogaster: Ir25a^{2} mutant*: w[*]; TI(w[+m*]=TI)Ir25a[2]/CyO*	Bloomington *Drosophila* Stock Center	BDSC: 41737; FlyBase: FBti0168524
D. melanogaster: double balancer: *y,w; Pin/CyO; Dh/TM6B*	N/A (Potter lab stock)	Derived from FBal0013831, FBba0000025, FBti0004009, FBba0000057, FBal0016730
D. melanogaster: double balancer: *y,w; S/CyO; Pr/TM6B*	N/A (Potter lab stock)	Derived from FBal0015108, FBba0000025, FBal0013944, FBba0000057, FBal0016730
D. melanogaster: double balancer: *19ADrok/FM7c; Pin/CyO*	N/A (Potter lab stock)	Derived from BDSC 6666, FBba0000009, FBal0013831, FBba0000025
D. melanogaster: single balancer: *y,w; S/CyO; +/+*	N/A (Potter lab stock)	Derived from FBal0015108, FBba0000025
D. melanogaster: single balancer: *y,w; +/+; Pr/TM6B*	N/A (Potter lab stock)	Derived from FBal0013944, FBba0000057, FBal0016730
D. melanogaster: wildtype: *w*^{1118} *IsoD1*	Gift from Thomas R. Clandinin	Derived from FBal0018186
Oligonucleotides		
Orco_gRNA_FOR: TCCGGGTGAACTTCGCACAGTGCGGAGGGGGCAAGTTTTAGAGCTAGAAATAGCAAGTTA	Integrated DNA Technologies; This paper	N/A
Orco_gRNA_REV: TTCTAGCTCTAAAACACTTTATGGTGCTGGTGCAGCGACGTTAAATTGAAAATAGGTC	Integrated DNA Technologies; This paper	N/A
Orco_5HA_FOR: CCCTTACGTAACGCGTCAGCTTGTTTGACTTACTTGATTAC	Integrated DNA Technologies; This paper	N/A
Orco_5HA_REV: CGCGGCCCTCACGCGTCTTGAGCTGTACAAGTACCATAAAGT	Integrated DNA Technologies; This paper	N/A

Orco_3HA_FOR: GTTATAGATCACTAGTCTCAGTACTATGCAACCAGCAATA	Integrated DNA Technologies; This paper	N/A
Orco_3HA_REV: AATTCAGATCACTAGTGTTTTATGAAAGCTGCAAGAAATAA	Integrated DNA Technologies; This paper	N/A
Ir8a_gRNA_FOR: TCCGGGTGAACTTCGTTTGTTTGTTCGGCCATGTGTTTTAGAGCTAGAAATAGCAAGTTA	Integrated DNA Technologies; This paper	N/A
Ir8a_gRNA_REV: TTCTAGCTCTAAAACCTGTGGGAGTCAGAGGCACCGACGTTAAATTGAAAATAGGTC	Integrated DNA Technologies; This paper	N/A
Ir8a_5HA_FOR: CCCTTACGTAACGCGtCTATTGGCTATTCGTCGTACTCATGC	Integrated DNA Technologies; This paper	N/A
Ir8a_5HA_REV: CGCGGCCCTCACGCGtCTCCATGTAGCCACTATGTGAGTCAGAT	Integrated DNA Technologies; This paper	N/A
Ir8a_3HA_FOR: GTTATAGATCACTAGtGTTTCTTGTCGCACCTAATTAACAAGTG	Integrated DNA Technologies; This paper	N/A
Ir8a_3HA_REV: AATTCAGATCACTAGtCATACTTAAGCTCCTTGAGGTCCAGC	Integrated DNA Technologies; This paper	N/A
Ir76b_gRNA_FOR: TCCGGGTGAACTTCGCAGTGATGCGAACTTCATAGTTTTAGAGCTAGAAATAGCAAGTTA	Integrated DNA Technologies; This paper	N/A
Ir76b_gRNA_REV: TTCTAGCTCTAAAACCGGCGGCCCTCTTTCAATACGACGTTAAATTGAAAATAGGTC	Integrated DNA Technologies; This paper	N/A
Ir76b_5HA_FOR: CCCTTACGTAACGCGtACCAATGAATCCTTGTCCATGCTAAA	Integrated DNA Technologies; This paper	N/A
Ir76b_5HA_REV: CGCGGCCCTCACGCGtCTCGGTGTAGCTGTCTTGAAGGAA	Integrated DNA Technologies; This paper	N/A
Ir76b_3HA_FOR: GTTATAGATCACTAGtGCCTAATTGGAATACCTTCTACATAATGGA	Integrated DNA Technologies; This paper	N/A
Ir76b_3HA_REV: AATTCAGATCACTAGtGGCAAGGCACAAAATAAAACGAAG	Integrated DNA Technologies; This paper	N/A
Ir25a_gRNA_FOR: TCCGGGTGAACTTCGCCGGATACTGATTAAAGCGGTTTTAGAGCTAGAAATAGCAAGTTA	Integrated DNA Technologies; This paper	N/A
Ir25a_gRNA_REV: TTCTAGCTCTAAAACAGTGCTCATTTTACCATAATCGACGTTAAATTGAAAATAGGTC	Integrated DNA Technologies; This paper	N/A
Ir25a_5HA_FOR: CCCTTACGTAACGCGtTGCATGACTTCATTGACACCTCAAG	Integrated DNA Technologies; This paper	N/A
Ir25a_5HA_REV: CGCGGCCCTCACGCGtGAAACGAGGCTTAAACGTAGCTGGATATT	Integrated DNA Technologies; This paper	N/A
Ir25a_3HA_FOR: GTTATAGATCACTAGtAATATTATGGTTAAGTGAGCTCTCGG	Integrated DNA Technologies; This paper	N/A
Ir25a_3HA_REV: AATTCAGATCACTAGtCAAAGCTAAGTTCATCGTCATAGAGAC	Integrated DNA Technologies; This paper	N/A
Orco_Seq_FOR: GATGTTCTGCTCTTGGCTGATATTC	Integrated DNA Technologies; This paper	N/A
Ir8a_Seq_FOR: CATCGACTTCATCATCAGGCTTTCG	Integrated DNA Technologies; This paper	N/A
Ir76b_Seq_FOR: CAACGATATCCTCACGAAGAACAAGC	Integrated DNA Technologies; This paper	N/A
Ir25a_Seq_FOR: CGAAAGGATACAAAGGATACTGCAT	Integrated DNA Technologies; This paper	N/A
HACK_Seq_REV: TGTATTCCGTCGCATTTCTCTC	Integrated DNA Technologies; This paper	N/A

IVS-FOR: TGGGTTGGACTCAGGGAATAGATCTAAAAGGTAGGTTCAACCACT	Integrated DNA Technologies; This paper	N/A
EcoRI-SV40-REV: GCTTACGTCAGAATTCAGATCGATCCAGACATGATAAGA	Integrated DNA Technologies; This paper	N/A
Tsp42Ej_FOR: GAGAAGTCGTTTCCCATAACACCCT	Integrated DNA Technologies; This paper	N/A
Tsp42Ej_REV: GAGGAGCAGTTTTCGGAGTCGCCTTC	Integrated DNA Technologies; This paper	N/A
Recombinant DNA		
pHACK-QF2	Addgene; (Lin and Potter, 2016a)	Plasmid# 80274; RRID: Addgene_80274
p10XQUAS-CsChrimson-SV40	This paper	Addgene #TBD
pHACK-QF2^{Orco}	This paper	N/A
pHACK-QF2^{Ir8a}	This paper	N/A
pHACK-QF2^{Ir76b}	This paper	N/A
pHACK-QF2^{Ir25a}	This paper	N/A
Software and Algorithms		
Fiji (ImageJ)	(Schindelin et al., 2012)	https://imagej.net/Fiji
GraphPad Prism 8.0	GraphPad Software	www.graphpad.com
AutoSpike	Syntech	http://www.ockenfels-syntech.com/products/signal-acquisition-systems-2/
LabChart Pro v8	ADInstruments	https://www.adinstruments.com/support/downloads/windows/labchart
Adobe Illustrator CS6	Adobe, Inc.	https://www.adobe.com/products/illustrator.html
Adobe Photoshop CS6	Adobe, Inc.	https://www.adobe.com/products/photoshop.html
MacVector 16.0	MacVector, Inc.	https://macvector.com/
Zen Black	Carl Zeiss Microscopy	https://www.zeiss.com/microscopy/us/products/microscope-software/zen.html
Venn Diagram web tool	VIB / UGent Bioinformatics & Evolutionary Genomics	http://bioinformatics.psb.ugent.be/webtools/Venn/
Amira	Thermo Fisher Scientific	https://www.thermofisher.com/us/en/home/industrial/electron-microscopy/electron-microscopy-instruments-workflow-solutions/3d-visualization-analysis-software/amira-life-sciences-biomedical.html
Q-Capture Pro 7	Teledyne QImaging	https://www.qimaging.com/home

Lead Contact

Further information and requests for resources and reagents should be directed to and will be fulfilled by the Lead Contact, Christopher J. Potter (cpotter@jhmi.edu).

Materials Availability

Fly lines generated in this study have been deposited to Bloomington *Drosophila* Stock Center (Stock #s TBD).

Data and Code Availability

Single-cell RNAseq raw data and preprocessed data are available from NCBI Gene Expression Omnibus (GSE143038). Python codes for figures are available from Github (https://github.com/Hongjie-Li/FlyORN). All other data are available upon request.

Fly Husbandry

Fly stocks were maintained at 20 – 25°C on standard cornmeal-agar food. Male and female flies used for experiments were 3 – 10 days old, unless otherwise noted.

Fly Stocks

Fly lines used in this paper can be found in the Key Resources Table.

Generation of *QUAS-CsChrimson*: the sequence of CsChrimson was PCR amplified from the genomic DNA of *UAS-CsChrimson* flies (Klapoetke et al., 2014) and cloned into the *10XQUAS* vector (Addgene #TBD). Fly line was established through random *P*-element insertion. Cloning was confirmed with Sanger sequencing (Genewiz) before being sent for injection (Rainbow Transgenic Flies, Inc). Primers used for PCR amplification and In-Fusion cloning:

IVS-FOR:

TGGGTTGGACTCAGGGAATAGATCTAAAAGGTAGGTTCAACCACT

EcoRI-SV40-REV:

GCTTACGTCAGAATTCAGATCGATCCAGACATGATAAGA

While performing co-labeling experiments, we discovered that several *OrX-Gal4* lines label multiple glomeruli, and thus do not accurately represent single olfactory sensory neuron classes. These lines were excluded from analyses, and should be used with caution: *Or33c-Gal4* (BDSC# 9966), *Or43b-Gal4* (BDSC# 23894), *Or59b-Gal4* (BDSC# 23897), *Or65a-Gal4* (BDSC# 9994), *Or85a-Gal4* (BDSC# 23133), *Or85b-Gal4* (BDSC# 23911).

Generation of HACK Knock-in Lines

In the HACK technique, the donor construct can be supplied in one of two ways (Fig S1). The first is to inject the HACK construct directly into embryos expressing Cas9 in their germline (direct injection method) (Fig S1D and E). The second approach is to establish transgenic donor lines through random *P*-element insertion or *ΦC31* integration (Bischof et al., 2007; Gloor et al., 1991; Groth et al., 2004) of the construct into the genome, followed by genetic crosses with germline Cas9 flies for generation of the knock-in (cross method)(Fig S1F). Only one (direct injection method) or two (cross method) generations of crosses are required for the creation of a knock-in line (Fig S1E and F). The HACK 3XP3-RFP selection marker is bright but shows positional effects (Fig S2A). Potential knock-in flies can be screened at the adult stage (Fig S2A), or at the larval or pupal stages (Fig S2B). We generated *T2A-QF2* knock-in lines for all four co-receptor genes using the direct injection method. Additionally, we tested the feasibility of the cross approach with two genes: *Orco* and *Ir25a*. Knock-ins were confirmed by PCR genotyping and sequencing (Fig S1A – C), and by crosses to a *QUAS-GFP* reporter to check for expression in the brain. We found no difference in expression pattern in the brain between these two approaches (Fig S2E). After establishing a knock-in line, the 3XP3-RFP marker can be removed via *Cre* recombination (Siegal and Hartl, 1996). This can be useful as 3XP3-RFP is expressed broadly throughout the fly nervous system and can interfere with red fluorescent reporters (Fig S2A-C). We produced two unmarked knock-in lines (for *Orco* and *Ir25a*) and confirmed no difference in brain GFP expression between marked and unmarked lines (Fig S2D).

Both approaches produced knock-ins at high rates (Table S1). Efficiency was calculated as the number of potentially HACKed knock-in flies (RFP+), divided by the total number of flies from the given cross (G_1 or F_2 progeny; see Fig S1D-F). We further calculated the percentage of founders producing knock-in lines, as this gives an indication of effort (how many initial crosses need to be set up to produce a knock-in). The aggregate efficiency rates for a given target locus ranged from 8% for Ir8a to 33% for Orco (Table S1); however, for individual crosses, efficiency rates were as high as 100% (See Supplemental Data 1), meaning that all progeny were potential RFP+ knock-ins. For the two genes for which we created knock-in lines via both direct injection and genetic cross (*Orco* and *Ir25a*), we found efficiency rates comparable between approaches (*Orco*: 33% for direct injection, 28% for cross; *Ir25a*: 23% for direct injection, 24% for cross). For the direct injection approach, we tested 51 independent knock-in lines across the four target genes and found 100% to be correctly targeted events (Table S1). However, for the genetic cross approach, of the 32 independent knock-in lines tested for the two target genes, 6 (~19%) had the HACK RFP eye marker, but did not have *QF2*-driven GFP expression in the brain.

Information on plasmid construction can be found in below. All *Drosophila* embryo injections were performed by Rainbow Transgenic Flies, Inc. (Camarillo, CA). For HACKing via genetic cross, *Orco-T2A-QF2*^{HACK} and *Ir25a-T2A-QF2*^{HACK} constructs were injected into w^{1118} flies for *P*-element insertion, and donor lines were established on the second or third chromosomes by crossing to double balancers (see Key Resources Table). Donor lines were then crossed to *Vas-Cas9* (BDSC# 51323). Knock-in lines were established from *cis*-chromosomal HACK (donor line on same chromosome as target gene) (Lin and Potter, 2016a). For HACKing via direct injection, knock-in constructs were injected into the following lines: *Vas-Cas9* (BDSC# 51324) for *Ir8a*; *Act5C-Cas9* (BDSC# 54590) for *Orco*, *Ir76b*, and *Ir25a*. The following lines were used to verify knock-in expression: *QUAS-mCD8::GFP* (BDSC# 30003), *10XQUAS-6XGFP* (BDSC# 52264). Knock-in lines were confirmed by PCR genotyping (Phusion, NEB) and Sanger sequencing (Genewiz). Unmarked *Orco-T2A-QF2*^{HACK} and *Ir25a-T2A-QF2*^{HACK} knock-in lines were generated by crossing RFP+ knock-in flies to the Crey+1B fly line (see Key Resources Table) (Siegal and Hartl, 1996).

Plasmid Construction

The construction of *QF2*$^{X\text{-}HACK}$ knock-in constructs requires three steps of cloning, as previously described (Lin and Potter, 2016a). All knock-in constructs were created using the *pHACK-QF2* plasmid (Addgene #80274) as the backbone. The backbone was digested with the following enzymes for cloning: *MluI* for the 5' homology arms; *SpeI* for the 3' homology arms; and *BbsI* for the gRNAs. All cloning was performed using In-Fusion Cloning (Clontech #639645). The homology arms were PCR amplified from genomic DNA extracted from *wildtype* flies using the DNeasy Blood and Tissue Kit (Qiagen #69506), while the gRNAs were PCR amplified using the *pHACK-QF2* backbone as a template, with the primers themselves containing the gRNA target sequences. All homology arms were approximately 1 kb (Orco: 5HA = 1012 bp, 3HA = 1027 bp; Ir8a: 5HA = 1027 bp, 3HA = 1079 bp; Ir76b: 5HA = 997 bp, 3HA = 956 bp; Ir25a: 5HA = 1119 bp, 3HA = 990 bp). gRNAs were selected by analyzing the region around the stop codon of each gene using an online tool (https://flycrispr.org/) (Gratz et al., 2014). When possible, gRNAs were chosen to minimize potential off-target cleavage sites (zero predicted for *Orco*, *Ir8a*, and *Ir76b*; one predicted for *Ir25a*, discussed below). They were selected such that: one gRNA targeted upstream of the stop codon, within the last exon of the gene; the second gRNA targeted downstream of the stop codon, within the 3'UTR; and, the two gRNAs were <100 bp apart. In order to prevent the gRNAs from targeting the homology arms, three synonymous nucleotide substitutions were made in each homology arm. The final knock-in lines did not always have all three substitutions (see Fig S1), possibly due to PCR or HDR error. Note that due to the way the primers are designed, each targeted gene loses a small portion of its native 3'UTR (Orco = 72 bp, Ir8a = 31 bp, Ir76b = 27 bp, Ir25a = 24 bp). Cloning was confirmed with Sanger sequencing (Genewiz) before being sent for injection (Rainbow Transgenic Flies, Inc).

gRNAs (PAM):

Orco:

CTGCACCAGCACCATAAAGT (AGG)

GCACAGTGCGGAGGGGGCAA (GGG)

Ir8a:

GTTTGTTTGTTCGGCCATGT (TGG)

GGTGCCTCTGACTCCCACAG (TGG)

Ir76b:

GCAGTGATGCGAACTTCATA (TGG)

GTATTGAAAGAGGGCCGCCG (AGG)

Ir25a:

GCCGGATACTGATTAAAGCG (CGG)

ATTATGGTAAAATGAGCACT (CGG)

PRIMERS

Italics = In-Fusion cloning 15 b.p. overhang; **bold** = gRNA; lowercase = adding back restriction site; underline = synonymous substitution to prevent Cas9 targeting of donor construct.

PCR Primers for Cloning:

Orco_gRNA_FOR:
*TCCGGGTGAACTTC***GCACAGTGCGGAGGGGGCAA**GTTTTAGAGCTAGAAATAGCAAGTTA

Orco_gRNA_REV:
*TTCTAGCTCTAAAAC***ACTTTATGGTGCTGGTGCAG**CGACGTTAAATTGAAAATAGGTC

Orco_5HA_FOR:

*CCCTTACGTAACGCG*tCAGCTTGTTTGACTTACTTGATTAC

Orco_5HA_REV:

*CGCGGCCCTCACGCG*tCTTGAGCTGTACAAGTACCATAAAGT

Orco_3HA_FOR:

*GTTATAGATCACTAG*tCTCAGTACTATGCAACCAGCAATA

Orco_3HA_REV:

*AATTCAGATCACTAG*tGTTTTATGAAAGCTGCAAGAAATAA

Ir8a_gRNA_FOR:
*TCCGGGTGAACTTCG***TTTGTTTGTTCGGCCATGT**GTTTTAGAGCTAGAAATAGCAAGTTA

Ir8a_gRNA_REV:
*TTCTAGCTCTAAAAC***CTGTGGGAGTCAGAGGCAC**CGACGTTAAATTGAAAATAGGTC

Ir8a_5HA_FOR:

*CCCTTACGTAACGCG*tCTATTGGCTATTCGTCGTACTCATGC

Ir8a_5HA_REV:

*CGCGGCCCTCACGCG*tCTCCATGTAGCCACTATGTGAGTCAGAT

Ir8a_3HA_FOR:

*GTTATAGATCACTAG*tGTTTCTTGTCGCACCTAATTAACAAGTG

Ir8a_3HA_REV:

*AATTCAGATCACTAG*tCATACTTAAGCTCCTTGAGGTCCAGC

Ir76b_gRNA_FOR:
*TCCGGGTGAACTTCG***CAGTGATGCGAACTTCATA**GTTTTAGAGCTAGAAATAGCAAGTTA

Ir76b_gRNA_REV:
*TTCTAGCTCTAAAAC***CGGCGGCCCTCTTTCAATAC**GACGTTAAATTGAAAATAGGTC

Ir76b_5HA_FOR:

*CCCTTACGTAACGCG*tACCAATGAATCCTTGTCCATGCTAAA

Ir76b_5HA_REV:

*CGCGGCCCTCACGCG*tCTCGGTGTAGCTGTCTTGAAGGAA

Ir76b_3HA_FOR:

*GTTATAGATCACTAG*tGCCTAATTGGAATACCTTCTACATAATGGA

Ir76b_3HA_REV:

*AATTCAGATCACTAG*tGGCAAGGCACAAAATAAAACGAAG

Ir25a_gRNA_FOR:
*TCCGGGTGAACTTC***GCCGGATACTGATTAAAGCG**GTTTTAGAGCTAGAAATAGCAAGTTA

Ir25a_gRNA_REV:
*TTCTAGCTCTAAAAC***AGTGCTCATTTTACCATAAT**CGACGTTAAATTGAAAATAGGTC

Ir25a_5HA_FOR:

*CCCTTACGTAACGCG*tTGCATGACTTCATTGACACCTCAAG

Ir25a_5HA_REV:

*CGCGGCCCTCACGCG*tGAAACGAGGCTTAAACGTAGCTGGATATT

Ir25a_3HA_FOR:

*GTTATAGATCACTAG*tAATATTATGGTTAAGTGAGCTCTCGG

Ir25a_3HA_REV:

*AATTCAGATCACTAG*tCAAAGCTAAGTTCATCGTCATAGAGAC

Genotyping and Sequencing Primers (PCR fragment size):

Orco_Seq_FOR (~2kb):

GATGTTCTGCTCTTGGCTGATATTC

Ir8a_Seq_FOR (~1.9kb):

CATCGACTTCATCATCAGGCTTTCG

Ir76b_Seq_FOR (~1.9kb):

CAACGATATCCTCACGAAGAACAAGC

Ir25a_Seq_FOR (~1.9kb):

CGAAAGGATACAAAGGATACTGCAT

HACK_Seq_REV (same for all):

TGTATTCCGTCGCATTTCTCTC

Checking for Off-target Effects

One of the gRNAs for *QF2*$^{Ir25a\text{-}HACK}$ had one predicted potential off-target cut site in the genome, in the *tetraspanin 42ej* (*Tsp42Ej*) gene. We sequenced this locus in the *Ir25a-T2A-QF2*^{HACK} knock-in line and compared the sequence to our *wildtype* lab stock. We found no evidence of indels in the knock-in line. Primers used:

Tsp42Ej_FOR:

GAGAAGTCGTTTCCCATAACACCCT

Tsp42Ej_REV:

GAGGAGCAGTTTTCGGAGTCGCCTTC

HACK Marker Screening

Adult flies were anaesthetized on a CO_2 pad and screened in one of two ways: either with a Nightsea Stereo Microscope Fluorescence Adapter with the green SFA-GR LED light source (Nightsea LLC, Lexington, MA) and viewed with a Zeiss Stemi SV6 stereo microscope; or illuminated with an X-Cite 120Q excitation light source and viewed with a Zeiss SteREO Discovery V8 microscope equipped with a ds-Red filter.

Whole Animal Imaging

Whole adults were anaesthetized on ice before imaging. Whole larvae, pupae, or freshly dissected adult heads were affixed to slides with clear nail polish before imaging. All animals were imaged on an Olympus SZX7 microscope equipped with GFP and RFP filters. Animals were illuminated with an X-Cite Series 120Q light source. Images were acquired using a QImaging QIClick Cooled digital CCD camera and Q-Capture Pro 7 software. Multiple images were taken at different focal planes and then merged in Photoshop (CS6). Gain was adjusted in Fiji. Images appear in the following figures/panels: Fig 2B, Fig 3A and E, Fig 4A, Fig S2A-B, Fig S4B.

Immunohistochemistry

All flies were used at 3- to 10-days old. Apart from the cryosection protocol, all immunostaining steps were done on a nutator. All steps involving or following the addition of fluorescently conjugated secondary antibodies were done in the dark.

Brain and ventral nerve cord (VNC) staining was performed as in (Xie et al., 2018). Tissue was dissected in PBS and then fixed for 20 minutes at room temperature (RT) in 4% paraformaldehyde in PBT (1XPBS with 0.3% Triton X-100). After fixation, tissue was quickly rinsed three times with PBT, then put through three longer washes in PBT at RT (at least 15 minutes each). Tissue was blocked in PBT + 5% normal goat serum (NGS) at RT for at least 30 minutes, then transferred to block + primary antibody solution, and incubated at 4°C in primary antibodies for 1-2 days. Tissue was then washed three times with PBT at RT (at least 15 minutes per wash) and incubated in secondary antibody solution in block at 4°C for 1 day. Tissue was washed three final times with PBT at RT for at least 15 minutes each times, then mounted in SlowFade gold (Thermo Fisher Scientific #S36936). For experiments in which the 10XQUAS-6XGFP or 20XUAS-6XGFP reporters were used, the endogenous, unstained GFP signal was visualized, and no secondary green antibodies were used. Primary antibodies used: mouse anti-nc82 (DSHB, 1:25), rat anti-mCD8 (Thermo Fisher #14-0081-82, 1:200). Secondary antibodies used: Cy3 goat anti-rat (Jackson ImmunoResearch #112-165-167, 1:200), Cy3 goat anti-mouse (Jackson ImmunoResearch #115-165-166, 1:200), Alexa 647 goat anti-rat (Jackson ImmunoResearch #112-605-167, 1:200), Alexa 647 goat anti-mouse (Jackson ImmunoResearch #115-605-166, 1:200).

Whole-mount staining of maxillary palps was performed according to the brain staining protocol above, with the exception of a shorter fixation step (15 minutes). Primary antibodies used: rabbit anti-Ir25a (gift from Richard Benton, University of Lausanne, 1:100), rabbit anti-Orco (gift from Leslie Vosshall, Rockefeller University, 1:100), rat anti-elav (DSHB, 1:100). Secondary antibodies used: Cy3 goat anti-rabbit (Jackson ImmunoResearch #111-165-144, 1:200), Alexa 647 goat anti-rabbit (Jackson ImmunoResearch #111-605-144, 1:200).

The cryosection protocol was adapted from (Spletter et al., 2007). Fly heads were dissected and lined up in cryomolds (Tissue-Tek #4565), covered with OCT compound (Tissue-Tek #4583), and frozen at -80°C. Samples were sectioned at ~12 µm on a Microm HM 500 cryostat (Microm International GmbH, Walldorf, Germany) and collected on SuperFrost Plus slides (Fisher #12-550-15). Slides were stored at -80°C until further processing. Slides were fixed at RT for 15 minutes in 4% paraformaldehyde in PBT (1XPBS with 0.3% Triton X-100), washed three times in PBT at RT (15 minutes each), blocked at RT for at least 30 minutes in PBT + 5% NGS, then incubated overnight at 4°C in primary antibodies in fresh block solution in a special humidified chamber. On the next day, slides were washed three times (15 minutes each) with PBT at RT, and then incubated in secondary antibodies in block at 4°C overnight in the same humidified chamber covered in foil. Finally, slides were washed three times (15 minutes each) with PBT at RT and mounted in SlowFade gold (Thermo Fisher Scientific #S36936). Primary antibodies used: rabbit anti-Ir25a (gift from Richard Benton, University of Lausanne, 1:1000), rabbit anti-Orco (gift from Leslie Vosshall, Rockefeller University, 1:1000). Secondary antibodies used: Cy3 goat anti-rabbit (Jackson ImmunoResearch #111-165-144, 1:200), Alexa 647 goat anti-rabbit (Jackson ImmunoResearch #111-605-144, 1:200).

Confocal Imaging and Analysis

Brains, ventral nerve cords, maxillary palps, and antennal cryosections were imaged on a Zeiss LSM 700 confocal microscope equipped with Fluar 10x/0.50 air M27, LCI Plan-Neofluar 25x/0.8 water Korr DIC M27, and C-Apochromat 63x/1.2 water Korr M27 objectives. Images were acquired at 512 x 512-pixel resolution with 0.58, 2.37 or 6.54 µm z-steps for each objective, respectively. For illustration purposes, confocal images were processed in either the native Zen Black software (Fig 2D) or Fiji/ImageJ (all other images) to collapse Z-stacks into a single image using maximum intensity projection. Where noted, single slices or partial z projections were used as opposed to full stacks. For co-labeling experiments, Fiji was used to convert red LUTs to orange for a colorblind-friendly palette. Similarly, in Fig S2C, Fiji was used to convert magenta LUT to blue for clarity. Fiji was also used to adjust the gain in separate channels; no other image processing was performed on the confocal data. For Fig 7A, glomeruli were assigned to the categories strong, intermediate, and weak by visual inspection of the strength of their innervation compared to the previously reported glomeruli for each respective knock-in line. Strong glomeruli generally have similar brightness/intensity of GFP signal as most of the originally reported glomeruli for the given knock-in line.

Magnification used:

10X: Fig 1D (Brain), Fig S2C

25X: Fig S2F, Fig S2D-E, Fig S4A

63X: Fig 2C-E, Fig 3B-D and F-G, Fig 4B-D, Fig 5A-B, Fig S5, Fig S7

Basiconic Single Sensillum Recordings

The glass recording electrode was filled with Beadle-Ephrussi Ringer's solution (7.5g of NaCl + 0.35g of KCl + 0.279g of $CaCl_2$-$2H_2O$ in 1L H_2O). Extracellular activity was recorded by inserting the glass electrode into the shaft or base of the sensillum of 3- to 10-day-old flies (unless otherwise specified in the young *Orco*^{2} mutant experiments). A tungsten reference electrode was inserted into the fly eye. Signals were amplified 100X (USB-IDAC System; Syntech, Hilversum, the Netherlands), inputted into a computer via a 16-bit analog-digital converter and analyzed off-line with AUTOSPIKE software (USB-IDAC System; Syntech). The low cutoff filter setting was 50 Hz, and the high cutoff was 5 kHz. Stimuli consisted of 1000 ms air pulses passed over odorant sources. The Δ spikes/second was calculated by counting the spikes in a 1000 ms window from ~500 ms after odorant stimuli were triggered, subtracting the spikes in a 1000 ms window prior to each stimulation. For ab3 recordings from *wildtype*, *Orco*^{2} mutant, and *Ir25a*^{2} mutant flies, spikes were counted in a 500 ms window from the start of the response, then multiplied by 2 to calculate the Δ spikes/second. Stimuli used: mineral oil (Sigma CAS #8042-47-5), ethyl acetate (Sigma CAS #141-78-6), pentyl acetate (Sigma CAS #628-63-7), benzaldehyde (Sigma CAS #100-52-7), ethyl butyrate (Sigma CAS #105-54-4), hexanol (Sigma CAS #111-27-3), e2-hexenal (Sigma CAS #6728-26-3), geranyl acetate (Sigma CAS # 105-87-3), 2-heptanone (Sigma CAS # 110-43-0), 1-octen-3-ol (Sigma CAS #3391-86-4), 2,3-butanedione (Sigma CAS #431-03-8), phenylacetaldehyde (Sigma CAS # 122-78-1), phenethylamine (Sigma CAS # 64-04-0), propionic acid (Sigma CAS #79-09-4), 1,4-diaminobutane (Sigma CAS #110-60-1), pyrrolidine (Sigma CAS #123-75-1), p-cresol (Sigma CAS #106-44-5), and methyl salicylate (Sigma CAS #119-36-8). Odorants were dissolved in mineral oil at a concentration of 1%, and 20 µl of solution was pipetted onto filter paper in a glass Pasteur pipette. Stimuli were delivered by placing the tip of the Pasteur pipette through a hole in a plastic pipette (Denville Scientific Inc, 10ml pipette) that carried a purified continuous air stream (8.3 ml/s) directed at the antenna or maxillary palp. A solenoid valve (Syntech) diverted delivery of a 1000 ms pulse of charcoal-filtered air (5 ml/s) to the Pasteur pipette containing the odorant dissolved on filter paper. Fresh odorant pipettes were used for no more than 5 odorant presentations. *Ir25a*^{2} and *Orco*^{2} mutant fly lines were outcrossed into the *w*^{1118} *wildtype* genetic background.

Coeloconic Single Sensillum Recordings

Coeloconic SSR was performed similarly as for basiconic sensilla. 3-5-day old female flies were wedged in the tip of a 200 µl pipette, with the antennae and half the head exposed. A tapered glass electrode was used to stabilize the antenna against a coverslip. A BX51WI microscope (Olympus) was used to visualize the prep, which was kept under a 2,000mL/min humidified and purified air stream. A borosilicate glass electrode was filled with sensillum recording solution (Kaissling and Thorson, 1980) and inserted into the eye as a reference electrode. An aluminosilicate glass electrode was filled with the same recording solution and inserted into individual sensilla. Different classes of coeloconic sensilla were identified by their known location on the antenna and confirmed with their responses to a small panel of diagnostic odors. No more than 4 sensilla per fly were recorded. Each sensillum was tested with multiple odorants, with a rest time of at least 10s between applications. The odorants used were acetic acid (Fisher, 1%, CAS# 64-19-7), ammonium hydroxide (Fisher, 0.1%, CAS# 7664-41-7), cadaverine (Sigma-Aldrich, 1%, CAS# 462-94-2), hexanol (ACROS Organics, 0.001%, CAS# 111-27-3), 2,3-butanedione (ACROS Organics, 1%, CAS# 431-03-8), phenethylamine (ACROS Organics, 1%, CAS# 64-04-0), propanal (ACROS Organics, 1%, CAS# 123-38-6), and 1,4-diaminobutane (ACROS Organics, 1%, CAS# 110-60-1). Odorants were diluted in water or paraffin oil. Odorant cartridges were made by placing a 13 mm antibiotic assay disc (Whatman) into a Pasteur pipette, pipetting 50 µl odorant onto the disc, and closing the end with a 1 mL plastic pipette tip. Each odorant cartridge was used a maximum of four times. The tip of the cartridge was inserted into a hole in the main airflow tube, and odorants were applied at 500mL/min for 500ms. Delivery was controlled via LabChart Pro v8 software (ADInstruments), which directed the opening and closing of a Lee valve (02-21-08i) linked to a ValveBank 4 controller (AutoMate Scientific). Extracellular action potentials were collected with an EXT-02F amplifier (NPI) with a custom 10X head stage. Data were acquired and AC filtered (300-1,700 Hz) at 10kHz with a PowerLab 4/35 digitizer and LabChart Pro v8 software. Spikes were summed in coeloconic recordings due to their similar sizes, and they were counted over a 500 ms window, starting at 100 ms after stimulus onset. Solvent corrected responses were calculated as the number of odor evoked spikes subtracting the number of solvent evoked spikes.

Optogenetics

Ir25a-T2A-QF2^{HACK} was crossed to *QUAS-CsChrimson* #11C and double balanced to establish a stable stock (*Ir25a-T2A-QF2*^{HACK}*/CyO; QUAS-CsChrimson* #11C/*TM6B)*. Newly eclosed flies (age < 1 day old) were transferred to fly vials containing 0.4 mM all trans-retinal in fly food (Sigma-Aldrich #R2500, dissolved in pure DMSO with stock concentration of 0.4 M). Vials with flies were kept in the dark for at least 4 days before experiments. 627nm LED light source (1-up LED Lighting Kit, PART #: ALK-1UP-EH-KIT) powered by an Arduino Uno (www.arduino.cc/en/Main/ArduinoBoardUno) was used to activate CsChrimson. By setting the voltage to 2V and the distance of the light source to 20 cm between the LED and the fly antenna, the light intensity was equivalent to 1.13 W/m^2. The antenna was stimulated for 500 ms followed by 5 s of recovery period for the total recording length of 20 s (3 stimulations). The identity of ab2 and ab3 sensilla were first verified with 1% ethyl acetate (Sigma #270989), and 1% pentyl acetate (Sigma #109584) before optogenetic experiments. Identification of ab9 sensilla was assisted by fluorescence-guided Single Sensillum Recording (fgSSR) (Lin and Potter, 2015) using *Or67b-Gal4* (BDSC #9995) recombined with *15XUAS-IVS-mCD8::GFP* (BDSC #32193).

Single-cell RNA-sequencing and Analysis

Dataset analyzed in this paper was published in (Li et al., 2020). Briefly, third antennal segments from *Drosophila* pupae 48 hours after puparium formation (APF) were dissected from specific Gal4 lines driving GFP expression in olfactory sensory neuron (OSN) subpopulations. Single-cell suspensions were then prepared from these antennae and FACS sorted. RNA was reverse-transcribed using SMART-seq2, and sequencing libraries were prepared using tagmentation (Nextera XT). Sequencing was done using Illumina Nextseq 500 with paired-end 75 bp reads. After sequence alignment to the *Drosophila* genome, gene counts were rescaled to counts per million (CPM) to normalize for variability in sequencing depth across cells. Analyses were done using principal component analysis (PCA), t-distributed Stochastic Neighbor Embedding (tSNE), and a custom machine learning algorithm called Iterative Clustering for Identifying Markers (ICIM) (Li et al., 2020).

The scRNAseq results were generally consistent with the *Ir25a-T2A-QF2*^{HACK} > *GFP* labeling in the antennal lobes: clusters with high proportions of Ir25a+ cells in the scRNAseq dataset tended to have glomeruli that were strongly labeled by the knock-in, such as the V glomerulus (Fig 5A, third row), and the VA2 glomerulus (fourth row). Conversely, clusters with few Ir25a+ cells tended to correspond to glomeruli weakly labeled or not labeled by the knock-in; intermediate clusters corresponded to weak or intermediate glomerular labeling (see Supplemental Data 3). There were two interesting exceptions to this trend. Clusters with the lowest proportions of Ir25a+ cells, such as clusters 12 (DM3) and 17 (VM3), corresponded to glomeruli not labeled by the knock-in, as expected. However, the cluster with the lowest proportion of Ir25a+ cells (cluster 5)

corresponded to a glomerulus that was labeled by the *Ir25a-T2A-QF2*^{HACK} knock-in (DA1), albeit weakly. Conversely, one cluster with a very high proportion of Ir25a+ cells (cluster 18) corresponded to a glomerulus which had consistent, but generally weak, GFP expression driven in the knock-in (DM4).

Quantification and Statistical Analysis

Cell Counting

To quantify knock-in co-expression with the corresponding antibody in the maxillary palps (Fig 2C and Fig 4D), the 3D reconstruction software Amira (FEI, Oregon, USA) was used to manually mark individual cell bodies throughout the z-stack in each channel (antibody in far red channel, knock-in in green channel) and inspect whether each labeled cell were present in one channel or both. For palp neurodegeneration experiments (Fig S7), elav+ cells were counted manually in Fiji (ImageJ).

Statistics

All statistical analyses on SSR recordings (Fig 6 and Fig S3) and maxillary palp neurodegeneration experiments (Fig S7) were done in GraphPad Prism (version 8). For all statistical analyses, significance level $\alpha = 0.05$. The following analyses were performed on all basiconic SSR data: within genotype, Kruskal-Wallis test with uncorrected Dunn's to determine which odorant responses were significantly different from mineral oil control; between genotype, Mann-Whitney *U* to compare responses of two genotypes to the same odorant (*wildtype* vs *Ir25a*^{2} mutant, or *wildtype* versus *Orco-T2A-QF2*^{HACK} knock-in). Summary tables in Fig 6D and Fig 6H are filled in based on the following criteria: no response means neither *wildtype* nor *Ir25a*^{2} mutant odor-evoked activity for given odorant was significantly different from its respective mineral oil control, nor was the difference between the genotypes statistically significant; no difference means that either *wildtype* or mutant or both had a significantly different odor-evoked response to the stimulus compared to mineral oil control, but the difference between the two genotypes was not statistically significant; higher response (in either *wildtype* or mutant) means that there was a statistically significant difference between genotypes for the given odorant. This could mean that: a) one genotype did not have a response, while the other did; b) both genotypes had a response, and one was higher; c) responses are different from each other, but not from their respective mineral oil controls; or d) neural activity was inhibited by the odorant in one genotype compared to mineral oil control, and either not inhibited in the other genotype, or inhibited to a lesser degree.

In the *Ir8a-T2A-QF2*^{HACK} knock-in, we recorded from coeloconic ac2 sensilla, which have one Ir8a+ neuron and two Ir25a+ neurons. We compared the odor-evoked activity of these neurons to *wildtype* ac2 in response to a panel of known ligands for Ir8a+ and Ir25a+ neurons, such as acids and amines, respectively (Abuin et al., 2011). Due to the difficulty of distinguishing individual neuronal responses in coeloconic sensilla (as seen in Fig S3C), responses of all neurons to a given stimulus were summed. The following analyses were performed on the coeloconic SSR data: two-way ANOVA with Sidak's post-hoc test to compare responses between *wildtype* and *Ir8a-T2A-QF2*^{HACK} knock-in flies across stimuli. There was a significant difference in responses between the two genotypes to one odorant, cadaverine, which elicited a higher response in the *wildtype* (Fig S3D). Cadaverine is typically considered an Ir25a-dependent odorant (Silbering et al., 2011); we found no difference in the responses of the two genotypes to the Ir8a-dependent odorants (Fig S3D; see also Supplemental Data 2). This suggests that the decreased response to cadaverine in the *Ir8a-T2A-QF2*^{HACK} knock-in line may be the result of genetic background, as opposed to a deficit induced by *T2A-QF2* knock-in.

In Fig 6I, stimulus responses which were statistically significantly different from mineral oil control were those whose Δ spike values were zero, due to the fact that the mineral oil control Δ spike value was non-zero (median = 1.2, range = 0 to 2). Because of this, we did not deem these differences as biologically relevant. Nevertheless, *p* values are reported in the figure legend of Fig 6, and detailed information can be found in Supplemental Data 2.

For neurodegeneration experiments, one-way ANOVA with Tukey's HSD post-hoc test was used to compare elav+ cell counts across both genotypes at the three timepoints.

Box plots were made using GraphPad Prism; bar graphs were made in Microsoft Excel.

SUPPLEMENTAL INFORMATION

Supplemental Figures

Figure S1. Confirmation of HACK knock-ins and crossing schematics. Related to Figure 2.

Figure S2. HACK marker expression and approach comparison. Related to Figure 2.

Figure S3. *T2A-QF2* HACK knock-in does not affect *Orco* function. Related to Figure 2.

Figure S4. Knock-in expression in the adult ventral nerve cord and in larva. Related to Figures 2, 3, and 4.

Figure S5. Transgenic co-receptor *Gal4* lines do not fully recapitulate knock-in expression. Related to Figures 2, 3, and 4.

Figure S6. Electrophysiological experiments to examine *Ir25a* expression and function in Orco+ neurons. Related to Figures 4 and 6.

Figure S7. Olfactory neurons lacking functional *Orco* degenerate in the maxillary palps. Related to Figure 6.

Table S1. Summary of HACK Knock-in Efficiency. Related to Figure 2.

Table S2. Validation of *Orco-T2A-QF2*^{HACK} knock-in expression in the maxillary palps. Related to Figure 2.

Table S3. Validation of *Ir25a-T2A-QF2*^{HACK} knock-in expression in the maxillary palps. Related to Figure 4.

Table S4. Summary of Expression Patterns for All Knock-in Lines. Related to Figures 2 – 5.

Supplemental Data

Supplemental Data 1. HACK knock-in screen and analyses.

Supplemental Data 2. Single Sensillum Recordings and analyses.

Supplemental Data 3. scRNAseq cell counts and correspondence to *Ir25a-T2A-QF2*^{HACK} knock-in.

Supplemental Data 4. Antennal lobe analyses.

Supplemental Data 5: Palp neurodegeneration analyses.

Supplemental Data 6: Example images of all glomeruli.

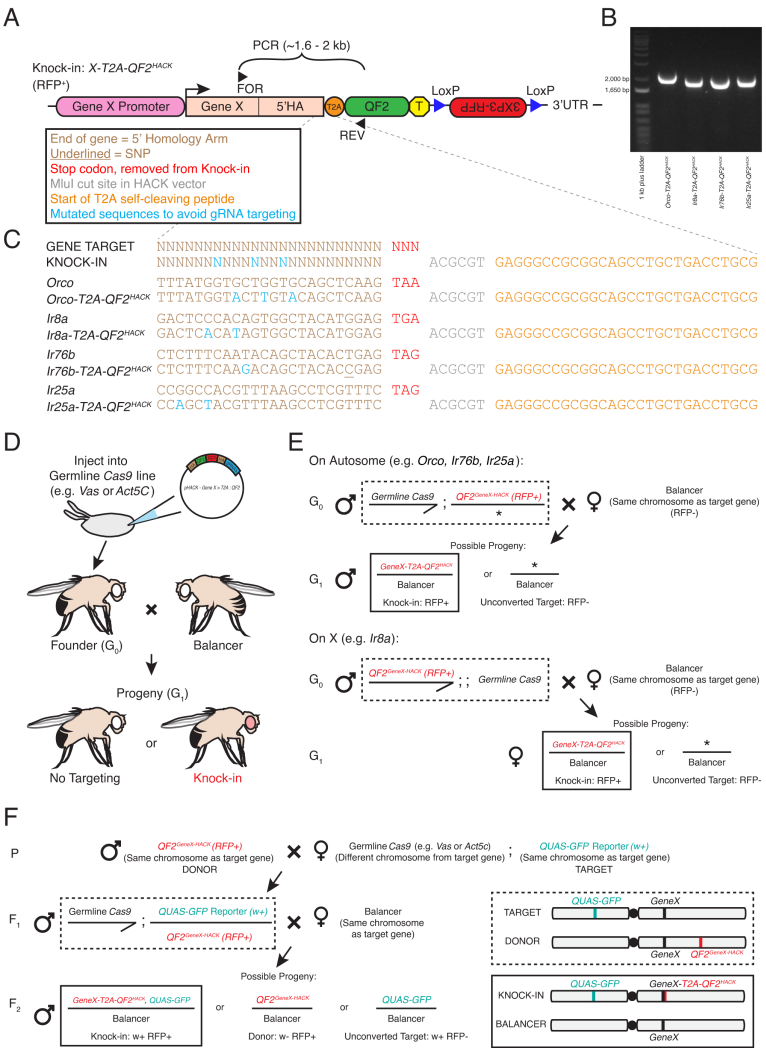

Figure S1. Confirmation of HACK knock-ins and crossing schematics. Related to Figure 2.

A. Schematic of targeted gene. Each knock-in line is generated by CRISPR-Cas9 mediated homology-directed insertion of a *T2A-QF2* cassette marked by RFP in front of the translational stop codon of the target gene. The 5' homology arm (5'HA) is ~1kb of the gene just before the stop codon. Successful knock-in lines were confirmed using forward primers upstream of the 5'HA (FOR), and a reverse primer within the *QF2* sequence (REV). Amplification of a ~1.6 to 2 kb sequence occurs only if a knock-in is present. See Fig 2A for target and donor construct schematics. **B.** PCR genotyping using the primers shown in (A) confirms successful knock-in of the four targeted genes. **C.** Knock-ins were confirmed with sequencing of the targeted genomic site. For each co-receptor, the first line shows the target sequence (based on the FlyBase reference genome[130]), and the second line shows the verified sequence of the knock-in. The stop codon (red) has been replaced with the HACK *T2A-QF2* cassette. The portion shown here includes the *MluI* restriction site used for cloning the 5'HA (grey), as well as the start of the *T2A* sequence (orange). In each knock-in construct, synonymous substitutions (blue) have been made to prevent the gRNA/Cas9 from cutting the donor construct. Each knock-in construct was designed with three substitutions. The underlined base pair in the *Ir76b* knock-in is a SNP discovered in the lab wildtype stock and considered when designing the knock-in construct. **D.** Schematic of the direct injection method to generate a HACK knock-in. The HACK KI construct is injected into a germline Cas9 expressing embryo (both *Act5C-Cas9* and *Vas-Cas9* yielded successful knock-ins; see Methods for more details). This approach requires one genetic cross to generate a knock-in: injected founder flies (G_0) are individually crossed to balancer flies, and progeny (G_1) are screened for the RFP knock-in marker. Each RFP+ G_1 represents an independent knock-in event; thus, single RFP+ flies are used to establish knock-in lines. **E.** Details of the genetic crosses used to establish knock-in lines for each target gene using the direct injection approach. For genes on autosomes (*Orco* and *Ir76b*, 3rd chromosome; *Ir25a*, 2nd chromosome), a *Cas9* line on the X chromosome was used, and RFP+ male progeny selected to remove the *Cas9* after successful HACKing. For *Ir8a* on the X chromosome, a *Cas9* line on the 3rd chromosome was used which was marked with GFP to facilitate its removal in subsequent generations. In addition to RFP marker screening, PCR genotyping, and sequencing, knock-in lines were confirmed by crossing to a *QUAS* reporter line and checking brain expression, either at the G_2 stage, or by crossing G_0 flies to balanced reporter lines to immediately check G_1 brain expression. **F.** Details of using the crossing method to generate HACK knock-ins. This involves the creation of donor lines, in which the HACK targeting construct is inserted into the genome, such as through *P*-element insertion or *ΦC31* integration. Donor lines are crossed to a germline *Cas9* line (Parental). The progeny, F_1, have all the components necessary for a knock-in to occur (gRNAs, Cas9, HDR cassette). An additional cross is required to select germline HACKing events at the F_2 generation. Because the donor lines also express RFP, as do the knock-ins, the target chromosome must be marked with a different marker (such as w+) for knock-in selection (see chromosome schematics at the right, illustrating the locations of the genetic elements in the F_1 and F_2 generations). F_2 knock-ins will have both markers (in this case, RFP+ w+), while donor flies will only have one (RFP+ w-). The cross approach was tested with two of the four genetic targets (*Orco* and *Ir25a*) and successfully produced knock-in lines for both. However, the cross approach can produce false positives (see Table S1 and Suppl Data 1) and is more time consuming. The direct injection approach is recommended for generation of targeted knock-ins.

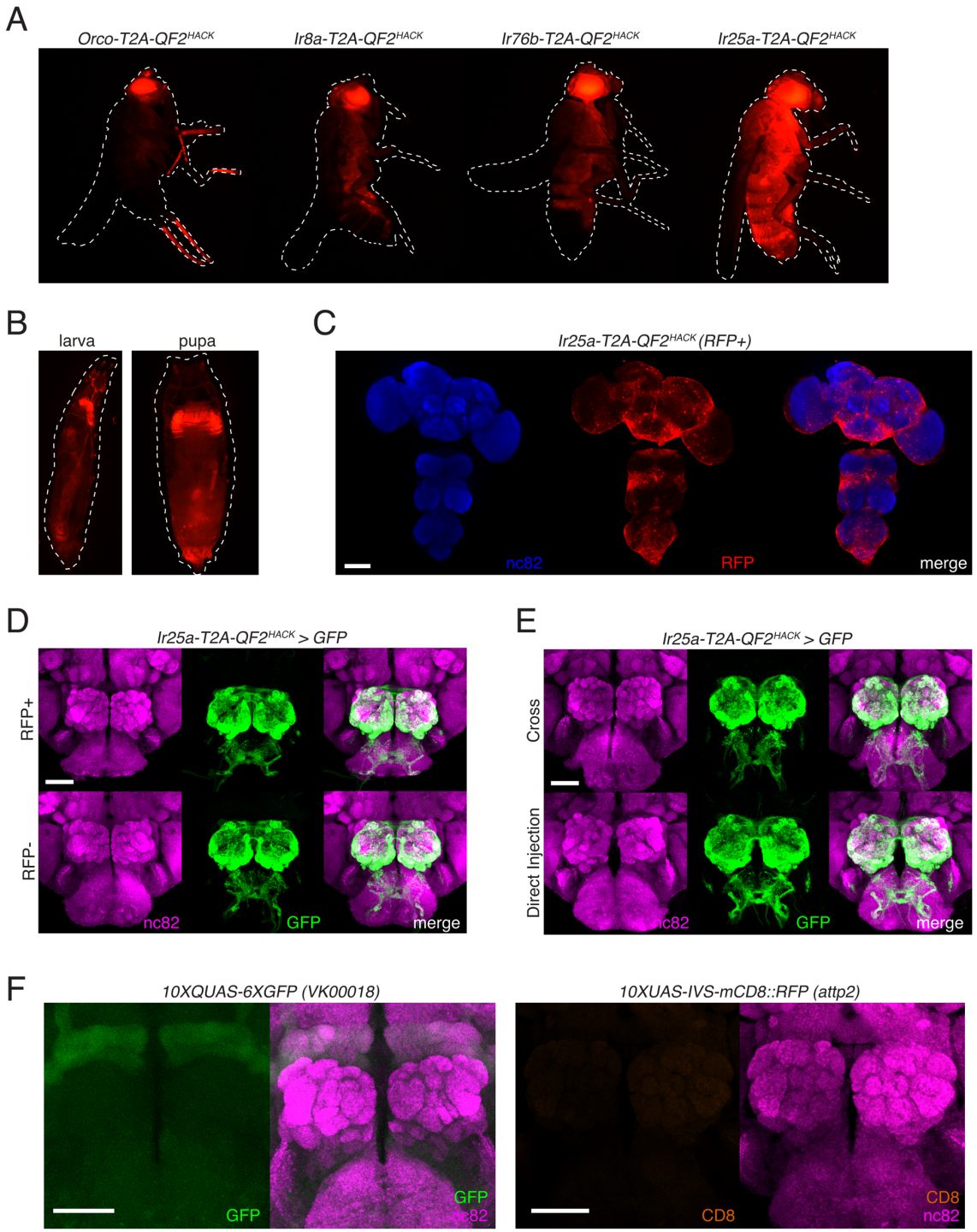

Figure S2. HACK marker expression and approach comparison. Related to Figure 2.
A. The HACK *3XP3-RFP* marker is expressed in the eyes and broadly throughout the fly nervous system and is subject to positional effects in expression. **B.** Knock-in screening can also be performed at the larval (left) and pupal (right) stages. **C.** The *3XP3-RFP* marker is expressed throughout the adult fly brain and ventral nerve cord. Nc82 channel has been pseudo-colored blue for clarity. **D.** The marker cassette is flanked by *loxP* sites and can be removed through *Cre* recombination[119] (see Methods for details). The *3XP3-RFP* marker does not affect knock-in expression. *Ir25a-T2A-QF2*^{HACK}-driven GFP expression in the brain was similar before (top row) and after (bottom row) *Cre*-mediated removal of the RFP marker. **E.** As outlined in Fig S1, HACK knock-ins can be generated either by direct injection or by genetic cross. No difference was found in the expression patterns of *Ir25a-T2A-QF2*^{HACK} knock-in lines generated via these two approaches. For (D) and (E): N = 5 for direct injection; N = 4 for cross, RFP+; N = 3 for cross, RFP-. Expression patterns were comparable across all three groups. **F.** Control brains showing the *QUAS-GFP* reporter alone (left) and the *UAS-mCD8::RFP* reporter alone (right). The *QUAS* reporter was used here in (D) and (E); these reporters were also used in Fig 2 – 5. The *QUAS* reporter weakly labels the mushroom bodies. Scale bars: 100 µm for (C), 50 µm for (D – F). The ventral nerve cord from the fly in (C) is also used in Fig S4A, row four.

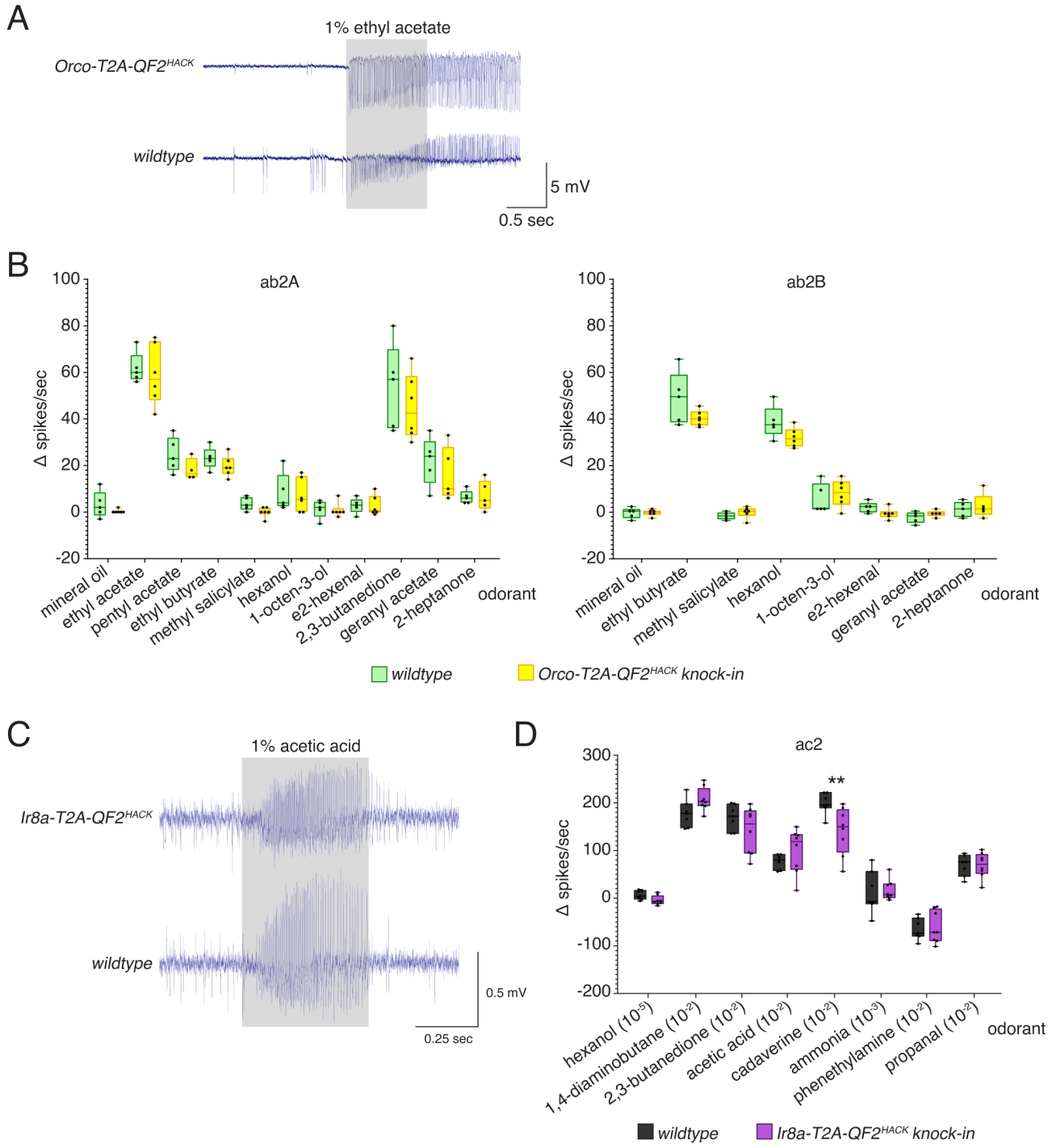

Figure S3. *T2A-QF2* HACK knock-in effects on target gene function. Related to Figures 2 and 3.
A. SSR experiments were performed in ab2 sensilla. Olfactory responses to ten odorants plus mineral oil control were compared in *wildtype* and homozygous *Orco-T2A-QF2*^{HACK} sensilla. Shown are example responses to 1% ethyl acetate. **B.** ab2 sensilla contain two neurons: A (left) and B (right). No differences were found in the responses of these two neurons between the two genotypes across all odorants tested (Mann-Whitney *U* test, $p > 0.05$ for all pairs; see Suppl Data 2 for *U* values and exact *p* values). A small difference in baseline activity (pre-stimulus) was found between the two genotypes, which can be seen in (A). Fewer stimuli are shown for ab2B because odorants that strongly activate the A neuron obscured the responses of the B neuron. N = 5 for *wildtype*, N = 6 for *Orco-T2A-QF2*^{HACK} knock-in. **C.** SSR experiments performed in ac2 sensilla. Olfactory responses to eight odorants plus paraffin oil or water solvent controls were compared in *wildtype* and homozygous *Ir8a-T2A-QF2*^{HACK} sensilla. Shown are example responses to 1% acetic acid. **D.** Two-way ANOVA revealed an interaction effect of genotype and odorant, $F(2,39) = 7.265$, $p = 0.0021$. Sidak's multiple comparison post-hoc test indicated that this was due to a statistically significantly higher response to cadaverine in the *wildtype*, $p = 0.0039$ (indicated by asterisks). Responses to all other stimuli were not significantly different between genotypes. N = 7 for *wildtype*, N = 8 for *Ir8a-T2A-QF2*^{HACK} knock-in.

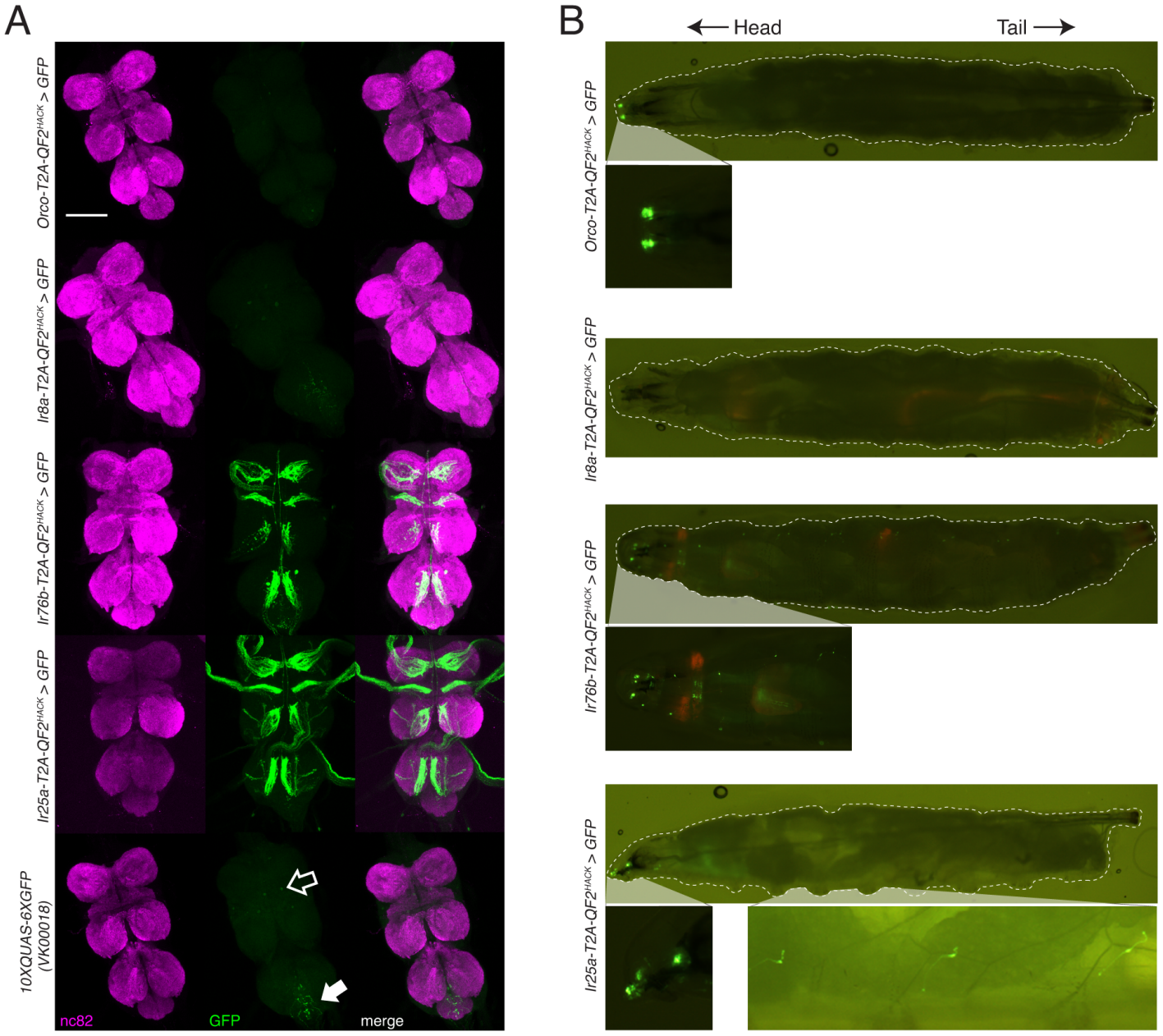

Figure S4. Knock-in expression in the adult ventral nerve cord and in larva. Related to Figures 2, 3, and 4.
A. In adult flies two of the four knock-ins (*Ir76b-T2A-QF2^{HACK}*, third row, and *Ir25a-T2A-QF2^{HACK}*, fourth row) drive GFP expression in neurons innervating the ventral nerve cord (VNC). This likely reflects the role of these co-receptors in gustation. There is weak GFP expression in the reporter control (bottom row) in the abdominal neuromere (filled arrow), as well as the accessory mesothoracic neuropil (empty arrow), which can be seen in the two other knock-ins (*Orco-T2A-QF2^{HACK}*, first row, and *Ir8a-T2A-QF2^{HACK}*, second row). This non-specific expression is likely from the reporter itself rather than driven by the two knock-ins. Scale bar = 100 µm. **B.** In the larval stage, the *Orco-T2A-QF2^{HACK}* knock-in (first row) appears to drive expression only in the dorsal organs (zoomed-in panel), as previously described[81]; the *Ir8a-T2A-QF2^{HACK}* knock-in, second row, does not appear to drive GFP expression in the larva (although very weak expression may not be visible at this magnification); and both *Ir76b-T2A-QF2^{HACK}*, third row, and *Ir25a-T2A-QF2^{HACK}*, fourth row, drive GFP expression in the larval head as well as throughout the body wall (zoomed-in panels), reflecting the role of these genes in additional, non-olfactory modalities. Weak red fluorescence from the *3XP3-RFP* knock-in marker can be detected in the *Ir8a-T2A-QF2^{HACK}* and *Ir76b-T2A-QF2^{HACK}* larvae. This is due to channel bleed-through and is not seen in the other knock-in lines (*Orco-T2A-QF2^{HACK}* and *Ir25a-T2A-QF2^{HACK}*) that have had the RFP marker removed (see Methods for details).

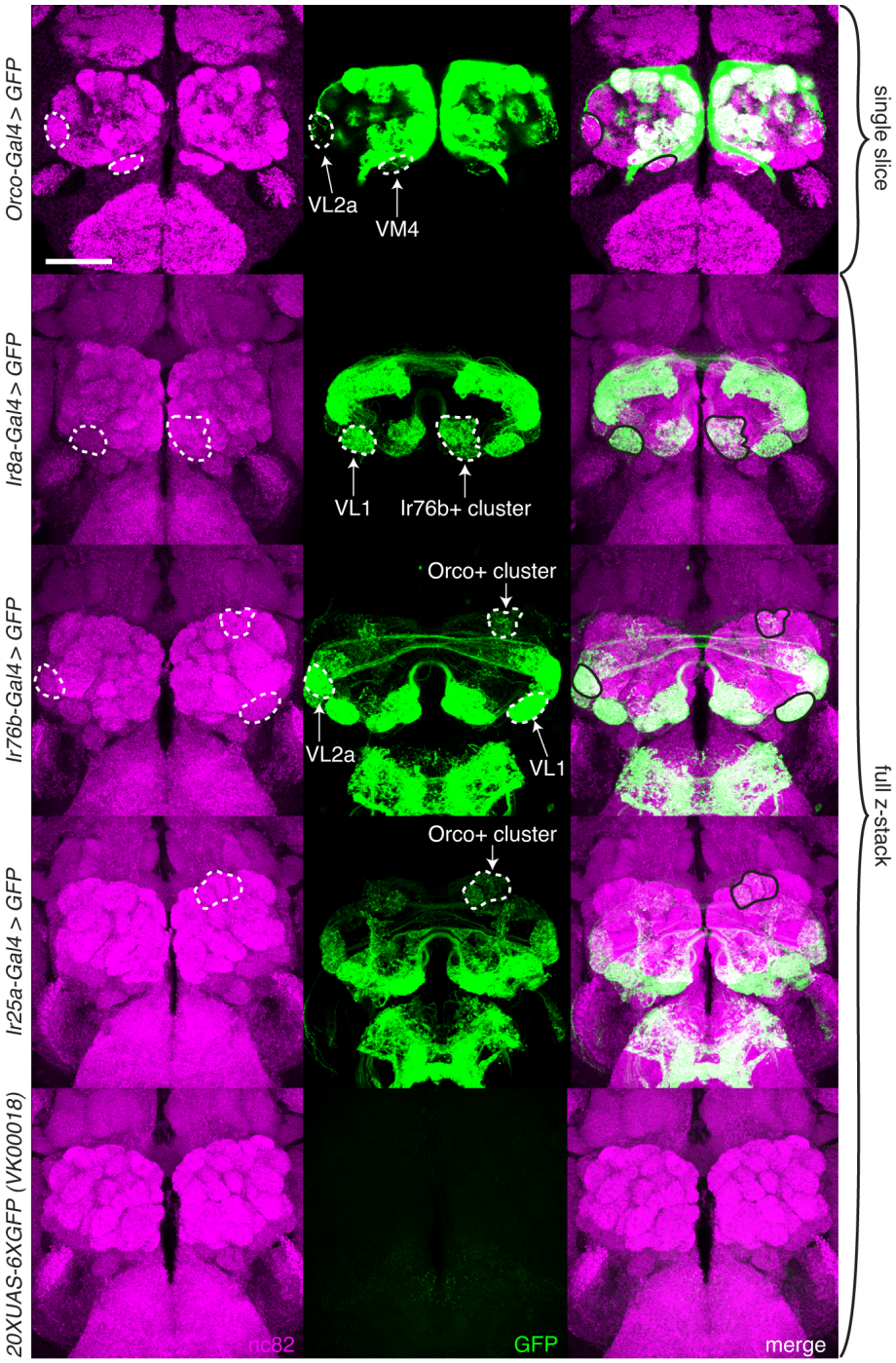

Figure S5. Transgenic co-receptor *Gal4* lines do not fully recapitulate knock-in expression. Related to Figures 2, 3, and 4.
Transgenic co-receptor *Gal4* lines crossed to a strong *UAS* reporter reveal expression in some, but not all, of the additional glomeruli labeled by the respective knock-ins. Outlined are example discrepancies between the *Gal4* and knock-in lines, but do not represent a comprehensive list. First row: *Orco-Gal4* drives weak GFP expression in VL2a (lateral dotted outline) and VM4 (medial dotted outline) glomeruli, but lacks expression in DL2, V, and VL1 glomeruli, which are labeled by the knock-in (see Fig 2 and Suppl Data 4). Second row: *Ir8a-Gal4>GFP* labels the previously reported Ir76b+ cluster (large medial dotted outline), as well as VL1 (lateral dotted outline); however, it lacks expression in the VM4 and VA3 glomeruli, which are labeled in the knock-in (see Fig 3 and Suppl Data 4). Third row: *Ir76b-Gal4* drives GFP expression in additional Orco+ glomeruli (dorsal outline) not seen in the knock-in. Additionally, it labels the VL1 (ventral dotted outline) and VL2a (dorsal dotted outline) glomeruli but lacks expression in the VA5 and DC3 glomeruli which are consistently labeled in the knock-in (see Fig 3 and Suppl Data 4). Fourth row: *Ir25a-Gal4* labels some Orco+ glomeruli (the white dotted outline includes DA2, DA3, DA4m, and DA4l), but is lacking expression in many glomeruli labeled by the knock-in (see Fig 5 and Suppl Data 4). Fifth row: the UAS-GFP control line has weak leaky expression in the subesophageal zone (SEZ), but no expression in the antennal lobes. Top row shows single slice to visualize weakly labeled glomeruli; all other rows are maximum intensity projections of z-stacks. All single channel outlines are white dotted lines, while composite image outlines are black solid lines. Scale bar = 50 µm.

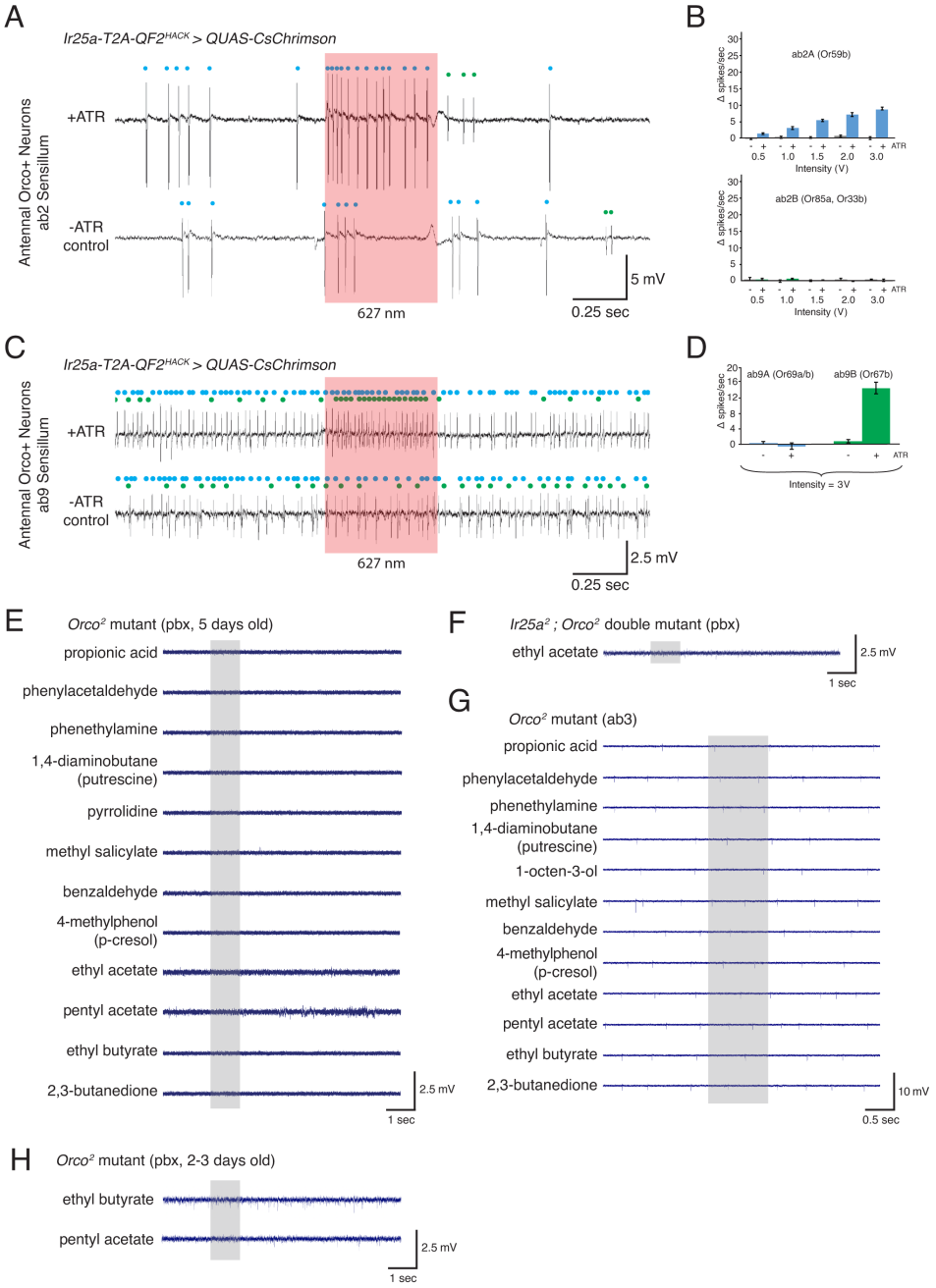

Figure S6. Electrophysiological experiments to examine *Ir25a* expression and function in Orco+ neurons. Related to Figures 4 and 6.

A.-D. Confirmation of *Ir25a* expression in ab2 and ab9 sensilla using optogenetic stimulation. *CsChrimson* expression is driven by the *Ir25a-T2A-QF2^{HACK}* knock-in, and recordings are performed in neurons previously determined to express only *Orco*. **A.** Representative SSR traces from ab2 using 1.5V of a 627 nm LED light (red box) to activate *CsChrimson*. Bottom trace is control animal which was not fed the necessary cofactor all-trans retinal (-ATR). ab2 has two neurons: blue dots indicate spikes from the A neuron, while green dots indicate spikes from the B neuron (genotype: *Ir25a-T2A-QF2^{HACK}*; *QUAS-CsChrimson*). **B.** Quantification of neuronal activity in response to light stimulation at various intensities (N = 7 – 12). Optogenetic experiments confirm *Ir25a* is expressed in ab2A (expressing *Or59b*, top; corresponding to DM4 glomerulus) and not in ab2B (expressing *Or85a* and *Or33b*, bottom; corresponding to DM5 glomerulus). **C.** Combination of optogenetics and fluorescent guided SSR^{86} (fgSSR) to examine *Ir25a* expression in ab9 sensilla (genotype: *Ir25a-T2A-QF2^{HACK}*; *QUAS-CsChrimson/Or67b-Gal4, 15XUAS-IVS-mcd8::GFP)*. Representative recording traces from ab9 in response to 3V of 627 nm LED light (red box). As in (A), -ATR indicates the inactive CsChrimson control; blue dots indicate responses of the A neuron, and green dots indicate responses of the B neuron. **D.** Quantification of neuronal activity in response to light stimulation verified that *Ir25a* is expressed in ab9B (*Or67b*, right; corresponding to VA3 glomerulus) but not in ab9A neurons (*Or69aA/aB*, left; corresponding to D glomerulus). N = 5. **E.** SSR recordings in *Orco^2* mutant palpal sensilla show neither baseline nor odor-evoked activity in response to a panel of odorants in 5-day old flies. N = 20 sensilla from 4 animals (3 male, 1 female). **F.** Like the *Orco^2* mutants in (E), *Ir25a^2; Orco^2* double mutant palpal sensilla showed neither baseline nor odor-evoked activity. Shown is one example trace. N = 42 sensilla from 5 animals (3 male, 2 female). **G.** Antennal ab3 sensilla did occasionally show baseline activity in the *Orco^2* mutant, but generally did not show odor-evoked activity (N = 5 flies; see also Fig 6). **H.** Similarly to older flies (E), young *Orco^2* mutant flies have neither spontaneous nor odor-evoked activity in their palpal neurons. In (E) through (H), the grey box indicates the time of stimulus delivery. See also Suppl Data 2.

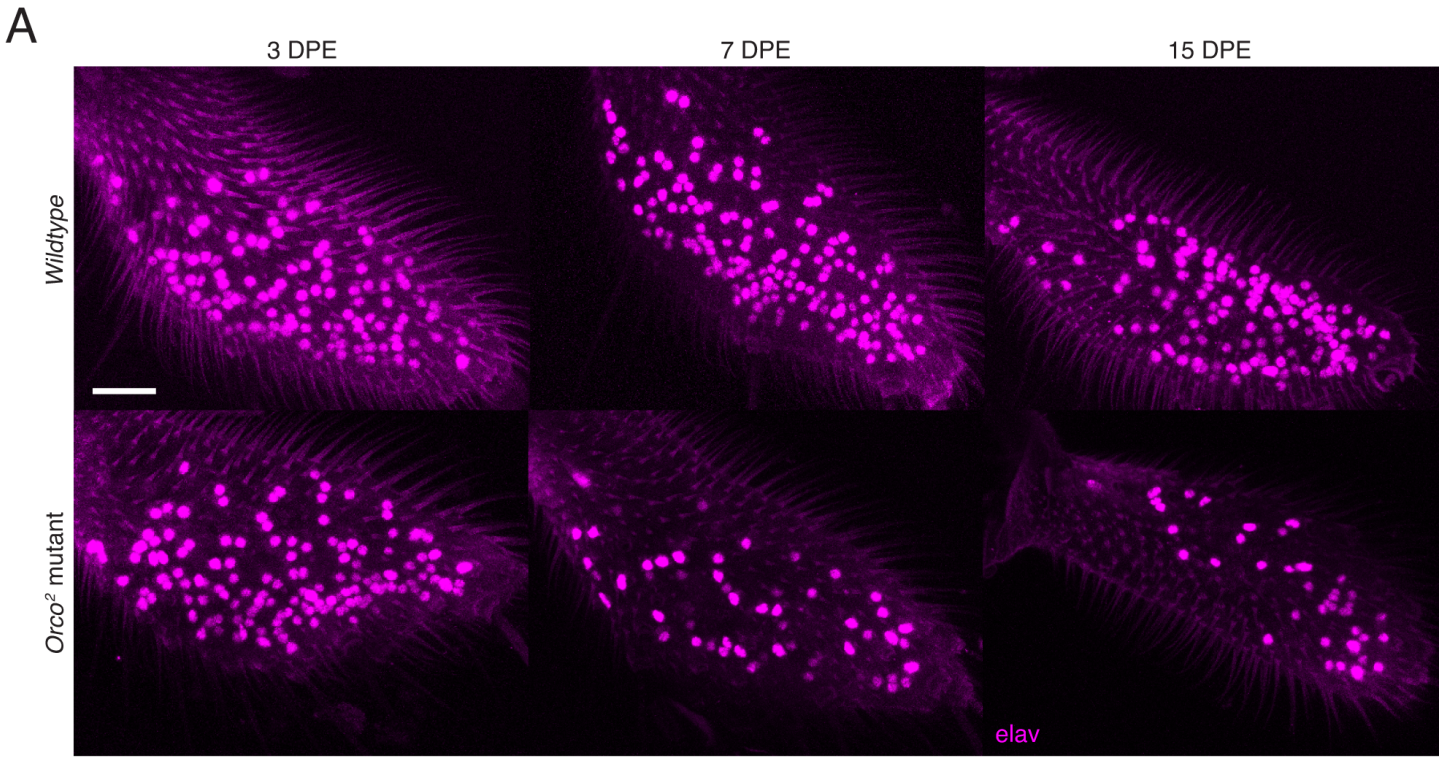

B

Genotype:	*Wildtype*			*Orco*^{2} Mutant		
Age:	3 DPE	7 DPE	15 DPE	3 DPE	7 DPE	15 DPE
Palp 1	123	121	138	141	56	42
Palp 2	136	152	145	108	56	35
Palp 3	147	143	138	135	72	49
Median:	136	143	138	135	56	42

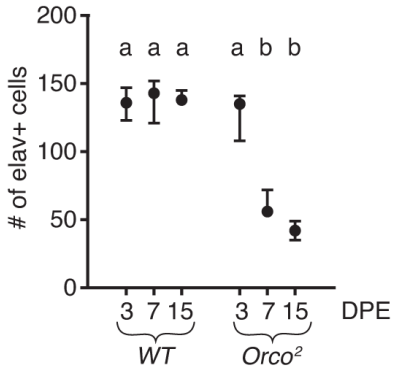

Figure S7. Olfactory neurons lacking functional *Orco* degenerate in the maxillary palps. Related to Figure 6.
A. *Orco*^{2} mutant olfactory neuron cell bodies are lost over time in the palps. An anti-elav antibody was used to visualize all neuronal cell bodies in the palps[97,110]. This includes all olfactory neurons (~120), as well as a small population of presumed mechanosensory neurons (~20)[121]. *Wildtype* (top row) and *Orco*^{2} mutant (bottom row) palps compared at three timepoints: 3 (left column), 7 (middle column) and 15 (right column) days post eclosion (DPE). **B.** Quantification of elav+ cells in *wildtype* and *Orco*^{2} mutant palps at the three timepoints (N = 3 per condition). *Wildtype* flies have consistent numbers of neurons throughout. *Orco*^{2} mutant palps appear normal at 3 DPE but lose approximately 60% of their neurons by day 7. At 15 DPE the *Orco*^{2} mutant phenotype is not significantly different from 7 DPE, with approximately 30% of neurons remaining. Graphed at right are medians with 95% confidence intervals. There was a statistically significant difference between groups as determined by an one-way ANOVA ($F(5,12) = 40.54$, $p < 0.0001$). A Tukey's post-hoc test for all pairwise comparisons revealed a statistically significant difference of the two oldest *Orco*^{2} mutant timepoints (7 and 15 DPE) from all other conditions (denoted with letter b; $p \leq 0.0002$), but no significant difference between these two conditions ($p = 0.4055$). There was no statistically significant difference between any of the *wildtype* conditions ($p > 0.99$), nor between the 3 DPE *Orco*^{2} mutant and any of the *wildtype* timepoints ($p > 0.79$) (denoted with letter a). See Suppl Data 5 for exact *p* values for all pairs.

Table S1. Summary of HACK Knock-in Efficiency. Related to Figure 2.

Gene	Approach	RFP+	RFP-	Total	Efficiency	Founders Producing Knock-in (#/Total)	Knock-ins Sampled	False Positives	Confirmed	Correct
Orco	Direct Injection	180	365	545	33%	43% (3/7)	30	0	30	100%
Ir8a	Direct Injection	53	609	662	8%	20% (4/20)	5	0	5	100%
Ir76b	Direct Injection	79	184	263	30%	100% (2/2)	10	0	10	100%
Ir25a	Direct Injection	82	268	350	23%	40% (2/5)	6	0	6	100%
Orco	Cross	37	96	133	28%	100% (3/3)	2	1	1	50%
Ir25a	Cross	30	95	125	24%	100% (2/2)	30	5	25	83%

Table S1. Summary of HACK Knock-in Efficiency. Related to Figure 2.
There are two ways to generate knock-ins via the HACK technique: by direct injection or by genetic cross[87] (see Fig S1 and Methods for details). All four co-receptor genes were targeted using the direct injection approach; additionally, the crossing approach was tested with *Orco* and *Ir25a*. Knock-in efficiency, as measured by the number of flies having the RFP+ marker divided by the total number of potentially HACKed flies, was high for all genes tested and both approaches. Efficiency appears to depend on the genetic locus, as has been previously demonstrated[87]. To further estimate the effort required to generate a HACK knock-in, we calculated the percentage of founder flies producing knock-in lines; this gives an indication of the number of independent crosses needed to successfully create a knock-in line. Two to five individual G_0 starting crosses were sufficient to produce a knock-in. For each gene, a sample of individual knock-in lines were tested via PCR genotyping, sequencing, and by crossing to a reporter line to confirm brain expression (knock-ins sampled). For all knock-ins generated via the direct injection method, every fly tested represented a correctly targeted knock-in. However, for the cross method, some lines had the RFP+ marker and yet did not drive expression in the brain when crossed to a reporter line (labeled here as false positives). See Fig S1 for crossing schematics.

Table S2. Validation of *Orco-T2A-QF2^{HACK}* knock-in expression in the maxillary palps with antibody staining. Related to Figure 2.

Genotype	Sample	Antibody (Ab)	Ab+ cells	GFP+ cells	Double-labeled cells	Total cells	Notes
Orco-T2A-QF2^{HACK} > GFP	Palp 1	anti-Orco	125	127	125	127	2 cell are GFP+ Orco-, 0 cells are GFP- Orco+, 125 cells are double labeled
Orco-T2A-QF2^{HACK} > GFP	Palp 2	anti-Orco	112	111	108	115	3 cell are GFP+ Orco-, 4 cells are GFP- Orco+, 108 cells are double labeled
Orco-T2A-QF2^{HACK} > GFP	Palp 6	anti-Orco	125	126	123	128	3 cell are GFP+ Orco-, 2 cells are GFP- Orco+, 123 cells are double labeled
		Total across tissue:	362	364	356	370	
			Proportion of Orco+ cells that are GFP+:	Proportion of GFP+ cells that are Orco+:	Proportion of all cells that are double labeled:		
			0.98	0.98	0.96		

Table S2. Validation of *Orco-T2A-QF2^{HACK}* knock-in expression in the maxillary palps. Related to Figure 2.
To verify that *Orco-T2A-QF2^{HACK}* recapitulates the endogenous expression pattern of *Orco*, maxillary palps of flies containing the knock-in driving GFP expression were co-stained with an anti-Orco antibody[81]. The overlap of Orco+ and GFP+ cells was examined. A high correspondence between the antibody staining and knock-in driven GFP was found, with 96% of cells being double-labeled.

Table S3. Validation of *Ir25a-T2A-QF2^{HACK}* knock-in expression in the maxillary palps with antibody staining. Related to Figure 4.

Genotype	Sample	Antibody (Ab)	Ab+ cells	GFP+ cells	Double-labeled cells	Total cells	Notes
Ir25a-T2A-QF2^{HACK} > GFP	Palp 1	anti-Ir25a	107	105	104	108	1 cell is GFP+ Ir25a-, 3 cells are GFP- Ir25a+, 104 cells are double labeled
Ir25a-T2A-QF2^{HACK} > GFP	Palp 2	anti-Ir25a	86	85	85	86	1 cell is GFP- Ir25a+, 85 cells are double labeled
Ir25a-T2A-QF2^{HACK} > GFP	Palp 3	anti-Ir25a	111	111	110	112	1 cell is GFP+ Ir25a-, 1 cell is GFP- Ir25a+, 110 cells are double labeled
Ir25a-T2A-QF2^{HACK} > GFP	Palp 4	anti-Ir25a	94	94	94	94	94 cells, all double labeled
Ir25a-T2A-QF2^{HACK} > GFP	Palp 5	anti-Ir25a	83	83	81	85	2 cells are GFP+ Ir25a-, 2 cells are GFP- Ir25a+, 81 cells are double labeled
		Total across tissue:	481	478	474	485	
			Proportion of Ir25a+ cells that are GFP+:	Proportion of GFP+ cells that are Ir25a+:	Proportion of all cells that are double labeled:		
			0.99	0.99	0.98		

Table S3. Validation of *Ir25a-T2A-QF2^{HACK}* knock-in expression in the maxillary palps. Related to Figure 4.
To verify Ir25a protein expression in the maxillary palps (which has not been previously reported) the *Ir25a-T2A-QF2^{HACK}* knock-in was used to drive *GFP* expression and maxillary palps co-stained with an anti-Ir25a antibody[10]. The overlap of Ir25a+ and GFP+ cells was examined. The anti-Ir25a antibody labels most olfactory neurons in the palps, and correlates highly with knock-in expression (98% of cells double-labeled).

Table S4. Summary of Expression Patterns for All Knock-in Lines. Related to Figures 2 – 5.

Glomerulus	Sensillum	Tuning Receptor(s)	Original Co-receptor(s)	*Orco-T2A-QF2^{HACK}*	*Ir8a-T2A-QF2^{HACK}*	*Ir76b-T2A-QF2^{HACK}*	*Ir25a-T2A-QF2^{HACK}*
D	Ab9A	Or69aA, Or69aB	Orco	Yes	No	No	No
DA1	At1A	Or67d	Orco	Yes	No	Variable	Yes
DA2	Ab4B	Or56a, Or33a	Orco	Yes	No	No	Yes
DA3	Ai2B (At2B)	Or23a	Orco	Yes	No	No	Yes
DA4l	Ai3C (At3C)	Or43a	Orco	Yes	No	No	Yes
DA4m	Ai3B (At3B)	Or2a	Orco	Yes	No	No	Yes
DC1	Ai3A (At3A)	Or19a, Or19b	Orco	Yes	No	No	Yes
DC2	Ai1A (Ab6A)	Or13a	Orco	Yes	No	No	Yes
DC3	Ai2A (At2A)	Or83c	Orco	Yes	No	Yes	Variable
DL1	Ab1D	Or10a, Gr10a	Orco	Yes	No	Yes	Yes
DL3	At4B	Or65a, Or65b, Or65c	Orco	Yes	No	No	Yes
DL4	Ab10B	Or49a, Or85f	Orco	Yes	No	No	Yes
DL5	Ab4A	Or7a	Orco	Yes	No	No	Variable
DM1	Ab1A	Or42b	Orco	Yes	No	No	Yes
DM2	Ab3A	Or22a, Or22b	Orco	Yes	No	No	Yes
DM3	Ab5B	Or47a, Or33b	Orco	Yes	No	No	No
DM4	Ab2A	Or59b	Orco	Yes	No	No	Yes
DM5	Ab2B	Or85a, Or33b	Orco	Yes	No	No	No
DM6	Ab10A	Or67a	Orco	Yes	No	No	Yes
VA1d	At4C	Or88a	Orco	Yes	No	No	Yes
VA1v	At4A	Or47b	Orco	Yes	No	No	Yes
VA2	Ab1B	Or92a	Orco	Yes	No	No	Yes
VA3	Ab9B	Or67b	Orco	Yes	Yes	Yes	Yes
VA4	Pb3B	Or85d	Orco	Yes	No	No	Yes
VA5	Ai1B (Ab6B)	Or49b	Orco	Yes	No	Yes	Yes
VA6	Ab5A	Or82a	Orco	Yes	No	Yes	Yes
VA7l	Pb2B	Or46a	Orco	Yes	No	No	Yes
VA7m	UNK	UNK	Orco	Yes	No	Variable	Yes
VC1	Pb2A	Or33c, Or85e	Orco	Yes	No	No	Yes
VC2	Pb1B	Or71a	Orco	Yes	No	No	Yes
VC4	Ab7B	Or67c	Orco	Yes	No	Yes	Yes
VM2	Ab8A	Or43b	Orco	Yes	No	No	No
VM3	Ab8B	Or9a	Orco	Yes	No	No	No
VM5d	Ab3B	Or85b	Orco	Yes	No	No	Yes

(continued on next page)

Table S4, continued.

Glomerulus	Sensillum	Tuning Receptor(s)	Original Co-receptor(s)	*Orco-T2A-QF2^{HACK}*	*Ir8a-T2A-QF2^{HACK}*	*Ir76b-T2A-QF2^{HACK}*	*Ir25a-T2A-QF2^{HACK}*
VM5v	Ab7A	Or98a	Orco	Yes	No	No	Yes
VM7d	Pb1A	Or42a	Orco	Yes	No	No	Yes
VM7v (1)	Pb3A	Or59c	Orco	Yes	No	No	Yes
VC3	Ac3B	Or35a	Orco, Ir76b	Yes	Yes	Yes	Yes
V	Ab1C	Gr21a, Gr63a	N/A	Yes	No	No	Yes
DC4	Sacculus, Chamber III	Ir64a	Ir8a	Variable	Yes	No	Yes
DL2	Ac3A	Ir75a, Ir75b, Ir75c	Ir8a	Yes	Yes	No	Yes
DP1l	Ac2	Ir75a	Ir8a	Yes	Yes	Yes	Yes
DP1m	Sacculus, Chamber III	Ir64a	Ir8a	No	Yes	Yes	Yes
VL2a	Ac4	Ir84a	Ir8a	Yes	Yes	Yes	Yes
VL2p	Ac1	Ir31a	Ir8a	No	Yes	Yes	Yes
VC5	Ac2	Ir41a	Ir25a, Ir76b	No	Yes	Yes	Yes
VM1	Ac1	Ir92a	Ir25a, Ir76b	No	Yes	Yes	Yes
VM4	Ac4	Ir76a	Ir25a, Ir76b	Yes	Yes	Yes	Yes
VL1	Ac1, Ac2, Ac4	Ir75d	Ir25a	Yes	Yes	Yes	Yes
VM6	UNK	UNK	Ir25a	No	Variable	No	Yes
VP1d	Sacculus, Chamber II	Ir40a, Ir93a	Ir25a	No	No	No	Yes
VP1l	Sacculus, Chamber I	Ir21a, Ir93a	Ir25a	No	No	No	Yes
VP1m	Sacculus, Chamber I	Ir68a, Ir93a	Ir25a	No	No	No	Yes
VP2	Arista	Gr28b.d	Ir25a	No	No	No	Yes
VP3	Arista	Ir21a	Ir25a	No	No	No	Yes
VP4	Sacculus, Chambers I + II	Ir40a, Ir93a	Ir25a	No	No	No	Yes
VP5	Sacculus, Chamber II	Ir68a, Ir93a	Ir25a	No	No	No	Yes
VC6	UNK	UNK	N/A (this paper)	No	Yes	No	Yes

Table S4. Summary of Expression Patterns for All Knock-in Lines. Related to Figures 2 – 5.
Summarized here are all of the OSN types innervating the 58 antennal lobe glomeruli; their corresponding sensilla and tuning receptors; the previously reported (original) co-receptors they express; and whether or not each of the four co-receptor knock-in lines labels those glomeruli. Variable indicates that the glomerulus was labeled in less than 50% of brains examined in the given knock-in line. UNK = unknown. Sensilla or glomeruli that have been renamed or reclassified have their former nomenclature listed in parentheses. See also Suppl Data 4 and 6.

REFERENCES

1. Abuin, L., Bargeton, B., Ulbrich, M.H., Isacoff, E.Y., Kellenberger, S., and Benton, R. (2011). Functional architecture of olfactory ionotropic glutamate receptors. Neuron *69*, 44-60.
2. Abuin, L., Prieto-Godino, L.L., Pan, H., Gutierrez, C., Huang, L., Jin, R., and Benton, R. (2019). In vivo assembly and trafficking of olfactory Ionotropic Receptors. BMC Biol *17*, 34.
3. Ache, B.W., and Young, J.M. (2005). Olfaction: diverse species, conserved principles. Neuron *48*, 417-430.
4. Ai, M., Blais, S., Park, J.Y., Min, S., Neubert, T.A., and Suh, G.S. (2013). Ionotropic glutamate receptors IR64a and IR8a form a functional odorant receptor complex in vivo in *Drosophila*. J Neurosci *33*, 10741-10749.
5. Ai, M., Min, S., Grosjean, Y., Leblanc, C., Bell, R., Benton, R., and Suh, G.S. (2010). Acid sensing by the *Drosophila* olfactory system. Nature *468*, 691-695.
6. Auer, T.O., Khallaf, M.A., Silbering, A.F., Zappia, G., Ellis, K., Alvarez-Ocana, R., Arguello, J.R., Hansson, B.S., Jefferis, G., Caron, S.J.C*., et al.* (2020). Olfactory receptor and circuit evolution promote host specialization. Nature *579*, 402-408.
7. Baena-Lopez, L.A., Alexandre, C., Mitchell, A., Pasakarnis, L., and Vincent, J.P. (2013). Accelerated homologous recombination and subsequent genome modification in *Drosophila*. Development *140*, 4818-4825.
8. Bates, A.S., Schlegel, P., Roberts, R.J.V., Drummond, N., Tamimi, I.F.M., Turnbull, R., Zhao, X., Marin, E.C., Popovici, P.D., Dhawan, S*., et al.* (2020). Complete Connectomic Reconstruction of Olfactory Projection Neurons in the Fly Brain. Curr Biol *30*, 3183-3199.e3186.
9. Benton, R., Sachse, S., Michnick, S.W., and Vosshall, L.B. (2006). Atypical membrane topology and heteromeric function of *Drosophila* odorant receptors in vivo. PLoS Biol *4*, e20.
10. Benton, R., Vannice, K.S., Gomez-Diaz, C., and Vosshall, L.B. (2009). Variant ionotropic glutamate receptors as chemosensory receptors in *Drosophila*. Cell *136*, 149-162.
11. Berck, M.E., Khandelwal, A., Claus, L., Hernandez-Nunez, L., Si, G., Tabone, C.J., Li, F., Truman, J.W., Fetter, R.D., Louis, M*., et al.* (2016). The wiring diagram of a glomerular olfactory system. eLIFE *5*.
12. Bhalerao, S., Sen, A., Stocker, R., and Rodrigues, V. (2003). Olfactory neurons expressing identified receptor genes project to subsets of glomeruli within the antennal lobe of *Drosophila melanogaster*. J Neurobiol *54*, 577-592.
13. Bischof, J., Maeda, R.K., Hediger, M., Karch, F., and Basler, K. (2007). An optimized transgenesis system for *Drosophila* using germ-line-specific *phiC31* integrases. PNAS *104*, 3312-3317.
14. Bosch, J.A., Knight, S., Kanca, O., Zirin, J., Yang-Zhou, D., Hu, Y., Rodiger, J., Amador, G., Bellen, H.J., Perrimon, N*., et al.* (2020). Use of the CRISPR-Cas9 System in *Drosophila* Cultured Cells to Introduce Fluorescent Tags into Endogenous Genes. Curr Protoc Mol Biol *130*, e112.
15. Brand, A.H., and Perrimon, N. (1993). Targeted gene expression as a means of altering cell fates and generating dominant phenotypes. Development *118*, 401-415.
16. Budelli, G., Ni, L., Berciu, C., van Giesen, L., Knecht, Z.A., Chang, E.C., Kaminski, B., Silbering, A.F., Samuel, A., Klein, M*., et al.* (2019). Ionotropic Receptors Specify the Morphogenesis of Phasic Sensors Controlling Rapid Thermal Preference in *Drosophila*. Neuron *101*, 738-747 e733.
17. Butterwick, J.A., Del Marmol, J., Kim, K.H., Kahlson, M.A., Rogow, J.A., Walz, T., and Ruta, V. (2018). Cryo-EM structure of the insect olfactory receptor Orco. Nature *560*, 447-452.
18. Carey, A.F., and Carlson, J.R. (2011). Insect olfaction from model systems to disease control. PNAS *108*, 12987-12995.
19. Chen, C., Buhl, E., Xu, M., Croset, V., Rees, J.S., Lilley, K.S., Benton, R., Hodge, J.J., and Stanewsky, R. (2015). *Drosophila* Ionotropic Receptor 25a mediates circadian clock resetting by temperature. Nature *527*, 516-520.
20. Chen, H.-M., Yao, X., Ren, Q., Chang, C.-C., Liu, L.-Y., Miyares, R.L., and Lee, T. (2020). Enhanced Golic+: highly effective CRISPR gene targeting and transgene HACKing in *Drosophila*. Development *147*.
21. Chen, Y., and Amrein, H. (2017). Ionotropic Receptors Mediate Drosophila Oviposition Preference through Sour Gustatory Receptor Neurons. Curr Biol *27*, 2741-2750 e2744.
22. Chen, Y.D., and Dahanukar, A. (2017). Molecular and Cellular Organization of Taste Neurons in Adult Drosophila Pharynx. Cell Rep *21*, 2978-2991.
23. Chiang, A., Priya, R., Ramaswami, M., Vijayraghavan, K., and Rodrigues, V. (2009). Neuronal activity and Wnt signaling act through Gsk3-beta to regulate axonal integrity in mature Drosophila olfactory sensory neurons. Development *136*, 1273-1282.
24. Clyne, P.J., Warr, C.G., Freeman, M.R., Lessing, D., Kim, J., and Carlson, J.R. (1999). A novel family of divergent seven-transmembrane proteins: candidate odorant receptors in Drosophila. Neuron *22*, 327-338.
25. Couto, A., Alenius, M., and Dickson, B.J. (2005). Molecular, anatomical, and functional organization of the Drosophila olfactory system. Curr Biol *15*, 1535-1547.
26. Croset, V., Rytz, R., Cummins, S.F., Budd, A., Brawand, D., Kaessmann, H., Gibson, T.J., and Benton, R. (2010). Ancient protostome origin of chemosensory ionotropic glutamate receptors and the evolution of insect taste and olfaction. PLoS Genet *6*, e1001064.
27. de Bruyne, M., Clyne, P.J., and Carlson, J.R. (1999). Odor Coding in a Model Olfactory Organ: The Drosophila Maxillary Palp. J Neurosci *19*, 4520-4532.
28. de Bruyne, M., Foster, K., and Carlson, J.R. (2001). Odor Coding in the *Drosophila* Antenna. Neuron *30*, 537-552.
29. DeGennaro, M., McBride, C.S., Seeholzer, L., Nakagawa, T., Dennis, E.J., Goldman, C., Jasinskiene, N., James, A.A., and Vosshall, L.B. (2013). orco mutant mosquitoes lose strong preference for humans and are not repelled by volatile DEET. Nature *498*, 487-491.
30. Depetris-Chauvin, A., Galagovsky, D., and Grosjean, Y. (2015). Chemicals and chemoreceptors: ecologically relevant signals driving behavior in *Drosophila*. Front Ecol Evol *3*, 41.
31. Diao, F., Ironfield, H., Luan, H., Diao, F., Shropshire, W.C., Ewer, J., Marr, E., Potter, C.J., Landgraf, M., and White, B.H. (2015). Plug-and-play genetic access to drosophila cell types using exchangeable exon cassettes. Cell Rep *10*, 1410-1421.
32. Diao, F., and White, B.H. (2012). A novel approach for directing transgene expression in Drosophila: T2A-Gal4 in-frame fusion. Genetics *190*, 1139-1144.
33. Dobritsa, A.A., Van der Goes van Naters, W., Warr, C.G., Steinbrecht, R.A., and Carlson, J.R. (2003). Integrating the molecular and cellular basis of odor coding in the *Drosophila* antenna. Neuron *37*, 827-841.
34. Du, L., Zhou, A., Sohr, A., and Roy, S. (2018). An Efficient Strategy for Generating Tissue-specific Binary Transcription Systems in Drosophila by Genome Editing. J Vis Exp.
35. Dubey, P., Joti, P., and Ray, K. (2016). A conditional Orco requirement in the somatic cyst cells for maintaining spermatids in a tight bundle in *Drosophila* testis. J Biosci *41*, 219-227.
36. Dunipace, L., Meister, S., McNealy, C., and Amrein, H. (2001). Spatially restricted expression of candidate taste receptors in the Drosophila gustatory system. Curr Biol *11*, 822-835.
37. Dweck, H.K.M., Ebrahim, S.A.M., Thoma, M., Mohamed, A.A.M., Keesey, I.W., Trona, F., Lavista-Llanos, S., Svatoš, A., Sachse, S., Knaden, M*., et al.* (2015). Pheromones mediating copulation and attraction in *Drosophila*. PNAS *112*, E2829-E2835.
38. Enjin, A., Zaharieva, E.E., Frank, D.D., Mansourian, S., Suh, G.S., Gallio, M., and Stensmyr, M.C. (2016). Humidity Sensing in Drosophila. Curr Biol *26*, 1352-1358.
39. Fandino, R.A., Haverkamp, A., Bisch-Knaden, S., Zhang, J., Bucks, S., Nguyen, T.A.T., Schroder, K., Werckenthin, A., Rybak, J., Stengl, M*., et al.* (2019). Mutagenesis of odorant coreceptor Orco fully disrupts foraging but

not oviposition behaviors in the hawkmoth *Manduca sexta*. PNAS *116*, 15677-15685.

40. Fishilevich, E., and Vosshall, L.B. (2005). Genetic and functional subdivision of the Drosophila antennal lobe. Curr Biol *15*, 1548-1553.

41. Frank, D.D., Enjin, A., Jouandet, G.C., Zaharieva, E.E., Para, A., Stensmyr, M.C., and Gallio, M. (2017). Early Integration of Temperature and Humidity Stimuli in the Drosophila Brain. Curr Biol *27*, 2381-2388 e2384.

42. Frechter, S., Bates, A.S., Tootoonian, S., Dolan, M.J., Manton, J., Jamasb, A.R., Kohl, J., Bock, D., and Jefferis, G. (2019). Functional and anatomical specificity in a higher olfactory centre. eLIFE *8*.

43. Ganguly, A., Pang, L., Duong, V.K., Lee, A., Schoniger, H., Varady, E., and Dahanukar, A. (2017). A Molecular and Cellular Context-Dependent Role for Ir76b in Detection of Amino Acid Taste. Cell Rep *18*, 737-750.

44. Gao, Q., and Chess, A. (1999). Identification of candidate *Drosophila* olfactory receptors from genomic DNA sequence. Genomics *60*, 31-39.

45. Gao, Q., Yuan, B., and Chess, A. (2000). Convergent projections of *Drosophila* olfactory neurons to specific glomeruli in the antennal lobe. Nat Neurosci *3*, 780-785.

46. Gloor, G.B., Nassif, N.A., Johnson-Schlitz, D.M., Preston, C.R., and Engels, W.R. (1991). Targeted gene replacement in *Drosophila* via P element-induced gap repair. Science *253*, 1110-1117.

47. Gnerer, J.P., Venken, K.J., and Dierick, H.A. (2015). Gene-specific cell labeling using MiMIC transposons. Nucleic Acids Res *43*, e56.

48. Goldman, A.L., Van der Goes van Naters, W., Lessing, D., Warr, C.G., and Carlson, J.R. (2005). Coexpression of two functional odor receptors in one neuron. Neuron *45*, 661-666.

49. Gomez-Diaz, C., Martin, F., Garcia-Fernandez, J.M., and Alcorta, E. (2018). The Two Main Olfactory Receptor Families in Drosophila, ORs and IRs: A Comparative Approach. Front Cell Neurosci *12*, 253.

50. Goulding, S.E., zur Lage, P., and Jarman, A.P. (2000). *amos*, a Proneural Gene for *Drosophila* Olfactory Sense Organs that Is Regulated by *lozenge*. Neuron *25*, 69-78.

51. Grabe, V., Baschwitz, A., Dweck, H.K.M., Lavista-Llanos, S., Hansson, B.S., and Sachse, S. (2016). Elucidating the Neuronal Architecture of Olfactory Glomeruli in the Drosophila Antennal Lobe. Cell Rep *16*, 3401-3413.

52. Grabe, V., and Sachse, S. (2018). Fundamental principles of the olfactory code. Biosystems *164*, 94-101.

53. Gratz, S.J., Rubinstein, C.D., Harrison, M.M., Wildonger, J., and O'Connor-Giles, K.M. (2015). CRISPR-Cas9 Genome Editing in Drosophila. Curr Protoc Mol Biol *111*, 31 32 31-20.

54. Gratz, S.J., Ukken, F.P., Rubinstein, C.D., Thiede, G., Donohue, L.K., Cummings, A.M., and O'Connor-Giles, K.M. (2014). Highly specific and efficient CRISPR/Cas9-catalyzed homology-directed repair in Drosophila. Genetics *196*, 961-971.

55. Groth, A.C., Fish, M., Nusse, R., and Calos, M.P. (2004). Construction of transgenic Drosophila by using the site-specific integrase from phage phiC31. Genetics *166*, 1775-1782.

56. Gupta, B.P., and Rodrigues, V. (1997). Atonal is a proneural gene for a subset of olfactory sense organs in Drosophila. Genes Cells *2*, 225-233.

57. Hallem, E.A., and Carlson, J.R. (2006). Coding of odors by a receptor repertoire. Cell *125*, 143-160.

58. Hallem, E.A., Ho, M.G., and Carlson, J.R. (2004). The molecular basis of odor coding in the Drosophila antenna. Cell *117*, 965-979.

59. Hansson, B.S., and Stensmyr, M.C. (2011). Evolution of insect olfaction. Neuron *72*, 698-711.

60. Harris, W.A. (1972). The maxillae of *Drosophila melanogaster* as revealed by scanning electron microscopy. J Morphol *138*, 451-456.

61. Haverkamp, A., Hansson, B.S., and Knaden, M. (2018). Combinatorial Codes and Labeled Lines: How Insects Use Olfactory Cues to Find and Judge Food, Mates, and Oviposition Sites in Complex Environments. Front Physiol *9*, 49.

62. Holt, R.A., Subramanian, G.M., Halpern, A., Sutton, G.G., Charlab, R., Nusskern, D.R., Wincker, P., Clark, A.G., Ribeiro, J.M.C., Wides, R.*, et al.* (2002). The Genome Sequence of the Malaria Mosquito *Anopheles gambiae*. Science *298*, 129-149.

63. Horne, J.A., Langille, C., McLin, S., Wiederman, M., Lu, Z., Xu, C.S., Plaza, S.M., Scheffer, L.K., Hess, H.F., and Meinertzhagen, I.A. (2018). A resource for the Drosophila antennal lobe provided by the connectome of glomerulus VA1v. eLIFE *7*.

64. Hueston, C.E., Olsen, D., Li, Q., Okuwa, S., Peng, B., Wu, J., and Volkan, P.C. (2016). Chromatin modulatory proteins and olfactory receptor signaling in the refinement and maintenance of fruitless expression in olfactory receptor neurons. PLoS Biol *14*, e1002443.

65. Hussain, A., Zhang, M., Ucpunar, H.K., Svensson, T., Quillery, E., Gompel, N., Ignell, R., and Grunwald Kadow, I.C. (2016). Ionotropic Chemosensory Receptors Mediate the Taste and Smell of Polyamines. PLoS Biol *14*, e1002454.

66. Jaeger, A.H., Stanley, M., Weiss, Z.F., Musso, P.Y., Chan, R.C., Zhang, H., Feldman-Kiss, D., and Gordon, M.D. (2018). A complex peripheral code for salt taste in Drosophila. eLIFE *7*.

67. Jhaveri, D., Sen, A., Reddy, G.V., and Rodrigues, V. (2000a). Sense organ identity in the *Drosophila* antenna is specified by the expression of the proneural gene atonal. Mech Dev *99*, 101-111.

68. Jhaveri, D., Sen, A., and Rodrigues, V. (2000b). Mechanisms underlying olfactory neuronal connectivity in Drosophila-the atonal lineage organizes the periphery while sensory neurons and glia pattern the olfactory lobe. Dev Biol *226*, 73-87.

69. Jinek, M., Chylinski, K., Fonfara, I., Hauer, M., Doudna, J.A., and Charpentier, E. (2012). A programmable dual-RNA-guided DNA endonuclease in adaptive bacterial immunity. Science *337*, 816-821.

70. Jones, W.D., Cayirlioglu, P., Kadow, I.G., and Vosshall, L.B. (2007). Two chemosensory receptors together mediate carbon dioxide detection in *Drosophila*. Nature *445*, 86-90.

71. Kaissling, K.-E., and Thorson, J. (1980). Insect olfactory sensilla: structural, chemical and electrical aspects of the functional organisation. In Receptors for neurotransmitters, hormones and pheromones in insects (Elsevier/North-Holland Biomedical Press), pp. 261-282.

72. Kanca, O., Zirin, J., Garcia-Marques, J., Knight, S.M., Yang-Zhou, D., Amador, G., Chung, H., Zuo, Z., Ma, L., He, Y.*, et al.* (2019). An efficient CRISPR-based strategy to insert small and large fragments of DNA using short homology arms. eLIFE *8*, e51539.

73. Klapoetke, N.C., Murata, Y., Kim, S.S., Pulver, S.R., Birdsey-Benson, A., Cho, Y.K., Morimoto, T.K., Chuong, A.S., Carpenter, E.J., Tian, Z.*, et al.* (2014). Independent optical excitation of distinct neural populations. Nat Methods *11*, 338-346.

74. Knecht, Z.A., Silbering, A.F., Cruz, J., Yang, L., Croset, V., Benton, R., and Garrity, P.A. (2017). Ionotropic Receptor-dependent moist and dry cells control hygrosensation in Drosophila. eLIFE *6*.

75. Knecht, Z.A., Silbering, A.F., Ni, L., Klein, M., Budelli, G., Bell, R., Abuin, L., Ferrer, A.J., Samuel, A.D., Benton, R.*, et al.* (2016). Distinct combinations of variant ionotropic glutamate receptors mediate thermosensation and hygrosensation in Drosophila. eLIFE *5*.

76. Kondoh, K., Lu, Z., Ye, X., Olson, D.P., Lowell, B.B., and Buck, L.B. (2016). A specific area of olfactory cortex involved in stress hormone responses to predator odours. Nature *532*, 103-106.

77. Kurtovic, A., Widmer, A., and Dickson, B.J. (2007). A single class of olfactory neurons mediates behavioural responses to a *Drosophila* sex pheromone. Nature *446*, 542-546.

78. Kwon, J.Y., Dahanukar, A., Weiss, L.A., and Carlson, J.R. (2007). The molecular basis of CO2 reception in *Drosophila*. PNAS *104*, 3574-3578.

79. Lai, S.-L., and Lee, T. (2006). Genetic mosaic with dual binary transcriptional systems in *Drosophila*. Nat Neurosci *9*, 703-709.

80. Laissue, P.P., Reiter, C.H., Hiesinger, P.R., Halter, S., Fischbach, K.F., and Stocker, R.F. (1999). Three-dimensional reconstruction of the antennal lobe in *Drosophila melanogaster*. J Comp Neurol *405*, 543-552.

81. Larsson, M.C., Domingos, A.I., Jones, W.D., Chiappe, M.E., Amrein, H., and Vosshall, L.B. (2004). *Or83b* encodes a broadly expressed odorant receptor essential for *Drosophila* olfaction. Neuron *43*, 703-714.

82. Lee, P.-T., Zirin, J., Kanca, O., Lin, W.-W., Schulze, K.L., Li-Kroeger, D., Tao, R., Devereaux, C., Hu, Y., Chung, V.*, et al.* (2018). A gene-specific T2A-GAL4 library for *Drosophila*. eLIFE *7*, e35574.

83. Li-Kroeger, D., Kanca, O., Lee, P.T., Cowan, S., Lee, M.T., Jaiswal, M., Salazar, J.L., He, Y., Zuo, Z., and Bellen, H.J. (2018). An expanded toolkit for gene tagging based on MiMIC and scarless CRISPR tagging in Drosophila. eLIFE *7*.

84. Li, H., Li, T., Horns, F., Li, J., Xie, Q., Xu, C., Wu, B., Kebschull, J.M., McLaughlin, C.N., Kolluru, S.S.*, et al.* (2020). Single-Cell Transcriptomes Reveal Diverse Regulatory Strategies for Olfactory Receptor Expression and Axon Targeting. Curr Biol *30*, 1189-1198 e1185.

85. Li, K., Wang, G., Andersen, T., Zhou, P., and Pu, W.T. (2014). Optimization of Genome Engineering Approaches with the CRISPR/Cas9 System. PLoS One *9*, e105779.

86. Lin, C.-C., and Potter, C.J. (2015). Re-Classification of *Drosophila melanogaster* Trichoid and Intermediate Sensilla Using Fluorescence-Guided Single Sensillum Recording. PLoS One *10*, e0139675.

87. Lin, C.-C., and Potter, C.J. (2016a). Editing Transgenic DNA Components by Inducible Gene Replacement in *Drosophila melanogaster*. Genetics *203*, 1613-1628.

88. Lin, C.-C., and Potter, C.J. (2016b). Non-mendelian dominant maternal effects caused by CRISPR/Cas9 transgenic components in *Drosophila melanogaster*. G3 (Bethesda) *6*, 3685-3691.

89. Lynd, A., and Lycett, G.J. (2012). Development of the Bi-Partite *Gal4-UAS* System in the African Malaria Mosquito, *Anopheles gambiae*. PLoS One *7*, e31552.

90. MacWilliam, D., Kowalewski, J., Kumar, A., Pontrello, C., and Ray, A. (2018). Signaling Mode of the Broad-Spectrum Conserved CO2 Receptor Is One of the Important Determinants of Odor Valence in *Drosophila*. Neuron *97*, 1153-1167.e1154.

91. Mansourian, S., Corcoran, J., Enjin, A., Löfstedt, C., Dacke, M., and Stensmyr, M.C. (2016). Fecal-Derived Phenol Induces Egg-Laying Aversion in *Drosophila*. Curr Biol *26*, 2762-2769.

92. Marin, E.C., Büld, L., Theiss, M., Sarkissian, T., Roberts, R.J.V., Turnbull, R., Tamimi, I.F.M., Pleijzier, M.W., Laursen, W.J., Drummond, N.*, et al.* (2020). Connectomics Analysis Reveals First-, Second-, and Third-Order Thermosensory and Hygrosensory Neurons in the Adult *Drosophila* Brain. Curr Biol *30*, 3167-3182.e3164.

93. Matthews, B.J., Younger, M.A., and Vosshall, L.B. (2019). The ion channel ppk301 controls freshwater egg-laying in the mosquito *Aedes aegypti*. eLIFE *8*, e43963.

94. McLaughlin, C.N., Brbić, M., Xie, Q., Li, T., Horns, F., Kolluru, S.S., Kebschull, J.M., Vacek, D., Xie, A., Li, J.*, et al.* (2020). Single-cell transcriptomes of developing and adult olfactory receptor neurons in *Drosophila*. bioRxiv, 2020.2010.2008.332130.

95. Menuz, K., Larter, N.K., Park, J., and Carlson, J.R. (2014). An RNA-seq screen of the *Drosophila* antenna identifies a transporter necessary for ammonia detection. PLoS Genet *10*, e1004810.

96. Nene, V., Wortman, J.R., Lawson, D., Haas, B., Kodira, C., Tu, Z., Loftus, B., Xi, Z., Megy, K., Grabherr, M.*, et al.* (2007). Genome Sequence of *Aedes aegypti*, a Major Arbovirus Vector. Science *316*, 1718-1723.

97. O'Neill, E.M., Rebay, I., Tjian, R., and Rubin, G.M. (1994). The activities of two Ets-related transcription factors required for *Drosophila* eye development are modulated by the Ras/MAPK pathway. Cell *78*, 137-147.

98. Papes, F., Logan, D.W., and Stowers, L. (2010). The Vomeronasal Organ Mediates Interspecies Defensive Behaviors through Detection of Protein Pheromone Homologs. Cell *141*, 692-703.

99. Park, J.H., and Kwon, J.Y. (2011). A systematic analysis of *Drosophila* gustatory receptor gene expression in abdominal neurons which project to the central nervous system. Mol Cells *32*, 375-381.

100. Pask, G.M., and Ray, A. (2016). Insect Olfactory Receptors: An Interface between Chemistry and Biology. In Chemosensory Transduction (Elsevier), pp. 101-122.

101. Persad, R., Reuter, D.N., Dice, L.T., Nguyen, M.-A., Rigoulot, S.B., Layton, J.S., Schmid, M.J., Poindexter, M.R., Occhialini, A., Stewart, C.N.*, et al.* (2020). The *Q*-System as a Synthetic Transcriptional Regulator in Plants. Front Plant Sci *11*.

102. Pinto, L., Stocker, R.F., and Rodrigues, V. (1988). Anatomical and neurochemical classification of the antennal glomeruli in Drosophila melanogaster meigen (Diptera: Drosophilidae). Int J Insect Morphol Embryol *17*, 335-344.

103. Pitts, R.J., Liu, C., Zhou, X., Malpartida, J.C., and Zwiebel, L.J. (2014). Odorant receptor-mediated sperm activation in disease vector mosquitoes. PNAS *111*, 2566-2571.

104. Port, F., Chen, H.M., Lee, T., and Bullock, S.L. (2014). Optimized CRISPR/Cas tools for efficient germline and somatic genome engineering in *Drosophila*. PNAS *111*, E2967-2976.

105. Potter, C.J., Tasic, B., Russler, E.V., Liang, L., and Luo, L. (2010). The Q system: a repressible binary system for transgene expression, lineage tracing, and mosaic analysis. Cell *141*, 536-548.

106. Ray, A., Van der Goes van Naters, W., and Carlson, J.R. (2008). A regulatory code for neuron-specific odor receptor expression. PLoS Biol *6*, e125.

107. Ray, A., Van der Goes van Naters, W., Shiraiwa, T., and Carlson, J.R. (2007). Mechanisms of odor receptor gene choice in *Drosophila*. Neuron *53*, 353-369.

108. Riabinina, O., Luginbuhl, D., Marr, E., Liu, S., Wu, M.N., Luo, L., and Potter, C.J. (2015). Improved and expanded Q-system reagents for genetic manipulations. Nat Methods *12*, 219-222, 215 p following 222.

109. Riabinina, O., Task, D., Marr, E., Lin, C.-C., Alford, R., O'Brochta, D.A., and Potter, C.J. (2016). Organization of olfactory centres in the malaria mosquito *Anopheles gambiae*. Nat Commun *7*, 13010.

110. Robinow, S., and White, K. (1991). Characterization and spatial distribution of the ELAV protein during *Drosophila melanogaster* development. J Neurobiol *22*, 443-461.

111. Sanchez-Alcaniz, J.A., Silbering, A.F., Croset, V., Zappia, G., Sivasubramaniam, A.K., Abuin, L., Sahai, S.Y., Munch, D., Steck, K., Auer, T.O.*, et al.* (2018). An expression atlas of variant ionotropic glutamate receptors identifies a molecular basis of carbonation sensing. Nat Commun *9*, 4252.

112. Sato, K., Pellegrino, M., Nakagawa, T., Nakagawa, T., Vosshall, L.B., and Touhara, K. (2008). Insect olfactory receptors are heteromeric ligand-gated ion channels. Nature *452*, 1002-1006.

113. Schindelin, J., Arganda-Carreras, I., Frise, E., Kaynig, V., Longair, M., Pietzsch, T., Preibisch, S., Rueden, C., Saalfeld, S., and Schmid, B. (2012). Fiji: an open-source platform for biological-image analysis. Nat Methods *9*, 676-682.

114. Scott, K. (2018). Gustatory Processing in *Drosophila melanogaster*. Annu Rev Entomol *63*, 15-30.

115. Scott, K., Brady, R., Cravchik, A., Morozov, P., Rzhetsky, A., Zuker, C., and Axel, R. (2001). A Chemosensory Gene Family Encoding Candidate Gustatory and Olfactory Receptors in *Drosophila*. Cell *104*, 661-673.

116. Seki, Y., Dweck, H.K.M., Rybak, J., Wicher, D., Sachse, S., and Hansson, B.S. (2017). Olfactory coding from the periphery to higher brain centers in the *Drosophila* brain. BMC Biol *15*, 56.

117. Shearin, H.K., Macdonald, I.S., Spector, L.P., and Stowers, R.S. (2014). Hexameric GFP and mCherry reporters for the *Drosophila* GAL4, Q, and LexA transcription systems. Genetics *196*, 951-960.

118. Siddiqi, O. (1987). Neurogenetics of olfaction in *Drosophila melanogaster*. Trends Genet *3*, 137-142.

119. Siegal, M.L., and Hartl, D.L. (1996). Transgene Coplacement and high efficiency site-specific recombination with the Cre/loxP system in *Drosophila*. Genetics *144*, 715-726.

120. Silbering, A.F., Rytz, R., Grosjean, Y., Abuin, L., Ramdya, P., Jefferis, G.S., and Benton, R. (2011). Complementary function and integrated wiring of the evolutionarily distinct *Drosophila* olfactory subsystems. J Neurosci *31*, 13357-13375.

121. Singh, R.N., and Nayak, S.V. (1985). Fine structure and primary sensory projections of sensilla on the maxillary palp of Drosophila melanogaster Meigen (Diptera: Drosophilidae). Int J Insect Morphol Embryol *14*, 291-306.

122. Spletter, M.L., Liu, J., Liu, J., Su, H., Giniger, E., Komiyama, T., Quake, S., and Luo, L. (2007). Lola regulates *Drosophila* olfactory projection neuron identity and targeting specificity. Neural Dev *2*, 14.

123. Stengl, M. (2010). Pheromone transduction in moths. Front Cell Neurosci *4*, 133-133.

124. Stensmyr, M.C., Dweck, H.K., Farhan, A., Ibba, I., Strutz, A., Mukunda, L., Linz, J., Grabe, V., Steck, K., Lavista-Llanos, S.*, et al.* (2012). A Conserved Dedicated Olfactory Circuit for Detecting Harmful Microbes in *Drosophila*. Cell *151*, 1345-1357.

125. Stocker, R.F. (1994). The organization of the chemosensory system in *Drosophila melanogaster*: a review. Cell Tissue Res *275*, 3-26.

126. Stocker, R.F. (2001). *Drosophila* as a focus in olfactory research: mapping of olfactory sensilla by fine structure, odor specificity, odorant receptor expression, and central connectivity. Microsc Res Tech *55*, 284-296.

127. Su, C.Y., Menuz, K., and Carlson, J.R. (2009). Olfactory perception: receptors, cells, and circuits. Cell *139*, 45-59.

128. Subedi, A., Macurak, M., Gee, S.T., Monge, E., Goll, M.G., Potter, C.J., Parsons, M.J., and Halpern, M.E. (2014). Adoption of the *Q* transcriptional regulatory system for zebrafish transgenesis. Methods *66*, 433-440.

129. Suh, G.S.B., Wong, A.M., Hergarden, A.C., Wang, J.W., Simon, A.F., Benzer, S., Axel, R., and Anderson, D.J. (2004). A single population of olfactory sensory neurons mediates an innate avoidance behaviour in *Drosophila*. Nature *431*, 854-859.

130. Thurmond, J., Goodman, J.L., Strelets, V.B., Attrill, H., Gramates, L.S., Marygold, S.J., Matthews, B.B., Millburn, G., Antonazzo, G., and Trovisco, V. (2019). FlyBase 2.0: the next generation. Nucleic Acids Res *47*, D759-D765.

131. Trible, W., Olivos-Cisneros, L., McKenzie, S.K., Saragosti, J., Chang, N.-C., Matthews, B.J., Oxley, P.R., and Kronauer, D.J.C. (2017). Orco mutagenesis causes loss of antennal lobe glomeruli and impaired social behavior in ants. Cell *170*, 727-735. e710.

132. van Breugel, F., Huda, A., and Dickinson, M.H. (2018). Distinct activity-gated pathways mediate attraction and aversion to CO2 in *Drosophila*. Nature *564*, 420-424.

133. Venkatesh, S., and Singh, R.N. (1984). Sensilla on the third antennal segment of *Drosophila melanogaster* meigen (Diptera : Drosophilidae). Int J Insect Morphol Embryol *13*, 51-63.

134. Vilain, S., Vanhauwaert, R., Maes, I., Schoovaerts, N., Zhou, L., Soukup, S., da Cunha, R., Lauwers, E., Fiers, M., and Verstreken, P. (2014). Fast and efficient *Drosophila melanogaster* gene knock-ins using MiMIC transposons. G3 (Bethesda) *4*, 2381-2387.

135. Vosshall, L.B., Amrein, H., Morozov, P.S., Rzhetsky, A., and Axel, R. (1999). A Spatial Map of Olfactory Receptor Expression in the *Drosophila* Antenna. Cell *96*, 725-736.

136. Vosshall, L.B., and Hansson, B.S. (2011). A unified nomenclature system for the insect olfactory coreceptor. Chem Senses *36*, 497-498.

137. Vosshall, L.B., and Stocker, R.F. (2007). Molecular architecture of smell and taste in *Drosophila*. Annu Rev Neurosci *30*, 505-533.

138. Vosshall, L.B., Wong, A.M., and Axel, R. (2000). An Olfactory Sensory Map in the Fly Brain. Cell *102*, 147-159.

139. Wei, X., Potter, C.J., Luo, L., and Shen, K. (2012). Controlling gene expression with the *Q* repressible binary expression system in *Caenorhabditis elegans*. Nat Methods *9*, 391-395.

140. Wilson, R.I. (2013). Early olfactory processing in *Drosophila*: mechanisms and principles. Annu Rev Neurosci *36*, 217-241.

141. Xie, T., Ho, M.C.W., Liu, Q., Horiuchi, W., Lin, C.-C., Task, D., Luan, H., White, B.H., Potter, C.J., and Wu, M.N. (2018). A genetic toolkit for dissecting dopamine circuit function in *Drosophila*. Cell Rep *23*, 652-665.

142. Xue, Z., Ren, M., Wu, M., Dai, J., Rong, Y.S., and Gao, G. (2014). Efficient gene knock-out and knock-in with transgenic Cas9 in *Drosophila*. G3 (Bethesda) *4*, 925-929.

143. Yan, H., Jafari, S., Pask, G., Zhou, X., Reinberg, D., and Desplan, C. (2020). Evolution, developmental expression and function of odorant receptors in insects. J Exp Biol *223*.

144. Yan, H., Opachaloemphan, C., Mancini, G., Yang, H., Gallitto, M., Mlejnek, J., Leibholz, A., Haight, K., Ghaninia, M., Huo, L.*, et al.* (2017). An Engineered *orco* Mutation Produces Aberrant Social Behavior and Defective Neural Development in Ants. Cell *170*, 736-747.e739.

145. Younger, M.A., Herre, M., Ehrlich, A.R., Gong, Z., Gilbert, Z.N., Rahiel, S., Matthews, B.J., and Vosshall, L.B. (2020). Non-canonical odor coding ensures unbreakable mosquito attraction to humans. BioRxiv.

146. Zhang, Y.V., Ni, J., and Montell, C. (2013). The molecular basis for attractive salt-taste coding in *Drosophila*. Science *340*, 1334-1338.

147. Zheng, Z., Lauritzen, J.S., Perlman, E., Robinson, C.G., Nichols, M., Milkie, D., Torrens, O., Price, J., Fisher, C.B., and Sharifi, N. (2018). A complete electron microscopy volume of the brain of adult *Drosophila melanogaster*. Cell *174*, 730-743. e722.